1996

An investigation of ethylene carbonate based, binary solvent electrolyte solutions for lithium-ion batteries.

Barry. Klassen
University of Windsor

NOTICE

AVIS

Canada

An Investigation of Ethylene Carbonate Based,

Binary Solvent Electrolyte Solutions for Lithium-

Ion Batteries.

BY

BARRY KLASSEN

A Dissertation

Submitted to the Faculty of Graduate Studies through the

Department of Chemistry and Biochemistry in partial

fulfilment of the requirements for the Degree of Doctor of

Philosophy at the University of Windsor

The author has granted an irrevocable non-exclusive licence allowing the National Library of Canada to reproduce, loan, distribute or sell copies of his/her thesis by any means and in any form or format, making this thesis available to interested persons.

L'auteur a accordé une licence irrévocable et non exclusive permettant à la Bibliothèque nationale du Canada de reproduire, prêter, distribuer ou vendre des copies de sa thèse de quelque manière et sous quelque forme que ce soit pour mettre des exemplaires de cette thèse à la disposition des personnes intéressées.

The author retains ownership of the copyright in his/her thesis. Neither the thesis nor substantial extracts from it may be printed or otherwise reproduced without his/her permission.

L'auteur conserve la propriété du droit d'auteur qui protège sa thèse. Ni la thèse ni des extraits substantiels de celle-ci ne doivent être imprimés ou autrement reproduits sans son autorisation.

ISBN   0-612-11006-0

Canada

Name _____

Dissertation Abstracts International and Masters Abstracts International are arranged by broad, general subject categories.
Please select the one subject which most nearly describes the content of your dissertation or thesis. Enter the corresponding
four-digit code in the spaces provided.

Physical Chemistry
SUBJECT TERM

$\boxed{0}\boxed{4}\boxed{9}\boxed{4}$ **UMI**
SUBJECT CODE

Subject Categories

THE HUMANITIES AND SOCIAL SCIENCES

COMMUNICATIONS AND THE ARTS
Architecture 0729
Art History 0377
Cinema 0900
Dance 0378
Fine Arts 0357
Information Science 0723
Journalism 0391
Library Science 0399
Mass Communications 0708
Music 0413
Speech Communication 0459
Theater 0465

EDUCATION
General 0515
Administration 0514
Adult and Continuing 0516
Agricultural 0517
Art 0273
Bilingual and Multicultural 0282
Business 0688
Community College 0275
Curriculum and Instruction 0727
Early Childhood 0518
Elementary 0524
Finance 0277
Guidance and Counseling 0519
Health 0680
Higher 0745
History of 0520
Home Economics 0278
Industrial 0521
Language and Literature 0279
Mathematics 0280
Music 0522
Philosophy of 0998
Physical 0523

Psychology 0525
Reading 0535
Religious 0527
Sciences 0714
Secondary 0533
Social Sciences 0534
Sociology of 0340
Special 0529
Teacher Training 0530
Technology 0710
Tests and Measurements 0288
Vocational 0747

LANGUAGE, LITERATURE AND LINGUISTICS
Language
 General 0679
 Ancient 0289
 Linguistics 0290
 Modern 0291
Literature
 General 0401
 Classical 0294
 Comparative 0295
 Medieval 0297
 Modern 0298
 African 0316
 American 0591
 Asian 0305
 Canadian (English) 0352
 Canadian (French) 0355
 English 0593
 Germanic 0311
 Latin American 0312
 Middle Eastern 0315
 Romance 0313
 Slavic and East European 0314

PHILOSOPHY, RELIGION AND THEOLOGY
Philosophy 0422
Religion
 General 0318
 Biblical Studies 0321
 Clergy 0319
 History of 0320
 Philosophy of 0322
Theology 0469

SOCIAL SCIENCES
American Studies 0323
Anthropology
 Archaeology 0324
 Cultural 0326
 Physical 0327
Business Administration
 General 0310
 Accounting 0272
 Banking 0770
 Management 0454
 Marketing 0338
Canadian Studies 0385
Economics
 General 0501
 Agricultural 0503
 Commerce-Business 0505
 Finance 0508
 History 0509
 Labor 0510
 Theory 0511
Folklore 0358
Geography 0366
Gerontology 0351
History
 General 0578

 Ancient 0579
 Medieval 0581
 Modern 0582
 Black 0328
 African 0331
 Asia, Australia and Oceania 0332
 Canadian 0334
 European 0335
 Latin American 0336
 Middle Eastern 0333
 United States 0337
History of Science 0585
Law 0398
Political Science
 General 0615
 International Law and
  Relations 0616
 Public Administration 0617
Recreation 0814
Social Work 0452
Sociology
 General 0626
 Criminology and Penology 0627
 Demography 0938
 Ethnic and Racial Studies 0631
 Individual and Family
  Studies 0628
 Industrial and Labor
  Relations 0629
 Public and Social Welfare 0630
 Social Structure and
  Development 0700
 Theory and Methods 0344
Transportation 0709
Urban and Regional Planning ... 0999
Women's Studies 0453

THE SCIENCES AND ENGINEERING

BIOLOGICAL SCIENCES
Agriculture
 General 0473
 Agronomy 0285
 Animal Culture and
  Nutrition 0475
 Animal Pathology 0476
 Food Science and
  Technology 0359
 Forestry and Wildlife 0478
 Plant Culture 0479
 Plant Pathology 0480
 Plant Physiology 0817
 Range Management 0777
 Wood Technology 0746
Biology
 General 0306
 Anatomy 0287
 Biostatistics 0308
 Botany 0309
 Cell 0379
 Ecology 0329
 Entomology 0353
 Genetics 0369
 Limnology 0793
 Microbiology 0410
 Molecular 0307
 Neuroscience 0317
 Oceanography 0416
 Physiology 0433
 Radiation 0821
 Veterinary Science 0778
 Zoology 0472
Biophysics
 General 0786
 Medical 0760

EARTH SCIENCES
Biogeochemistry 0425
Geochemistry 0996

Geodesy 0370
Geology 0372
Geophysics 0373
Hydrology 0388
Mineralogy 0411
Paleobotany 0345
Paleoecology 0426
Paleontology 0418
Paleozoology 0985
Palynology 0427
Physical Geography 0368
Physical Oceanography 0415

HEALTH AND ENVIRONMENTAL SCIENCES
Environmental Sciences 0768
Health Sciences
 General 0566
 Audiology 0300
 Chemotherapy 0992
 Dentistry 0567
 Education 0350
 Hospital Management 0769
 Human Development 0758
 Immunology 0982
 Medicine and Surgery 0564
 Mental Health 0347
 Nursing 0569
 Nutrition 0570
 Obstetrics and Gynecology .. 0380
 Occupational Health and
  Therapy 0354
 Ophthalmology 0381
 Pathology 0571
 Pharmacology 0419
 Pharmacy 0572
 Physical Therapy 0382
 Public Health 0573
 Radiology 0574
 Recreation 0575

 Speech Pathology 0460
 Toxicology 0383
Home Economics 0386

PHYSICAL SCIENCES
Pure Sciences
Chemistry
 General 0485
 Agricultural 0749
 Analytical 0486
 Biochemistry 0487
 Inorganic 0488
 Nuclear 0738
 Organic 0490
 Pharmaceutical 0491
 Physical 0494
 Polymer 0495
 Radiation 0754
Mathematics 0405
Physics
 General 0605
 Acoustics 0986
 Astronomy and
  Astrophysics 0606
 Atmospheric Science 0608
 Atomic 0748
 Electronics and Electricity 0607
 Elementary Particles and
  High Energy 0798
 Fluid and Plasma 0759
 Molecular 0609
 Nuclear 0610
 Optics 0752
 Radiation 0756
 Solid State 0611
Statistics 0463

Applied Sciences
Applied Mechanics 0346
Computer Science 0984

Engineering
 General 0537
 Aerospace 0538
 Agricultural 0539
 Automotive 0540
 Biomedical 0541
 Chemical 0542
 Civil 0543
 Electronics and Electrical 0544
 Heat and Thermodynamics ... 0348
 Hydraulic 0545
 Industrial 0546
 Marine 0547
 Materials Science 0794
 Mechanical 0548
 Metallurgy 0743
 Mining 0551
 Nuclear 0552
 Packaging 0549
 Petroleum 0765
 Sanitary and Municipal 0554
 System Science 0790
Geotechnology 0428
Operations Research 0796
Plastics Technology 0795
Textile Technology 0994

PSYCHOLOGY
General 0621
Behavioral 0384
Clinical 0622
Developmental 0620
Experimental 0623
Industrial 0624
Personality 0625
Physiological 0989
Psychobiology 0349
Psychometrics 0632
Social 0451

ABSTRACT

Mixtures of solvents are commonly used in non-aqueous lithium-ion battery electrolytes. Structures comprised of the solvents and ions determine many of the electrolyte properties. Solvation structures which could exist in the electrolyte solution include separated-solvated ions, solvent separated ion pairs, solvated contact ion pairs, and polyionic aggregates. An understanding of these solvent-ion interactions will aid in the selection of solvent mixtures. The experimental techniques that were used in this investigation were Raman scattering, conductivity measurements, and viscosity measurements. The experimental results were supplemented by quantum mechanical *ab initio* calculations in order to gain further insight into the solvation structures. Where the possibility of the formation of ion-pairs and the predicted structure of the ion-pair is calculated. The solvent mixtures were made up of ethylene carbonate combined with one of the following solvents: propylene carbonate, diethyl carbonate, or dimethyl carbonate. Lithium perchlorate was used as the electrolyte. This research was the result of constant collaboration between the Unversity of Windsor and General Motors.

DEDICATION

To my understanding parents, sisters, and brothers.

ACKNOWLEDGEMENTS

TABLE OF CONTENTS

APPENDICES

LIST OF TABLES

LIST OF FIGURES

CHAPTER 1

INTRODUCTION

1.1 LITHIUM BATTERIES

Interest in the study of lithium continues to grow because of its actual and potential applications in industry[1] and biology[2]. The recent progress made in the field of portable compact electronic equipment (cellular telephones, microcomputers, video cameras. etc.) in the last ten years or so has dramatically increased the demand for new rechargeable high energy density batteries. In response to this demand, lithium batteries in particular have been the focus of intense fundamental and industrial research activity, which has led to commercialization of the first lithium-ion batteries by Sony Energetic in their portable phones. Lithium-ion batteries are characterized by a weight and volume that are both three times less than those of the conventional lead/acid batteries for the same energy capacity, which is due to their high energy density[3]. The most prominent merits of the lithium-ion battery are that the working voltage is three times as high and possesses twice the capacity of nickel-cadmium battery. Research and development of multimedia information systems allowing transmission of characters, sounds, and pictures have also been pursued by computer manufacturers. The performance of these information systems is determined by the performance
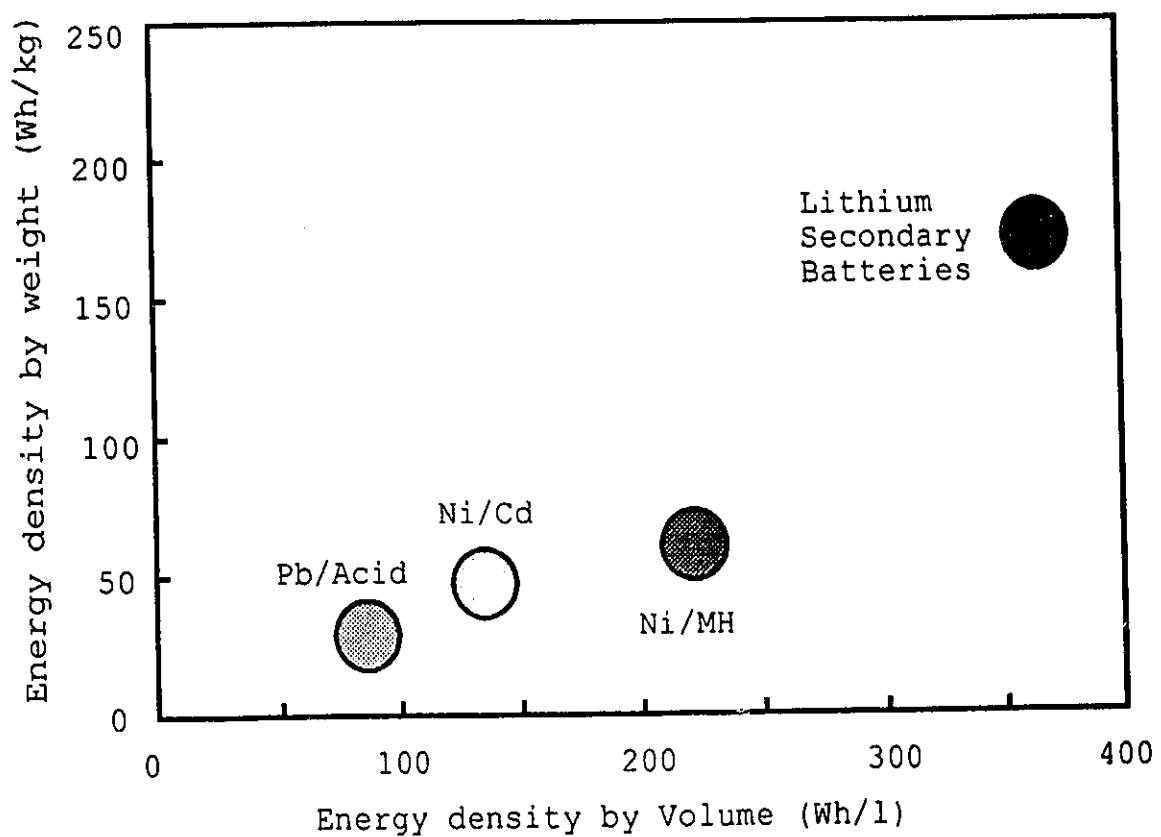
Figure 1.1 Comparison of Energy Densities for Various Types of Batteries.

of a small rechargeable battery. Figure 1.1 illustrates the advantages of lithium-ion batteries over three other main systems on the market, which include lead/acid, nickel/cadmium and nickel/metallic hydride[4]. The high degree of ionic conductivity shown by non aqueous electrolytic solutions made up of organic solvents such as propylene carbonate or ethylene carbonate, or in many cases, polymers such as poly (propylene carbonate and poly (ethylene oxides))[5 - 10] suggests their possible use in high energy density batteries. Further research is required to obtain improvement in the cyclability, cost and reliability of lithium batteries. The final objective is to produce large-scale, economically viable systems, for the application to electric vehicles.

The operating principle, based on the "rocking chair" concept[11,12], of the lithium battery is based on the reversible transfer of lithium ions between two electrodes made of lithium insertion materials as shown in Figure 1.2. In a lithium-ion battery, the anode is made up of carbonaceous material[13], which is well known for its good ionic lithium insertion-disinsertion properties[14,15]. The "ideal" anode is produced by the insertion of one lithium atom for every six atoms of carbon, LiC_6. Candidates for the make up of the cathode are transition metal oxides, chalcogenides, $LiMO_2$ (M = Co, Ni, Mn, Fe) or $LiMn_2O_4$ which
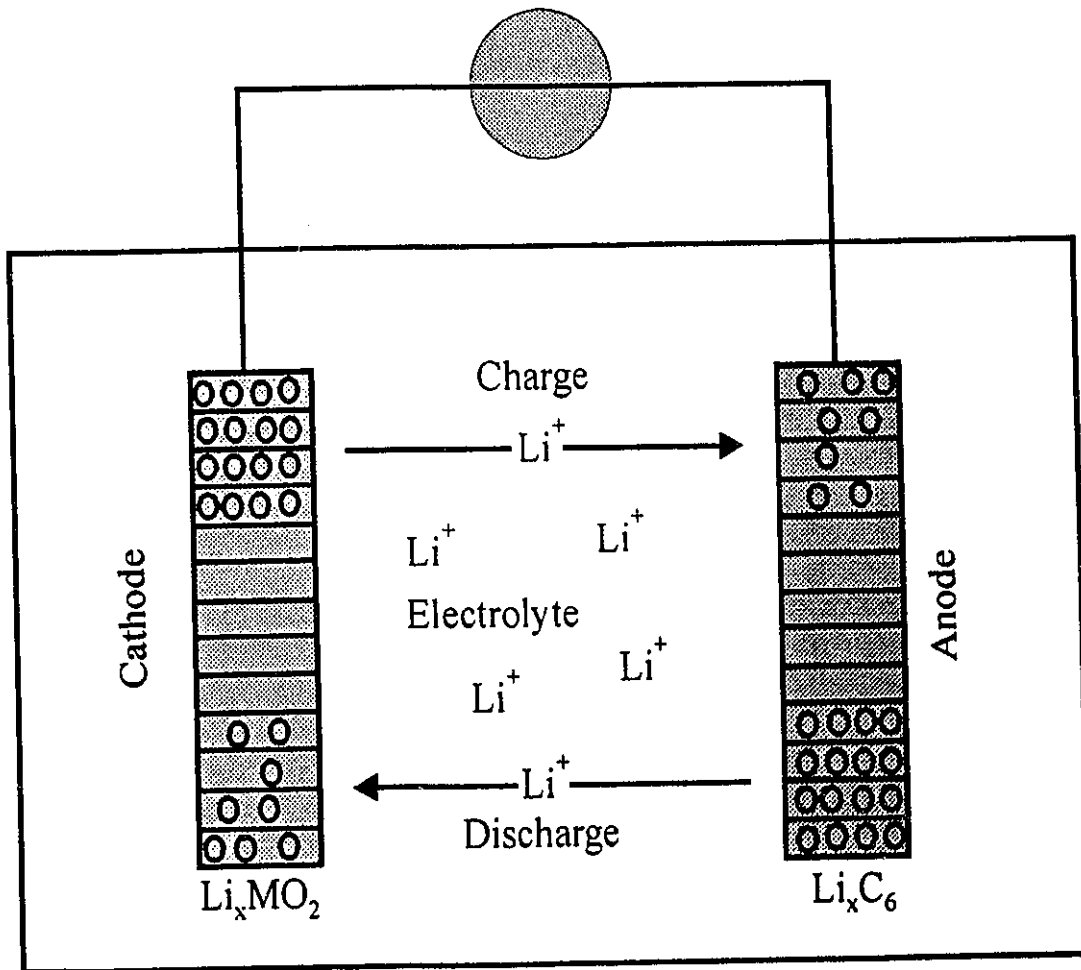
Figure 1.2 Operating Principle of a Lithium-ion (Rocking Chair) Type Battery.

show a good aptitude for lithium insertion-desinsertion and have relatively high discharge potential (3 to 4 V). Electrolytes are composed of a lithium salt (LiClO$_4$, LiPF$_6$, LiCF$_3$SO$_3$, etc)[16,17] dissolved in an organic solvent or more commonly a mixture of organic solvents such as ethylene carbonate, propylene carbonate, 2-methyl-tetrahydrofuran, etc.[18]. There are also examples of ternary solvent blends[19] which have been used in an attempt to improve low temperature performance. The structure and transport properties of non-aqueous electrolyte solutions used in ambient temperature lithium batteries are examined in this work. Composition of non-aqueous electrolyte solutions for secondary lithium batteries plays an important role in determining cycle life, cell performance, operating temperature range, and storage temperature range. There have been numerous studies and reviews concerning the conductivity and properties of non-aqueous electrolyte solutions[20,21,22]. Since a battery is an interactive system, many of the problems encountered in lithium batteries concerning the solution phase actually involve interactions between the components of the electrolyte solution. The characterization of these interactions that determine the performance of binary-solvent electrolyte solution will be the focus of this study.

1.2 COMPONENTS OF THE ELECTROLYTE SOLUTIONS

The choice of the solvents for the electrolyte solutions are based upon the following important factors: First, there are the practical considerations, since these are of significant importance in industry, the availability and cost of the solvents are important. The properties of the solvent must be considered when choosing a solvent for an electrolyte solution. An ideal solvent should have a high dielectric constant[23], a low viscosity, high boiling point, low freezing point, in other words, a broad temperature range of operation and be stable chemically in contact with the cell components and electrochemically stable over a broad voltage range. The solvents that were chosen for this study were ethylene carbonate (EC), propylene carbonate (PC), diethylene carbonate (DEC), and dimethyl carbonate (DMC), some of their physical properties are summarized in Table 1.1. Another important property of a solvent, obviously, is its ability to dissolve lithium salts. Ethylene carbonate has the highest dielectric constant and a high boiling point making it an ideal choice for a solvent in a non-aqueous electrolyte solution, however, it has a major draw back, it is a solid at room temperature (melting pt = 36 °C). The three other solvents PC, DEC, and DMC have a broad temperature range and low viscosities. While PC has

Li˙ Cation

Anion
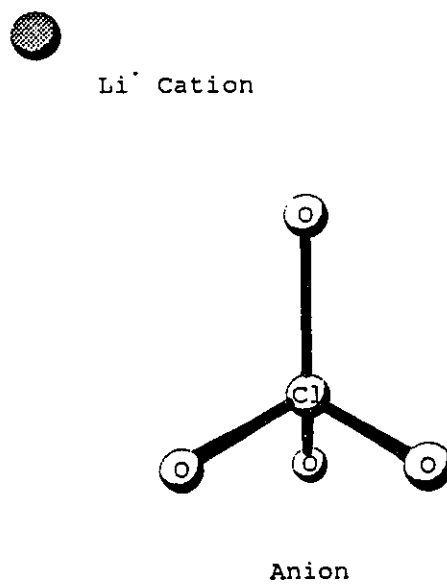
Figure 1.3 Structure of Dissociated Lithium
Perchlorate.

Ethylene carbonate
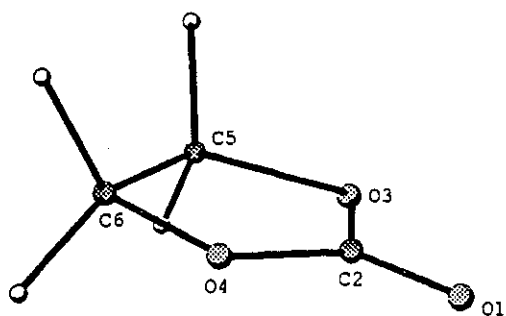
Propylene carbonate
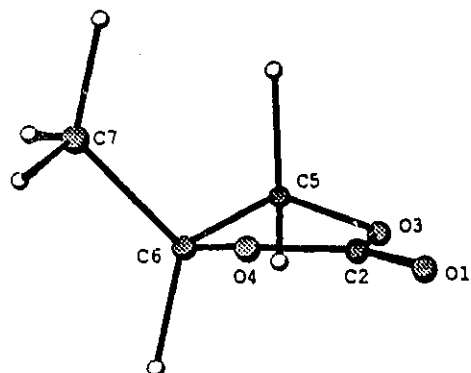
Diethyl carbonate
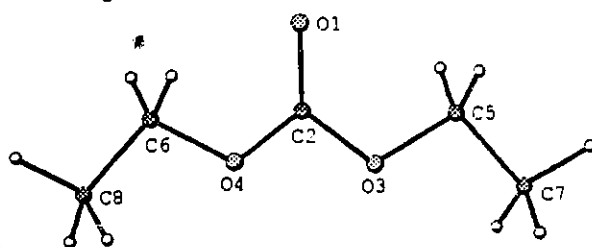
Diemethyl carbonate
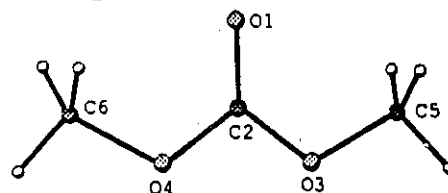
Figure 1.4 Molecular Structures of the Four Compounds Used as Solvents for the Electrolytes.

a relatively high dielectric constant, DEC and DMC have
relatively low dielectric constants, however, as will be
shown in Chapter 6, both DEC and DMC contribute in
maintaining a low electrolyte viscosity. A logical step
would be to combine solvents to obtain the desired
properties. When EC is combined with any of the other

Table 1.1 Properties of solvents used in this work

Solvent	Melting[24] Point(°C)	Boiling[16] Point (°C)	Viscosity (η) (cP)[25] (25°C)	Dielectric constant[12] (ε) (25°)
EC	36	238	solid	95.3
PC	−49	241	6.38	64.4
DEC	−43	126	2.18	3.12
DMC	0.5	90	1.20	2.82

solvents, the resulting binary solvent is a liquid at room
temperature and the properties can be adjusted by varying
the relative concentrations of each solvent. Thus we take
full advantage of the high dielectric constant of EC and the
low viscosities of the other three solvents. Possible binary
solvents that are addressed are EC/PC, EC/DEC, and EC/DMC.

As mentioned, there are many choices for a lithium
salt, the lithium salt chosen for this project is lithium
perchlorate. Lithium perchlorate is dissociated when

dissolved at low concentrations. The structure of the perchlorate anion is shown in Figure 1.3, it is simply four oxygen atoms around a chlorine atom in a tetrahedral geometry.

The molecular structures of the four compounds used as solvents for the electrolytes are depicted in Figure 1.4. Both EC and PC have five membered ring structures with PC having an extra methyl group. The compounds DMC and DEC have a methyl group and ethyl group respectively attached to either side of the carbonate group.

Interactions between the ions and solvents within the electrolyte are complex. The possible interactions that could occur in an electrolyte include separated solvated ions, solvent separated ion-pair, solvated contact ion-pair and lithium perchlorate aggregates[26] (refer to Figures 1.5) and 1.6. Existence of different types of ion pairs (contact ion-pairs, solvent separated ion-pairs) was originally postulated in order to explain the stereochemical course of solvolysis and electrophilic substitution reactions[27,28]. Since then the existence of both types of ion-pairs has been widely accepted. The electrolyte performance depends upon the mobility of ions. A central factor affecting the mobility of these ions and thereby the conductivity of the electrolytic solutions, is the formation of ion-pairs in non aqueous electrolytes. Numerous reports have illustrated the

Separated Solvated ions
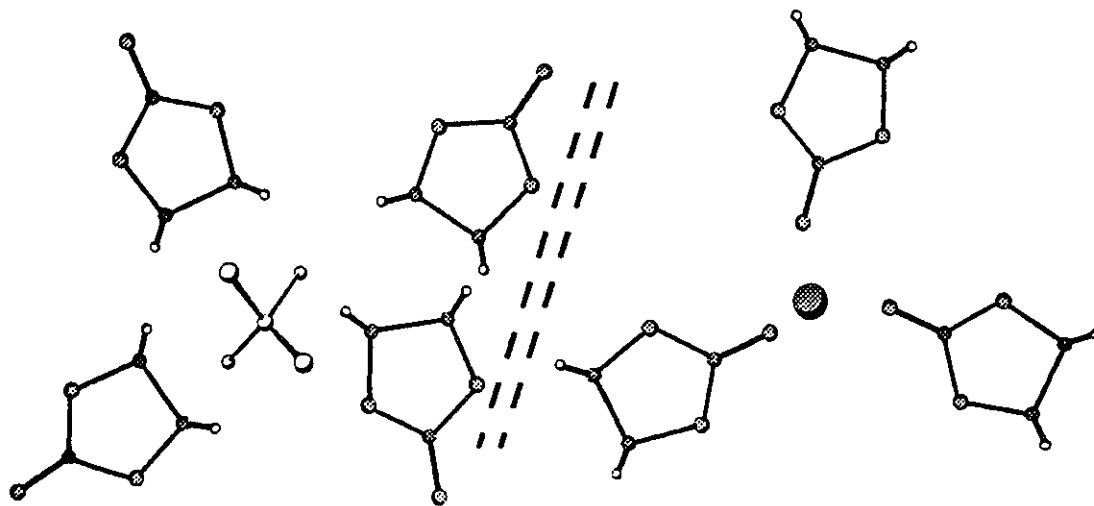
Solvent Separated ion - pair
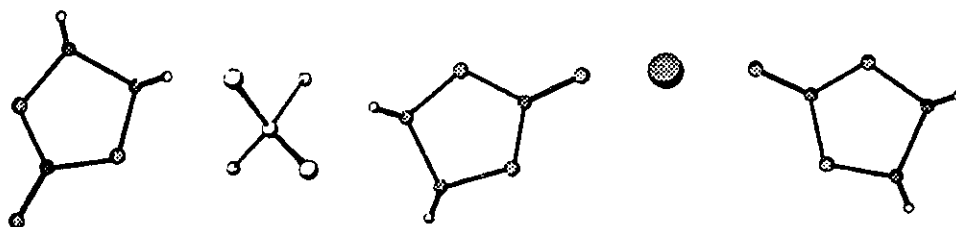
Solvated Contact ion - pair
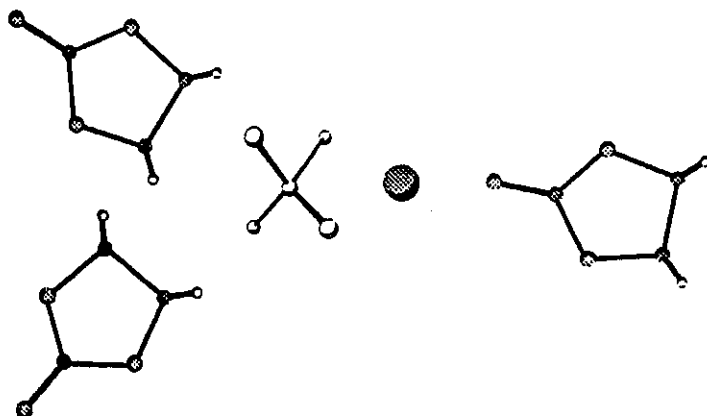
Figure 1.5 Possible interactions that could occur in an electrolyte solution.
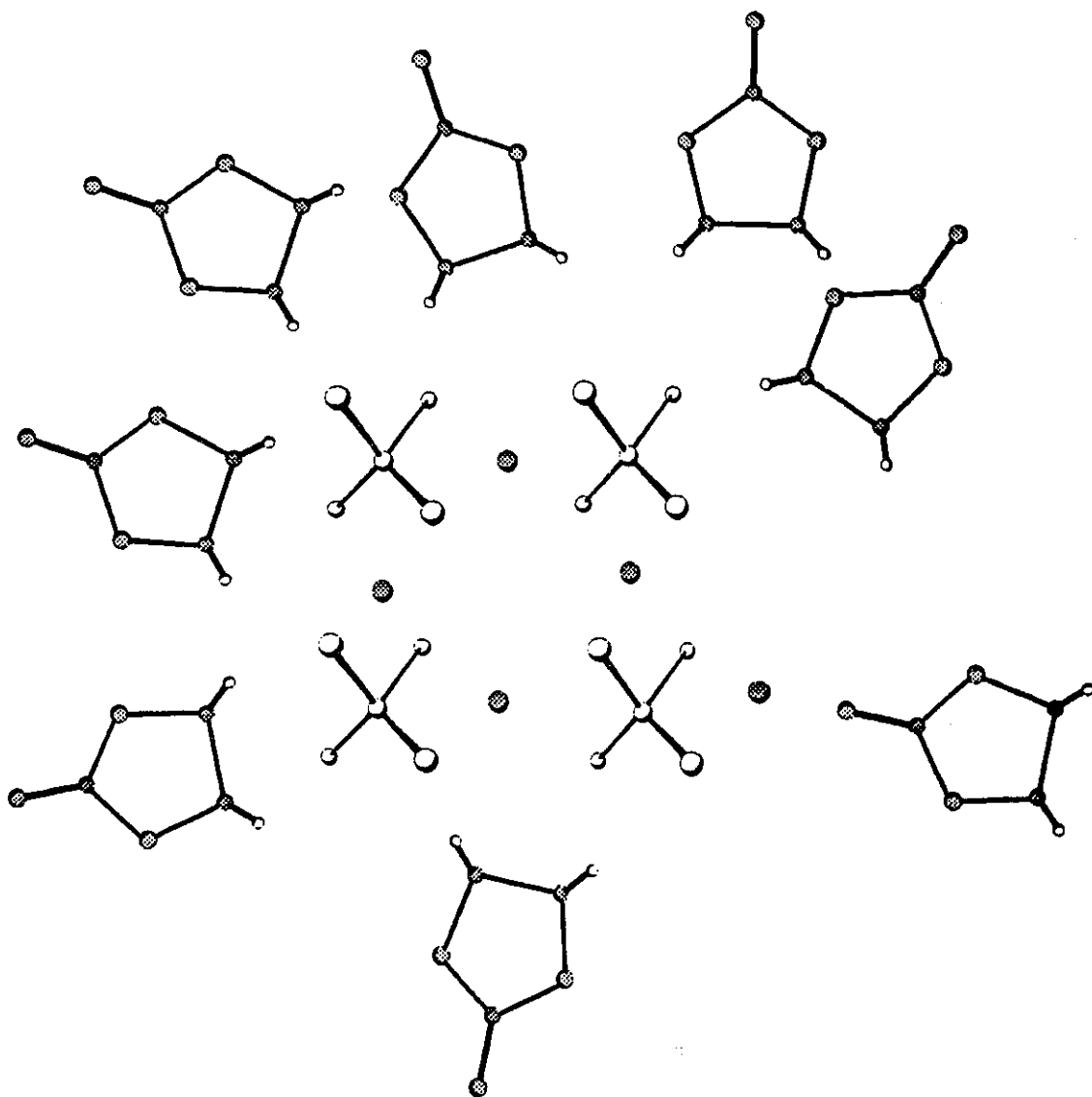
Figure 1.6 Possible structure of lithium perchlorate aggregates in a concentrated electrolyte solution

role of NMR[29], vibrational spectroscopy[30-33], and absorption spectra[34,35] as tools to probe solvent-salt interactions in electrolytes. The formation of $Li^+ClO_4^-$ ion-pairs and aggregates has been associated in the infrared and Raman spectra with frequency shifts and splitting of the vibrational bands of the conjugated anion in the lithium salt[36,37].

For instance, in a previous study[26] evidence of ion-pairing was found in electrolytes made up of lithium perchlorate salt dissolved in propylene carbonate which provided an explanation for the rapid decrease in the conductivity with electrolyte concentration. The totally symmetric Cl-O stretch of the free perchlorate anion was observed at 933 cm^{-1}. The bands at 938 cm^{-1} and 944 cm^{-1} were assigned to solvent-shared ion-pairs and contact ion-pairs respectively. These features were observed at the same time that the conductivity in the electrolytes dropped off at higher concentrations of lithium salt.

In order to provide a more complete physical picture of the electrolyte species, theoretical methods, such as *ab initio* calculations, may be applied to study the likelihood of occurrence of ion-pairing and the most stable structure associated with ion-pairing. The value of *ab initio* calculations for molecular geometries is well established[38]

and advances in *ab initio* quantum chemistry have made possible the accurate prediction of vibrational frequencies[39,40]. Therefore, it is possible to accurately calculate ion-pair vibrational states and then compare with observed vibrational spectra (Raman and/or infrared)[41]. For instance, the possible geometries and vibrational spectra of the most stable ion-paired structures have been discussed[42] for the $BF_4^-Li^+$ ion pair. The formation of the ion-pair was energetically favourable and a bidentate C_{2v} geometry was preferred over the monodentate or tridentate C_{3v} geometry.

In this work, *ab initio* calculations were performed on lithium perchlorate and the organic solvents that make up the binary-solvent solution. The calculations gave detailed structural information along with a complete vibrational assignment for each of the components of the lithium perchlorate binary-solvent solution. Insight into the overall structure of the lithium perchlorate binary solvent solution can also be obtained from *ab initio* calculations.

1.3 OUTLINE OF THESIS

The thesis is arranged in the following sections: The experimental techniques and the instrumentation used to study the binary-solvent solutions are described in Chapter 2. Raman spectroscopy, conductivity and viscosity

measurements constituted the bulk of the experimental work. Chapter 3 contains the theoretical background for the quantum mechanical calculations that were performed using Gaussian 92. The formation of $Li^+ClO_4^-$ ion-pairs in concentrated binary-solvent solutions is discussed in Chapter 4. The geometry and Raman spectrum of the resulting ion-pair is predicted using Gaussian 92. Chapter 5 deals with the individual solvent molecules. The geometries and a detailed assignment of the vibrational bands is provided for EC, PC, DEC, and DMC. The individual components that were described in the previous chapters are combined to form the binary-solvent solutions in Chapter 6. The properties of the resulting binary solvent solutions upon dissolving lithium perchlorate in EC combined with one of PC, DEC, or DMC is discussed in detail. The interactions that occur within the binary-solvent solution when going from a dilute to a concentrated solution is discussed in terms of conductivity, viscosity, and spectral changes.

REFERENCES

1. *Lithium-Current Applications in Science, Medicine, and Technology,* ed. R. O. Bach, Wiley-Interscience, New York, 1985.

2. Symposium Proceedings: *Power Sources for Biomedical Implantable Applications and Ambient Temperature Lithium Batteries;* Owens, B. B., Margalit, N., Eds.; Electrochem. Soc.; Princeton, NJ, 1977.

3. Zaghib, K. *The Prospects for Lithium-Ion Batteries in Japan: Workshop for Li-Ion Batteries and Supercapacitors,* Reno, Nevada, USA, 1995.

4. Ohzuku, T. *Lithium Batteries: New Materials, Developments and perspectives.* Vol. 5, G. Pistoia ed., Elsevier, pp 239-280, (1994)

5. Blonsky, P. M.; Shriver, D. F.; Austin, P.; Allcock, H. R. *J. Am. Chem. Soc.* **1984**, *106*, 6854.

6. Ratner, M. A.; Shriver, D. F. *Chem. Rev.*, **1988**, *88*, 109.

7. Fringant, C.; Tranchant, A.; Messina, R. *Electrochemica Acta.* **1995**, *40*, 513.

8. Nazri, G.-A.; Meibuhr, S. G. *J. Electrochem. Soc.*, **1989**, *136*, 2450.

9. Zhuang, G.; Chottiner, G.; Scherson, D. A. *J. Phys. Chem.* **1995**, *99*, 7009.

10. Allcock, H. R.; Austin, P. E.; Sisko, J. T.; Blonsky, P. M.; Shriver, D. F. *Macromolecules*, **1986**, *19*, 1921.

11. Armand, M. In *Materials for Advanced Batteries;* Murphy, D. W., Broodhead, J., Steele, B. C. H., Eds.; Plenum Press: New York, 1980, p 145.

12. Scrosati, B. *J. Electrochem. Soc.*, **1992**, *139*(10), 383.

13. Sawai, K.; Iwakoshi, Y.; Ohzuku, T. *Solid State Ionics* **1994**, *69*, 273.

14. Takehara, Z. *Electrochim. Acta*, **1993**, *38*, 1169.

15. Sacken, U. v.; Nodwell, E.; Sundher, A. *Solid State Ionics*, **1995**, *69*, 284.

16. Dudley, J. T.; Wilkinson, D. P.; Thomas, G.; LeVae, R.; Woo, S.; Blom, H.; Horvath, C.; Juzkow, M. W.; Deis, B.; Juric, P.; Aghakian, P.; Dahn, J. R. *J. Power Sources*. **1991**, *35*, 59.

17. Strauss, S. H. *Chem. Rev.*, **1993**, *93*, 927.

18. Tobishima, S., Arakawa, M. *Electrochim. Acta*, **1986**, *35*, 383.

19. Abraham, K. M., Pasquariello, D. M. *Proc. 32nd Int. Power Sources Symp.*, 1986, The Electrochemical Society, Pennington, NJ, 1986, p. 136.

20. Blomgren, G. E., *Lithium Batteries*, Academic Press, New York, J. P. Gabano ed., 1983, pp 13-41.

21. Kumar, G.; Janaklraman; Namboodiri, N.; Gangadharan *J. Chem. Eng. Data*, **1991**, *36*, 467.

22. Jansen, M. L.; Yeager, H. L. *J. Phys. Chem.* **1974**, *78*, 1380.

23. Dudley, J. T.; Wilkinson, D. P.; Thomas, G.; LeVae, R.; Woo, S.; Blom, H.; Horvath, C.; Juzkow, M. W.; Denis, B.; Juric, P.; Aghakian, P.; Dahn, J. R. *J. Power Sources*, **1991** , *35*, 59.

24. CRC Hand Book of chemistry and physics, CRC Press, Boca Raton handbook

25. Viscosity data were obtained from experimental data results from this work as presented in chapter 6.

26. Battisti, D.; Nazri, G. A.; Klassen, B.; Aroca, R. *J. Phys. Chem.*, **1993**, *97*, 5826.

27. Grunwald, E. *Anal. Chem.* **1954**, *26*, 1696.

28. Winstein, S.; Clippinger, E.; Fainberg, A. H.; Robinson, G. C., *J. Am. Chem. Soc.* **1954**, *76*, 2597.

29. Schneider, H. *Eletrochim. Acta.* **1974**, *21*, 711.

30. Nazri, G. A.; MacAuthur, D. M.; O'Gara, J. F.; Aroca, R., In *Materials Research Society Symposium*

Proceedings, Nazri, G. A.; Shriver, D. F.; Huggins, R. A.; Balkanski, M., Eds.; Materials Research Society: Pittsburgh, 1990; Vol. 210, p 163.

31. Irish, D. E.; Ozeki, T. *Analytical Raman Spectroscopy*, Grasselli, J. G., Bulkin, B. J. Eds. **1991**, *114*, 59.

32. Wong, M. K.; Mckinney, W. J.; Popov, A. I. *J. Phys. Chem.*, **1971**, *75*, 56.

33. Ratcliffe, C. I.; Irish, D. E. *Can. J. Chem.* **1990**, *62*, 1134.

34. Hogen-Esch, T. E.; Smid, J. *J. Am. Chem. Soc.*, **1966**, *88*, 307.

35. Hogen-Esch, T. E.; Smid, J. *ibid.*, 318.

36. Jones, M. M.; Jones, E. A.; Harmon, D. F.; Semmes, R. T. *J. Am. Chem. Soc.* **1961**, *83*, 2038.

37. Deng, Z.; Irish, D. E. *Chem. Soc. Faraday Trans.* **1992**, *88(19)*, 2891.

38. Foresman, J. B.; Frisch, A. *Exploring Chemistry with Electronic Structure Methods: A Guide to Using Gaussian*, Gaussian Inc., Pittsburgh, 1993.

39. Defrees, D. J.; McLean, A. D. *J. Chem. Phys.*, **1985**, *82*, 333.

40. Pulay, P.; Forgeries, G.; Pang, F.; Biggs, J. E. *J. Am. Chem. Soc.* **1979**, *79*, 2550.

41. Ohio, K.; Acedia, H.; Watanabe, H.; Fujita, T.; Matsuura, H. *J. Phys. Chem.* **1994**, *98*, 6924.

42. Francisco, J. S.; Williams, I. H. *J. Phys. Chem.* **1990**, *94*, 8522.

CHAPTER 2

INSTRUMENTATION AND EXPERIMENTAL TECHNIQUES

2.1 RAMAN SPECTROSCOPY

Raman scattering was applied to explore molecular structure[1,2,3]. Group theory shows that Raman scattering and infrared absorption are complementary and especially powerful when used together for studies in molecular structure[4,5]. Raman spectra were collected using a Spex 1403 spectrometer interfaced to an IBM computer. The spectrometer was stationed on an optical table. The software was written in our laboratory and has been described elsewhere.[6] The double monochronometer contains holographic gratings (1800 grooves/nm). Photons were detected by a thermoelectrical and water cooled Hamamatsu R928 multialkali photomultiplier tube followed by conventional photon counting electronics. The spectral data collected were more conveniently manipulated by importing the data to the program Spectra Calc produced by Galactic Industries.

The 514.5 nm laser line from a Spectra-Physics model 164 Ar^+ laser was used for Raman excitation. Optical filters supplied from Spectra-Physics were used to remove plasma lines. The incident laser light was plane polarized and could be rotated by a Spectra-Physics model 310-21 polarization rotator. Scattered light was passed through a scrambler before passing through the entrance slit of the
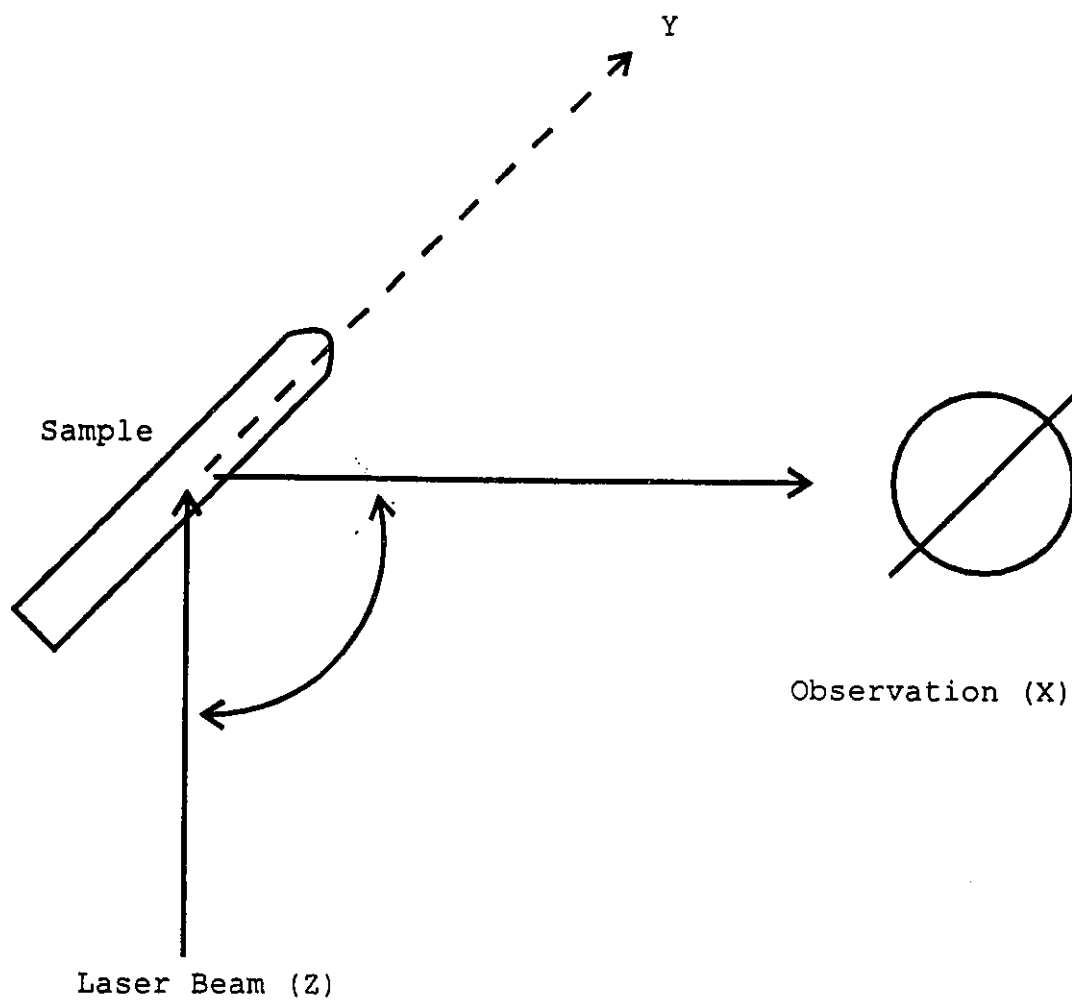
Figure 2.1 A schematic representation of the 90° scattering geometry.

spectrometer to ensure similar sensitivities towards

polarized light in different directions. The liquid samples

were contained in high quality glass capillaries having 2 mm

inside diameter. All spectra were collected using 90°

geometry and an xyz-positioner was used to secure and align

the sample as shown in Figure 2.1.

2.2 CONDUCTIVITY MEASUREMENTS

Conductivity of a completely dissociated electrolyte in

dilute solutions correlates well with the concentration of

mobile ions[7] and is given by:

$$\sigma = \frac{(N/V)eD}{k_B T} \qquad\qquad 2.1$$

where N is the number of mobile ions with charge e contained

in a volume V, k_B is Boltzmanns constant, and D is the

diffusion coefficient of the mobile ion. Equation 2.1 can be

associated to viscosity[5,9], η, of the electrolyte according

to the Stokes-Einstein relation, where the diffusion

coefficient of the mobile species is inversely proportional

to the viscosity and the radius of the charged particle, r:

$$D = \frac{k_B T}{6\pi\eta r} \qquad\qquad 2.2$$

Substituting Equation 2.1 into equation 2.2 results gives:

$$\sigma = \frac{(N/V)e}{6\pi\eta r} \qquad 2.3$$

Equation 2.3 indicates an inverse relationship between the conductivity and the viscosity of electrolytes. This relationship is also valid when equivalent conductance is applied. Equivalent conductance is given by the relationship:

$$\Lambda = \frac{1000\sigma}{c} \qquad 2.4$$

where σ is the conductivity (ohm^{-1} cm^{-1}) and c is the equivalent concentration (equiv/dm^3). Substitution of equation 2.3 into equation 2.4 produces:

$$\Lambda = 1000(\frac{N}{cV})e\frac{1}{6\pi\eta r} \qquad 2.5$$

The Walden product, $\Lambda\eta$, which is inversely proportional to the radius of charged particles in the solution can be obtained from Equation 2.5. Walden has proposed that for nonassociated electrolytes, the product of conductivity and viscosity is constant. The Walden product is represented by:

$$\Lambda\eta = constant \qquad 2.6$$

The linear relationship between conductivity and inverse viscosity (fluidity) only applies with complete dissociation of ions in solution (very dilute solutions). Deviation from ideal behaviour is observed and the linearity of the relationship is lost when ion association occurs. Solutions with maximum conductivity contain complex electrolyte species resulting from ion association, and frequently the ideal treatment of dilute solutions no longer holds. Despite the complex nature of concentrated solutions, the inverse relationship between conductivity and viscosity has been proven to be a useful guide for formulation of solutions with high fluidity and enhanced ionic conductivity. For practical applications, the main goal is to select mixed solvents with a reduced viscosity, and enhanced ionic conductivity.

Conductivity measurements were performed using dip cells (model A-01 with cell constant 0.1 from Rosemount Analytical Inc.). This cell uses two platinized parallel plates fixed in a cylindrical glass cavity. The electrode is dipped in the solution and the conductivity was allowed to stabilize before measurements were started (typically 3-5 minutes). Conductivity measurements were consistently reproducible following the above technique. The cell was connected to a Genrad model GR1689/1689M precision RLC

Digibridge. The Genrad Digibridge is a microprocessor controlled programmable RLC measuring instrument with long term stability and better than 0.02% accuracy[10]. The Digibridge measures the resistance of the electrolyte, where conductivity is simply obtained from the inverse resistance. Conductometers usually operated at 1000Hz, the digibridge operates at 1000Hz if another frequency is not specified. All data reported in this work were taken at 1000Hz.

2.3 VISCOSITY MEASUREMENTS

Solution viscosities were measured using a Brookfield dial viscometer model M/85-150E. This instrument measures the viscosity of fluids at a given shear rate (viscosity is a measure of the fluids resistance to flow)[11]. The viscometer measures the torque required to rotate a cylindrical spindle immersed in a fluid. Viscosity is proportional to the spindle speed of rotation and is related to the spindle size and geometry. The drag will increase with spindle size and rotation speed. Viscosity is defined by the formula:

$$\eta = viscosity = \frac{F'}{S} = \frac{shear\ stress}{shear\ rate} \qquad 2.7$$

Where S, the "shear rate" have the units "reciprocal

seconds" (sec $^{-1}$). The term F', called "shear stress", with the unit of measurement "dynes per square centimeter" (dynes/cm^2). For the rotating cylinder used in this work the shear stress is represented as:

$$Shear\ stress = \frac{M}{2\pi R_b^2 L} \qquad 2.8$$

and the shear rate is given by:

$$Shear\ rate = \frac{\omega R_c^2 R_b^2}{[x^2(R_c^2 - R_b^2)]} \qquad 2.9$$

Where ω is the angular velocity of the spindle used (rad/sec), R_c is the radius of container (cm), R_b is the radius of the spindle, x is the radius at which the shear rate is being calculated, M is the torque input of the instrument, and L is the effective length of the spindle $(2\pi/60)N$ (N = RPM). The fundamental unit of viscosity is the "poise". A material requiring a shear stress of one dyne per square centimeter to produce a shear rate of one reciprocal second has a viscosity of one poise. The viscosity unit used

Conductivity
Bridge

Viscometer

To Circulating
Bath

From Circulating
Bath
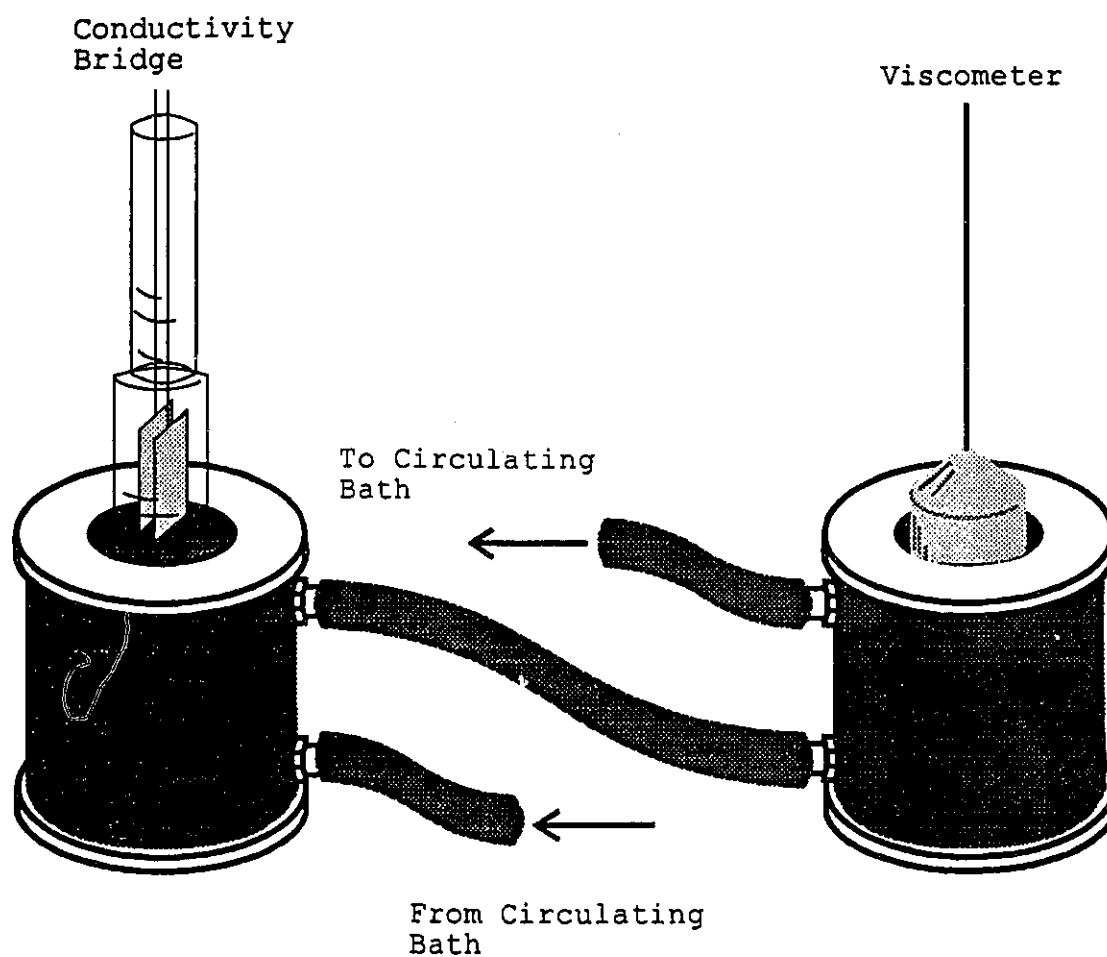
Figure 2.2 Schematic of conductometer and viscometer system
Temperature of conductometer and viscometer was
controlled by a circulating bath.

throughout this work is centipoise (cP). The measured value on the Brookfield viscometer is translated to centipoise according to the dial reading multiplied by a speed factor.

During conductivity and viscosity measurements, it is important to maintain the temperature of the electrolyte constant. A circulating bath with an accuracy of ± 0.1 ºc was used to control the temperature while performing measurements over a temperature range of -20 to 60 ºC. Both the conductivity and viscosity were measured at exactly the same temperature. This was accomplished by using a double pass circulating bath in which fluid at a constant temperature circulates around both the conductivity cell and the conductivity sample chamber jackets, as illustrated in Figure 2.2. The tubing connecting the circulating bath to the sample chambers were kept to a minimum length along with being insulated to prevent temperature variance between the circulating bath and sample chambers. The circulating bath fluid was commercial automobile antifreeze. The main components of the automobile antifreeze is a glycol derivative with low melting and high boiling points well within the temperature range used.

Considering that the solutions were potentially moisture sensitive, the setup had to be isolated from the outside atmosphere. This was accomplished by surrounding the

entire apparatus by a glove bag filled with 99.999% argon gas. Before each set of measurements, the glove bag was thoroughly purged.

2.4 MATERIALS

High purity cyclic ester solvents and linear carbonates; ethylene carbonate, propylene carbonate, dimethyl carbonate, and diethyl carbonate, were purchased from Fluka. In order to reduce the residual moisture, the solvents were stored over molecular sieves for at least 24 hours. Lithium perchlorate was also obtained from Fluka. Before preparing the electrolyte solutions, the lithium perchlorate was dried at 120 ºc under 10^{-4} torr vacuum for approximately 24 hours. After dissolution of salt in the ultra pure solvents, the concentration of residual water in the solution was negligible according to IR measurements.

All electrolyte solutions were prepared in a dry box filled with 99.999% argon. The atmosphere of the box was continuously circulated over Cu shaving catalyst and over titanium sponge at 700 ºc to remove residual oxygen, moisture, and nitrogen. The dry box was a Vacuum Atmosphere model MO-40-2H/DRI, equipped with a Nitrain and a catalyst recirculation unit. A 40 watt tungsten light bulb was cracked by a file and installed in the box to monitor the

purity of the dry box atmosphere. Usually each lamp lasts over two months before burning out. The open filament of the lamp is very sensitive to reactive gasses. If there is a leak in the box, the lamp burns off in less than 5 minutes. For each entry to the dry box the antechamber was purged with argon gas at least three times before opening to the main box.

REFERENCES

1. Wilson, E. B.; Decius, J. C.; Cross, P. C. *Molecular Vibrations*, Dover, New York, 1955.

2. Woodward, L. A. *Introduction to the Theory of Molecular Vibrations and Vibrational Spectroscopy*, Oxford University Press, Oxford, 1972.

3. Banwell, C. N. *Fundamentals of Molecular Spectroscopy*, McGraw-Hill, London, 1983.

4. Ferraro, J. R.; Ziomek, J. S. *Introductory Group Theory and Its Application to Molecular Structure*, Plenum, New York, 1969.

5. Cotten, F. A. *Chemical Applications of Group Theory*, Wiley-Interscience, New York, 1977.

6. Aroca, R.; Cook, P. *Am. Lab* **16**, 138, !1984).

7. Newman, J. S. *Electrochemical Systems*, Prentice-Hall Inc., NJ, **1973**, pp 3-25.

8. Jasinski, R. in Delahey, P. and Tobias, C. W. (eds.), *Advances in Electrochemistry and Electrochemical Engineering*, Vol. 8, Wiley, New York, 1971, p. 253.

9. Nazri, M. M.Sc. Thesis, Oakland University, 1995.

10. Genrad users manual.

11. Brookfield dial viscometer users manual

CHAPTER 3

COMPUTATIONAL TECHNIQUES

3.1 THEORETICAL BACKGROUND

There are many good text books for the theoretical background in quantum chemistry (i. e. I. N. Levine[1]). A good description of computational chemistry and applications is by Warren et al[2]. This chapter begins with a brief description of computational quantum mechanics as applied to chemistry problems. This leads to the program Gaussian 92, which was used throughout this work with success.

According to quantum mechanics, properties of physical systems are represented by operators. In particular energy is represented by H, the Hamiltonian operator. The energy of a stationary state of a molecule can be found by the solution of the nonrelativistic Schrödinger partial differential equation:

$$\hat{H}\Psi = E\Psi \qquad\qquad (3.1)$$

Where $\hat{H}$ is a differential operator representing the total energy. The numerical value of the energy minimum of the state, the energy relative to a state in which the nuclei and electrons are infinitely separated and at rest, is given by E. Ψ is the state wavefunction which depends on the Cartesian coordinates of all particles and also the spin coordinates. Spin coordinates may take on only a finite

number of values corresponding to spin angular momentum components in a certain direction. Since we are dealing with fermions, the wavefunction must also be antisymmetric with respect to interchange of the coordinates of any pair of electrons. This is called the antisymmetry principle.

The Hamiltonian is the sum of kinetic and potential terms:

$$\hat{H} = \hat{T} + \hat{V} \tag{3.2}$$

The kinetic energy operator is a sum of differential operators. The sum is over all particles i, nuclei and electrons where m_i is the mass of particle i, h is Plank's constant:

$$\hat{T} = -\frac{h^2}{8m_i\pi^2}\sum_i (\frac{\partial^2}{\partial x_i^2} + \frac{\partial^2}{\partial y_i^2} + \frac{\partial^2}{\partial z_i^2}) \tag{3.3}$$

The Potential energy operator is the coulomb interaction:

$$\hat{V} = \sum_i \sum_j (\frac{e_i e_j}{r_{ij}}) \tag{3.4}$$

Where $i < j$. The sum is over distinct particles (i, j) which have electric charges e_i, and e_j separated by a distance r_{ij}. For electrons, $e_i = -e$, while for a nucleus with atomic number Z_i, $e_i = +Z_i e$.

To facilitate solving the Schrödinger equation, the first major step in simplifying the general molecular problem in quantum mechanics is the separation of the nuclear and electronic motions. This can be done since the nuclear masses are much greater than those of the electrons. In general, the electrons in a molecule adjust their distribution to changing nuclear positions very rapidly. This leads to the assumption that the electron distribution depends only on the instantaneous positions of the nuclei and not their velocities. The separation of the general problem into two parts is called the Born-Oppenheimer approximation[3] and is valid so long as the ratio of electron to nuclear mass is sufficiently small.

Now the Schrödinger equation for electrons in the field of fixed nuclei can be rewritten with the Born-Oppenheimer approximation included:

$$\hat{H}^{ele}\Psi^{ele}(r,R)=E^{eff}(R)\Psi^{ele}(r,R) \tag{3.5}$$

Here, the effective electronic energy $E^{eff}(R)$ depends on the relative nuclear coordinates, denoted by R. The term $E^{eff}(R)$ is referred to as the potential surface for the molecule. Ψ^{ele} is the electronic wavefunction which depends on the electronic coordinates r as well as on the nuclear coordinates R. The electronic Hamiltonian now corresponds to

the motion of electrons in the field of fixed nuclei:

$$\hat{H}^{ele} = \hat{T}^{ele} + \hat{V} \qquad (3.6)$$

where electronic kinetic energy can be rewritten as:

$$\hat{T}^{ele} = -\left(\frac{h^2}{8\pi^2 m}\right) \sum_{i}^{electrons} \left(\frac{\partial^2}{\partial x_i^2} + \frac{\partial^2}{\partial y_i^2} + \frac{\partial^2}{\partial z_i^2}\right) \qquad (3.7)$$

and the coulomb potential energy becomes:

$$\hat{V} = -\sum_{i}^{electrons}\sum_{s}^{nuclei}\frac{Z_s e^2}{r_{is}} + \sum_{i}^{electrons}\sum_{j}\frac{e^2}{r_{ij}} + \sum_{s}^{nuclei}\sum_{t}\frac{Z_s Z_t e^2}{R_{st}} \qquad (3.8)$$

Where the first part corresponds to electron-nuclear attraction, the second part to electron-electron repulsion, and the third part to nuclear-nuclear repulsion. The third part is independent of the electronic coordinates and is a constant contribution for a nuclear configuration.

Molecular orbital theory is a quantum mechanical approach which uses one-electron functions, which are referred to as orbitals, to approximate the full wavefunction. A molecular orbital $\psi(x,y,z)$ is a function of the Cartesian coordinates x,y,z of a single electron. The probability distribution of the electron in space is given by $|\psi|^2$. The dependence on spin coordinates (ξ) must be included to completely describe the wavefunction. The spin

angular momentum component along the z axis in units of $h/2\pi$ can take on one of two possible values, $+\frac{1}{2}$ or $-\frac{1}{2}$, . Spin aligned along the positive z axis the wavefunction is written as $\alpha(+\frac{1}{2}) = 1$ and $\alpha(-\frac{1}{2}) = 0$, while spin aligned along the negative z axis the wavefunction is written as $\beta(+\frac{1}{2}) = 0$ and $\beta(-\frac{1}{2}) = 1$. The complete wavefunction for a single electron is then the product of a molecular orbital and a spin function, $\psi(x,y,z)\alpha(\xi)$ or $\psi(x,y,z)\beta(\xi)$, giving a spin orbital, $\chi(x,y,z,\xi)$.

To build a determinantial wavefunction, a set of monoelectronic functions (molecular orbitals) is chosen, $\psi_1, \psi_2, \psi_3, \ldots$, then electrons of α (spin up) or β (spin down) spin are assigned to these orbitals. The wavefunction must comply with the Pauli exclusion principle, which states that it is not possible for a molecular orbital to be occupied by two electrons of the same spin[4]. Therefore the determinant wavefunction must vanish if two columns are identical. Orbitals may be classified as doubly occupied, singly occupied, or empty. In this present study, all of the calculations are of molecules that contain an even number of electrons in their ground state with empty or doubly occupied orbits known as close-shell wavefunctions. Molecular orbital wavefunctions must also be orthogonal to each other, that is:

$$S_{ij} = \int \psi_i^* \psi_j dxdydz = 0 \quad \textit{for } i \neq j \tag{3.9}$$

Spin functions are orthogonal by integration over spin space, or in other words, they are actually summed over the two possible values of ξ:

$$\sum_\xi \alpha(\xi)\beta(\xi) = \alpha(+\tfrac{1}{2})\beta(+\tfrac{1}{2}) + \alpha(-\tfrac{1}{2})\beta(-\tfrac{1}{2}) = 0 \tag{3.10}$$

Molecular orbitals are also normalized:

$$S_{ii} = \int \psi_i^* \psi_i dxdydz = 1 \tag{3.11}$$

Which is accomplished by multiplication of the individual ψ_i by a constant. Normalization corresponds to the requirement that the probability of finding an electron in space is unity. The determinantal wavefunction may then be normalized by a multiplication factor of $(n!)^{-\frac{1}{2}}$. The resulting determinant is called a Slater determinant[5].

$$\Psi = (n!)^{1/2} \begin{vmatrix} \psi_1(1)\alpha(1) & \psi_1(1)\beta(1) & \psi_2(1)\alpha(1) & \cdot & \cdot & \cdot & \psi_{n/2}(1)\beta(1) \\ \psi_1(2)\alpha(2) & \psi_1(2)\beta(2) & \psi_2(2)\alpha(2) & \cdot & \cdot & \cdot & \psi_{n/2}(2)\beta(2) \\ & & & \cdot & & & \\ & & & \cdot & & & \\ & & & \cdot & & & \\ \psi_1(n)\alpha(n) & \psi_1(n)\beta(n) & \psi_2(n)\alpha(n) & \cdot & \cdot & \cdot & \psi_{n/2}(n)\beta(n) \end{vmatrix} \tag{3.12}$$

For practical applications of quantum mechanics the

individual orbitals may be expressed as linear combinations

of a finite set of N, one-electron functions which are known

as basis functions. Consider the basis functions to be ϕ_1,

ϕ_2, ..., ϕ_N, then an orbital can be written as:

$$\psi_i = \sum_{\mu=1}^{N} c_{\mu i} \phi_\mu \qquad (3.13)$$

Where $c_{\mu i}$ are the molecular expansion coefficients. Two

types of atomic basis functions are commonly used, Slater-

type atomic orbitals (STO) and Gaussian-type atomic

functions. STOs have exponential radial terms, they are

labeled like hydrogen atomic orbitals, 1s, 2s, $2p_x$, ... The

first three are given below:

$$\phi_{1s} = (\frac{\zeta_1^3}{\pi})^{1/2} \exp(-\zeta_1 r) \qquad (3.14)$$

$$\phi_{2s} = (\frac{\zeta_2^5}{96\pi})^{1/2} r \exp(\frac{-\zeta_2 r}{2}) \qquad (3.15)$$

$$\phi_{2p_x} = (\frac{\zeta_2^5}{32\pi})^{1/2} x \exp(\frac{-\zeta_2 r}{2}) \qquad (3.16)$$

Where ζ_1 and ζ_2 are constants which determine the size of

the orbitals. STOs are not well suited for numerical calculations and their use is limited.

The second type, Gaussian-type atomic functions (GTO), is the more widely used function in the calculation of large molecular systems and in the normalized form the first ten functions are [6,7]:

$$g_s(\alpha,r)=(\frac{2\alpha}{\pi})^{3/4}\exp(-\alpha r^2) \tag{3.17}$$

$$g_x(\alpha,r)=(\frac{128\alpha^5}{\pi^3})^{1/4}x\,\exp(-\alpha r^2) \tag{3.18}$$

$$g_y(\alpha,r)=(\frac{128\alpha^5}{\pi^3})^{1/4}y\,\exp(-\alpha r^2) \tag{3.19}$$

$$g_z(\alpha,r)=(\frac{128\alpha^5}{\pi^3})^{1/4}z\,\exp(-\alpha r^2) \tag{3.20}$$

$$g_{xx}(\alpha,r)=(\frac{2048\alpha^7}{9\pi^3})^{1/4}x^2\,\exp(-\alpha r^2) \tag{3.21}$$

$$g_{yy}(\alpha,r)=(\frac{2048\alpha^7}{9\pi^3})^{1/4}y^2\,\exp(-\alpha r^2) \tag{3.22}$$

$$g_{zz}(\alpha,r)=(\frac{2048\alpha^7}{9\pi^3})^{1/4}z^2\,\exp(-\alpha r^2) \tag{3.23}$$

$$g_{xy}(\alpha,r)=(\frac{2048\alpha^7}{\pi^3})^{1/4}xy\ \exp(-\alpha r^2) \qquad (3.24)$$

$$g_{xz}(\alpha,r)=(\frac{2048\alpha^7}{\pi^3})^{1/4}xz\ \exp(-\alpha r^2) \qquad (3.25)$$

$$g_{yz}(\alpha,r)=(\frac{2048\alpha^7}{\pi^3})^{1/4}yz\ \exp(-\alpha r^2) \qquad (3.26)$$

The Gaussian functions g_s, g_x, g_y, and g_z have angular symmetries of the s-type and p-type atomic orbitals. The next six second order functions do not all represent the angular symmetry of atomic orbitals. They may be combined to give the proper set of five d-type atomic functions which include g_{xy}, g_{xz}, g_{yz}, and the remaining two functions g_{3zz-rr} and g_{xx-yyN} have the form:

$$g_{3zz-rr}=\frac{1}{2}(2g_{zz}-g_{xx}-g_{yy}) \qquad (3.27)$$

$$g_{xx-yy}=(\frac{3}{4})^{1/2}(g_{xx}-g_{yy}) \qquad (3.28)$$

A s-type function can also be constructed from a sixth linear combination:

$$g_{rr}=5^{-1/2}(g_{xx}+g_{yy}+g_{zz}) \qquad (3.29)$$

The ten third-order Gaussian functions can be used to

construct a set of seven f-type atomic functions and an additional set of p functions. The GTOs have the advantage over STOs that all integrals in the calculations can be evaluated explicitly without using numerical integration, however, GTOs are less satisfactory than STOs. The Gaussian program solves this problem by using linear combinations of GTOs. For example, a s-type basis function can be expanded in terms of s-type gaussians:

$$\phi_\mu = \sum_s d_{\mu s} g_s \qquad (3.30)$$

where the coefficients $d_{\mu s}$ are fixed. These basis functions are called contracted gaussians and the terms g_s, are called primitive gaussians.

Description of the determinantial wavefunctions constructed from molecular orbitals has been given, the next step is to describe the method by which the expansion coefficients are determined. This brings us to Hartree-Fock (HF) theory. Hartree-Fock theory is based on the variational method in quantum mechanics[8]. Given a system with Hamiltonian operator $\hat{H}$, then if Φ is any antisymmetric normalized function of the electronic coordinates then the expectation value of the energy corresponding to this function is obtained from the integration over the coordinates of all electrons:

$$E' = \int \Phi^* \hat{H} \Phi d\tau \qquad (3.31)$$

When Φ is an exact wavefunction, Ψ, for the electronic ground state it will satisfy the Schrödinger equation. Since Ψ is normalized, E' will be the exact energy E:

$$E' = E \int \Psi^* \Psi d\tau = E \qquad (3.32)$$

Now, if Φ is any other normalized antisymmetric function, this results in E' will then be greater than E:

$$E' = \int \Phi^* \hat{H} \Phi d\tau > E \qquad (3.33)$$

So that if Φ is the antisymmetric molecular orbital function the energy E' calculated will be above the minimum value E.

The variational method is used to determine optimum orbitals in single determinant wavefunctions. A basis set for molecular orbital expansion is chosen and then the coefficients $c_{\mu i}$, are then adjusted to minimize the expectation value of the energy E'. The resulting energy E' will then be as close to the exact energy E depending on the single determinant wavefunction and the basis set that was applied. In an energy sense, the best single determinant wavefunction is determined by minimizing E' with respect to the coefficient $c_{\mu i}$. In other words:

$$\frac{\partial E'}{\partial c_{\mu i}} = 0 \ (all \ \mu, i) \tag{3.34}$$

In all cases, the calculations performed in this work are on closed shell systems using Hartree-Fock theory, so that we can focus on the methods relating to closed shell systems. The variational condition described above leads to a set of algebraic equations for $c_{\mu i}$ and were derived for the closed shell wavefunction by both Roothaan[9] and Hall [10]:

$$\sum_{v=1}^{N} (F_{\mu v} - \epsilon_i S_{\mu v}) = 0 \quad \mu = 1, 2, \dots, N \tag{3.35}$$

having the normalized conditions:

$$\sum_{\mu=1}^{N} \sum_{v=1}^{N} c_{\mu i}^* S_{\mu v} c_{v i} = 1 \tag{3.36}$$

Where ϵ_i is the one-electron energy of the molecular orbital ψ_i, $S_{\mu v}$ are the elements of an $N \times N$ matrix called the overlap matrix:

$$S_{\mu v} = \int \phi_{\mu}^*(1) \phi_{v}(1) dx_1 dy_1 dz_1 \tag{3.37}$$

The term $F_{\mu v}$ has the elements of another $N \times N$ matrix called the Fock matrix:

$$F_{\mu\nu} = H_{\mu\nu}^{core} + \sum_{\lambda=1}^{N} \sum_{\sigma=1}^{N} P_{\lambda\sigma}[(\mu\nu|\lambda\sigma) - \tfrac{1}{2}(\mu\lambda|\nu\sigma)] \qquad (3.38)$$

In the above expression, $H^{core}{}_{\mu\nu}$ is a matrix representing the energy of a single electron in a field of nuclei:

$$H_{\mu\nu}^{core} = \int \phi_\mu^*(1) \hat{H}^{core}(1) \phi_\nu(1) dx_1 dy_1 dz_1 \qquad (3.39)$$

$$\hat{H}^{core}(1) = -\frac{1}{2}\left(\frac{\partial^2}{\partial x_1^2} + \frac{\partial^2}{\partial y_1^2} + \frac{\partial^2}{\partial z_1^2}\right) - \sum_{A=1}^{M} \frac{Z_A}{r_{1A}} \qquad (3.40)$$

Where Z_A is the atomic number of atom A, the summation is over all atoms. The quantities $(\mu\nu|\lambda\sigma)$ are two-electron repulsion integrals:

$$\nu|\lambda\sigma) = \int\int \phi_\mu^*(1) \phi_\nu(1) \left(\frac{1}{r_{12}}\right) \phi_\lambda^*(2) \phi_\sigma(2) dx_1 dy_1 dz_1 dx_2 dy_2 d \qquad (3.41)$$

Which is multiplies by the elements of the one-electron density matrix, $P_{\lambda\sigma}$:

$$P_{\lambda\sigma} = 2 \sum_{i=1}^{occ} c_{\lambda i}^* c_{\sigma i} \qquad (3.42)$$

Here the summation is over occupied molecular orbitals. The number 2 indicates that two electrons occupy each molecular orbital. The electronic energy, E^{ee}, is given by:

$$E^{ee} = \frac{1}{2} \sum_{\mu=1}^{N} \sum_{\nu=1}^{N} P_{\mu\nu}(F_{\mu\nu} + H_{\mu\nu}^{core}) \tag{3.43}$$

The internuclear repulsion energy is given by the equation:

$$E^{nr} = \sum_{A<B}^{M} \sum \frac{Z_A Z_B}{R_{AB}} \tag{3.44}$$

So that the total energy is the combination of the above two terms ($E^{ee} + E^{nr}$). The terms Z_A and Z_B are the atomic numbers of atoms A and B, and R_{AB} is their separation. Considering that the Roothaan-Hall equations are non linear since the Fock matrix $F_{\mu\nu}$ depends on the molecular coefficients $c_{\mu i}$ through the density matrix expression, the solutions involves an iterative process. The resulting molecular orbitals are derived from their own effective potential and the technique is commonly called the self-consistent-field (SCF) theory.

3.2 UNITS

When a quantum chemical calculation is performed on the Gaussian 92 program the energy units are in what is called Hartrees. These units have been adopted in order to eliminate the fundamental physical constants from the

electronic Schrödinger equation. We start with the introduction of the Bohr radius, a_o, which is defined by:

$$a_o = \frac{h^2}{(4\pi^2 m e^2)}$$
(3.45)

This is the atomic unit of length, the bohr and new coordinates (x', y', z') are introduced:

$$x' = \frac{x}{a_o}$$
(3.46)

Then a new atomic unit of energy, E_H, which is the Coulomb repulsion between two electrons separated by 1 bohr:

$$E_H = \frac{e^2}{a_o}$$
(3.47)

This unit is called the hartree and the new energies, E', are given by:

$$E' = \frac{E}{E_H}$$
(3.48)

If the above are substituted into the Schrödinger equation:

$$\hat{H}'\Psi' = E'\Psi'$$
(3.49)

One hartree is equal to 2625 kJ mol^{-1}.

3.3 BASIS SET DESCRIPTION AND OPTIONS

Ab initio self consistent field (SCF) molecular orbital calculations were performed with the program Gaussian 92[11]. Full geometry optimization was performed according to Schegel's method[12]. Employing analytical gradients, to better than 10^{-3} Å for bond lengths and 10^{-2} for angles. The basis sets utilized were 3-21G[13] where each inner-shell atomic orbital is represented by a single function which in turn are made up of three Gaussian primitives:

$$\phi_{nl}(r)=\sum_{k=1}^{K} d_{nl,k}g_l(\alpha_{n,k},r) \qquad (3.50)$$

with $K = 3$. Valence-shell orbitals are made up of two contracted ($K' = 2$) and one diffuse basis functions ($K'' = 1$):

$$\phi_{nl}'(r)=\sum_{k'=1}^{K'} d_{nl,k}'g_l(\alpha_{n,k}',r) \qquad (3.51)$$

$$\phi_{nl}''(r)=\sum_{k'=1}^{K''} d_{nl,k}''g_l(\alpha_{n,k}'',r) \qquad (3.52)$$

The double-zeta basis set, 6-31G[14] where each inner-shell

atomic orbital is represented by a single function made up
of six Gaussian primitives ($K = 6$) and the valence-shell
orbitals are made up three contracted ($K' = 3$) and one
diffuse basis function ($K'' = 1$).

So far the basis sets discussed have functions that are
constrained to be centered at the nuclear positions. There
is evidence that the descriptions of highly polar molecules
and systems consisting of small strained rings requires that
some allowance be made for the possibility of nonuniform
displacement of charge away from the atomic centers. The way
that the Gaussian 92 program deals with the problem is to
include functions of higher angular quantum number. Thus d-
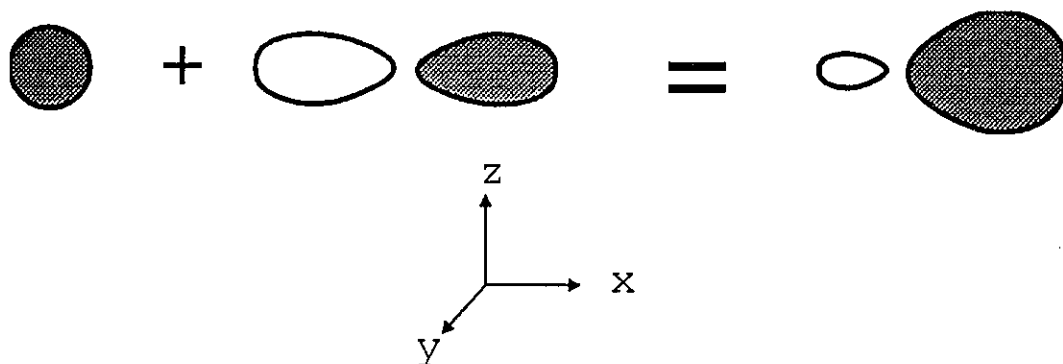
Figure 3.1 Combination of p-type function with a s-type
function.

type functions are included on heavy atoms and p-type
functions are included on hydrogen in the basis sets. For
example, when combining a p_x-type function with a valence s
function of hydrogen the centre of the basis function is

displaced along the x-axis and away from the hydrogen nucleus as seen in Figure 3.1[15].

The same approach is made when combining s-type with p_y-type or p_z-type functions and leads to the analogous displacements along the y and z axis respectively. The displacements of p-type functions can be achieved in the same manner, by the combination of d-type functions with the p-type functions, for an example, shown in Figure 3.2 is the combination of d_{xz} with p_z which results in the displacement of charge along the x axis. In a similar manner, f-type functions effect the charge distribution of valence d-type functions. From the above discussion, a basis set that incorporates functions of higher angular quantum number than are needed by the atom in its electronic ground state is referred to as a polarization basis set; they provide for the displacement of electronic charge away from the nuclear centres, or in other words, charge polarization. A double-zeta basis set with d-type polarization functions on heavy atoms (i.e. C, N, O, ... etc.) is represented in Gaussian as 6-31G*. A double-zeta basis set with d-type polarization functions on heavy atoms and p-type polarizations functions added to hydrogens is represented by 6-31G**[16].

Included in this work are *ab-initio* calculations that
are performed on the perchlorate anion (ClO_4^-).
Calculations involving anions are more difficult to deal
with and are not adequately dealt with the basis sets
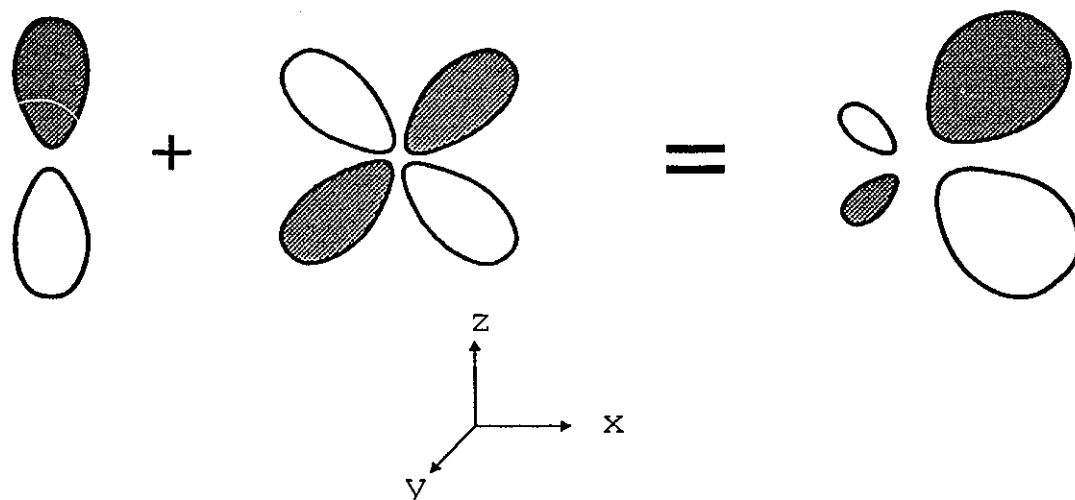
Figure 3.2 The combination of a *p*-type function with a
d-type function.

discussed so far [17]. Considering that the electron
affinities of the corresponding neutral molecules are
typically low, the extra electron is weakly bound[18]. To
overcome this problem, one or more sets of highly diffuse
functions is included in the basis set. **The double-zeta
basis function with diffuse functions is represented in
Gaussian 92 by 6-31+G[19] and is able to properly describe the**
long range behavior of molecular orbitals with energies
close to the ionization limit.

The largest basis sets used in this work are the triple-zeta basis sets 6-311G*, 6-311G**, 6-311+G*, 6-311+G**[20] where the valence region is split into three parts represented by three, one and one primitives. The triple-zeta basis set increases the flexibility of the representation and improve the description of the outer valence region.

Hartree-Fock methods do not adequately account for the correlation of electron motion. The most economical methods for electron correlation are based on the perturbation theory of Møller and Plesset[21].

3.4 GEOMETRY OPTIMIZATION

To perform geometry optimizations, the size of the molecule and properties to be investigated as well as the available computational resources need to be considered in determining the level of theory to be applied. Since the goal of all of the calculations performed in this work was a complete understanding of the molecular structure. A complete optimization of all geometrical parameters was carried out. These parameters are: bond lengths, bond angles, and dihedral angles. A typical calculation is started with the position or coordinates for each of the atoms in the system that must be decided upon. The starting geometry of the molecule must be carefully chosen in order

to avoid unwanted transition structures or a geometry that will not optimize and would essentially force the calculation into an endless cycle.

The type of *ab initio* calculation in Gaussian 92 is controlled by specific keywords[22]. For instance, in a geometry optimization, the keyword "opt", which is short for a full optimization, is used, this is followed by the level of theory that the calculation is to be performed at (i.e. RHF/6-31G opt is asking the program to perform a full optimization using the 6-31G basis set at the restricted Hartree-Fock level of theory). Next, the title for the job is supplied, the molecular charge, and the required multiplicity (singlet, triplet, etc.). The geometry is specified in the form of a z-matrix using internal coordinates which specifies atoms, bond lengths, bond angles, and dihedral angles. The z-matrix is simply a geometrical device used to define the position of the atoms from which the program finds the Cartesian coordinates upon starting the calculation[23]. Optimization is often carried out for a molecule constrained to a specific symmetry. This is accomplished by forcing two or more parameters to optimize at the same value. For example, the first calculation that is performed is the geometry optimization of the perchlorate anion. The anion is known to have a tetrahedral structure[24] so that the four bond lengths can be

optimized together and all bond angles and dihedral angles can be held constant to retain the geometry. A typical input file has the form:

RHF/6-31G* opt

Perchlorate ion.

```
-1   1
O
Cl   1   r1
O    2   r1   1   109.4712206
O    2   r1   1   109.4712206   3   -120.0
O    2   r1   1   109.4712206   3    120.0

r1=1.877
```

refer to appendix I for an example of the Gaussian92 output for this calculation.

3.5 VIBRATIONAL ANALYSIS

The total energy of a molecule comprising N atoms near its equilibrium structure can be written as:

$$E=T+V=\frac{1}{2}\sum_{i=1}^{3N}\dot{q}_i^2+V_{eq}+\frac{1}{2}\sum_{i=1}^{3N}\sum_{j=1}^{3N}(\frac{\partial^2 V}{\partial q_i\partial q_j})_{eq}q_iq_j. \tag{3.53}$$

Where the mass-weighted Cartesian displacements, q_i, are defined in terms of the locations x_i of the nuclei relative to their equilibrium positions $x_{i,eq}$ and their masses M_i:

$$q_i=M_i^{\frac{1}{2}}(x_i-x_{i,eq}). \tag{3.54}$$

Where V_{eq} is the potential energy at the equilibrium nuclear

position. The expansion of the vibrational energy in terms of a power series is truncated at the second order[25]. The classical mechanical equations then become:

$$q^{..} = -\sum_{i=1}^{3N} f_{ij}q_i \quad j=1,2,...,3N.$$ (3.55)

Where f_{ij} is termed the quadratic force constants and are the second derivatives of the potential energy with respect to mass-weighted Cartesian displacements, evaluated at the equilibrium positions nuclear configuration, shown as:

$$f_{ij} = (\frac{\partial^2 V}{\partial q_i \partial q_j})_{eq}.$$ (3.56)

the force constants can be evaluated by numerical second differentiation,

$$\frac{\partial^2 V}{\partial q_i \partial q_j} \approx \frac{\Delta(\Delta V)}{\Delta q_i \Delta q_j}$$ (3.57)

by numerical first differentiation of analytical first derivatives,

$$\frac{\partial^2 V}{\partial q_i \partial q_j} \approx \frac{\Delta(\partial V/\partial q_j)}{\Delta q_i}$$ (3.58)

or by direct analytical second differentiation. The choice

of procedure depends upon the quantum mechanical model used.

In the present work Cartesian force constants were computed analytically at each stationary point and transformed to valence force constants; harmonic vibrational frequencies were found by diagonalization of the matrix of mass-weighted Cartesian force constants from which residual translational and rotational contributions had first been excluded[26]. Symmetry constraints were applied for each coordination geometry, forcing the structure to optimize within the desired point group symmetry, which also serves to minimize the computational time to perform the calculations. All calculations were performed on an IBM RISC 6000 computer.

Normal coordinate representation is done using our program (Ptolemy). I developed a program that would read in the ground state coordinates and then subtract the relative displacements for each vibration from the ground state coordinates whereupon the program would display them graphically to make the assignment of the vibrations easier. The program was written in Pascal computer language and the code is listed in appendix II.

3.6 COMPUTERS AND COMPUTER TIMES

Actually performing *ab initio* calculations depends highly on computer resources. The size of molecule that can

be studied and the level of theory that can be realistically
applied is directly related to the speed of the computer and
the disk space. An IBM RISC6000 located at the General
Motors tech center in Warren MI was used to perform most of
the *ab initio* calculations. Some of the smaller calculations
were performed on an IBM compatible PC. Gaussian 92 jobs
report the CPU time used upon completion of a calculation.
Table 3.1 gives a summary of the calculation times for the
perchlorate anion (ClO_4^-) using various basis sets.

Table 3.1 Computer Resource Usage for the Perchlorate Anion
geometry optimization and Various Basis Sets.

Basis Set	# Basis Functions	IBM PC	IBM RISC6000
HF/3-21G	45	430 s	—
HF/6-31G	60	1980 s	—
HF/6-31G*	75	9180 s	130 s
HF/6-31+G*	95	—	297 s
HF/6-311G*	90	—	318 s
HF/6-311+G*	110	—	545 s
MP2/6-31G*	75	—	720 s
MP2/6-31+G*	95	—	2220 s
MP2/6-311G*	90	—	2224 s
MP2/6-311+G*	110	—	4140 s

REFERENCES

1. Levine, I. N., *Quantum Chemistry*, 3rd ed., Allyn and
    Bacon, Boston, **1983**.

2. Hehre, W. J.; Radom, L.; Schleyer, P. v. R.; Pople, J.
    A. *Ab Initio Molecular Orbital Theory*, John Wiley and
    Sons, **1986**.

3. Born, M.; Oppenheimer, J. R., *Ann. Physik.*, **1927, 84,**
    457.

4. Pauli, W., *Z. Physik*, **1925,** *31,* 765.

5. Slater, J. C., *Phys. Rev.*, **1929,** *34,* 1293.

6. R. Poirier, R. Kari, I. G. Csizmadia, *Handbook of
    Gaussian Basis Sets*, Elsevier, **1985.**

7. Stewart, R. F., *J. Chem. Phys.*, **1969,** *52,* 431.

8. I. N. Levine, *Quantum Mechanics Volume 1: Quantum
    Mechanics and Electronic Structure*, Allyn and Bacon,
    1970, pp184-189.

9. Roothaan, C. C. J. *Rev. Mod. Phys.* **1951** *23,* 69.

10. Hall, G. G. *Proc. Roy. Soc. (London)*, **1951,** *A205,* 541.

11. Gaussian 92, Revision G.1, M. J. Frisch, G. W. Truck,
    M. Head-Gordon, P. M. W. Gill, M. W. Wong, J. B.
    Forseman, B. G. Johnson, H. B. Schegel, M. A. Robb, E.
    S. Replogle, R. Gomperts, J. L. Martin, D. J. Fox, D.
    J. Defrees, J. Baker, J. J. P. Stewart, and J. A.
    Pople, Gaussian, Inc., Pittsburg PA, 1992.

12. Schlegel, H. B. *J. Comput. Chem.* **1982,** *3,* 214.

13. Binkley, J. S.; Pople, J. A.; Hehre, W. J. *J. Am. Chem.
    Soc.* **1980,** *102,* 939.

14. Dill, J. D.; Pople, J. A. *J. Am. Chem.* **1975,** *62,* 2921.

15. Warren J. Hehre, Leo Radom, Paul v.R. Schleyer, John A.
    Pople, *Ab Initio Molecular Orbital Theory*, John Wiley
    and Sons, **1986,** pp81.

16. Binkley, J. S.; Pople, J. A. *J. Chem. Phys.* **1977,** *66,*
    879.

17. Simons, J. *Ann. Rev. Phys. Chem.,* **1977,** *28,* 15.

18. B. K. Janousek and J. I. Brauman in *Gas Phase Ion Chemistry,* M. T. Bowers, ed., Academic Press, New York, **1979,** vol. 2 p. 53.

19. Clark, T.; Chandrasekhar, J.; Spitznagel, G. W.; Schleyer, P. v. R *J. Comput. Chem.* **1983,** *4,* 294.

20. Binkley, J. S.; Pople, J. A. *J. Chem. Phys.* **1977,** *66,* 879.

21. Krishnan, R.; Pople, J. A. *Int. J. Quantum Chem. Symp.* 1980, *14,* 91.

22. Foresman, J. B.; Frisch, A. *Exploring Chemistry with Electronic Structure Methods: A Guide to Using Gaussian* Gaussian Inc., Pittsburgh, PA, **1993,** p 111.

23. T. Clark, *A Handbook of Computational Chemistry,* John Wiley and Sons, **1985,** pp 102-4.

24. R. J. Gillespie, *Molecular Geometry,* Van Nostrand Reinhold company, London, **1972.**

25. Warren J. Hehre, Leo Radom, Paul v.R. Schleyer, John A. Pople, *Ab Initio Molecular Orbital Theory,* John Wiley and Sons, **1986.**

26. Williams, I. H. *J. Mol. Struct.* **1983,** *94,* 275.

CHAPTER 4

LITHIUM PERCHLORATE, STRUCTURAL AND SPECTRAL

CHANGES ASSOCIATED WITH ION PAIRING

4.1 INTRODUCTION

The first component to be studied is the lithium perchlorate salt that is used in all the electrolyte solutions discussed in this work. In this chapter experimental results and theoretical calculations are correlated to characterize the lithium perchlorate salt used in all of the solutions. The anion ClO_4^- and the ion pair of $Li^+ClO_4^-$ have been studied by *Ab Initio* quantum chemical methods. Optimized geometries for monodentate, bidentate, and tridentate structures were determined up to the MP2/6-311+G* level of theory. Vibrational frequencies were determined for the ClO_4^- anion and the $Li^+ClO_4^-$ ion-pair up to the HF/6-311+G* level of theory. Comparisons are made with experimental Raman spectra of electrolyte solutions.

The electrolyte solution performance depends upon the mobility of ions. A central factor affecting the mobility of these ions and thereby the conductivity of the solution, is the formation of ion-pairs and higher aggregates. Therefore, the examination of the likelihood of occurrence and the experimental detection of ion-pairs in nonaqueous electrolytes is of great interest. Numerous reports have already illustrated the role of vibrational spectroscopy as a tool to probe solvent-salt interactions in electrolytes[1-4]. The formation of $Li^+ClO_4^-$ ion-pairs and aggregates has

been associated in the infrared and Raman spectra with frequency shifts and splitting of the vibrational bands of the conjugated anion in the lithium salt.

There are numerous reports on the coordination geometry of Li^+ complexes. Insight into coordination of the litium cations can be gained from macrocylic complexes[5]. Small preorganized cavity calixarenes are shown to bind with the lithium cation in a tetrahedral geometry to oxygens with a $O-Li^+$ bond length of 1.61 and 1.71 Å[6,7,8]. There is also evidence that Li^+ can coordinate to three oxygens in a trigonal planar geometry in highly preorganized chromogenic cryptahemispherands[9]. A bidentate geometry has been shown to exist in the lithium triflate ion-pair[10] with Li^+-O bond distance of 1.63 Å.

Frequency shifts for the perchlorate anion are observed in the spectra of nonaqueous electrolytes and have been attributed to the formation of ion-pairs, however, the structure of the resulting complex is unclear. The object of this chapter is to determine the formation of ion-pair $Li^+ClO_4^-$ that are energetically possible using *ab initio* methods and establish the most stable structure of the ion-pair. Further, using the energetically favourable structure, the vibrational spectra and the frequency shifts for the vibrations of the perchlorate anion in different

coordinating environments are discussed. The inelastic

scattering of light (Raman spectroscopy) is well suited for

the study of the perchlorate anion, the anion has T_d point

group symmetry and all of the harmonic vibrational modes are

Raman active. Whereas, only the degenerate modes are

infrared active and difficult to obtain information from in

nonaqueous electrolyte solutions[1,2]. The results from the

calculations will thus be compared with experimental results

obtained from Raman spectroscopy of an electrolyte solution

made up of a solvent mixture of diethylene carbonate and

ethylene carbonate.

4.2 METHODS

Ab initio self consistent field (SCF) molecular orbital

calculations were performed with the program gaussian92[11].

Full geometry optimization was performed according to

Schegel's method[12]. Employing analytical gradients, to

better than 10^{-3} Å for bond lengths and 10^{-2} for angles. The

basis sets utilized were 3-21G[13] where each inner-shell

atomic orbital is represented by a single function which in

turn are made up of three Gaussian primitives and the

valence-shell orbitals are made up of two contracted and one

diffuse basis functions. The double-zeta basis set, 6-31G[14]

where each inner-shell atomic orbital is represented by a

single function made up of six Gaussian primitives and the
valence-shell orbitals are made up three contracted and one
diffuse basis function. The double-zeta basis function with
diffuse functions 6-31±G[15] and/or polarization functions[16] 6-
31G* and 6-31+G*. The triple-zeta basis sets 6-311G* and 6-
311+G*[17] where the valence region is split into three parts
represented by three, one and one primitives. Geometry was
optimized at the Hartree-Fock level as well as Møller-
Plesset perturbation theory[18] at the second-order MP2 (full)
level, with all the orbitals active. Cartesian force
constants were computed analytically at each stationary
point and transformed to valence force constants; harmonic
vibrational frequencies were found by diagonalization of the
matrix of mass-weighted Cartesian force constants from which
residual translational and rotational contributions had
first been excluded[19]. Symmetry constraints were applied for
each coordination geometry, forcing the structure to
optimize in the desired geometry, which also serves to
minimize the computational time to perform the calculations.
All calculation were performed on an IBM RISC 6000.

4.3 PERCHLORATE ANION GEOMETRY

The first step in this chapter was to analyse the
effect of basis sets on the results of the calculations. The

results for the optimized Cl-O bond lengths and total

energies from SCF MO calculations for the free anion having

tetrahedral geometry using various basis sets are given in

Table 4.1. For the free anion, the basis sets 3-21G, 6-31G,

and the diffuse-function 6-31+G give an unrealistic Cl-O

bond length. The resulting values of 1.851Å, 1.877Å, and

1.893Å for these basis sets respectively are obviously too

large compared to known Cl-O bond length values considering

that experimental values are typically ≈1.47Å[20]. With the

addition of the polarization function (6-31G*, 6-31+G*, 6-

311G*, and 6-311+G*), which essentially introduces d-type

function added to the heavy atoms[21], gave results that were

in closer agreement to the known experimental values. This

produces the reasonable bond lengths of 1.450Å for 6-31G*.

The addition of diffuse-function 6-31+G* lengthens the Cl-O

bond length to 1.452Å. Applying the larger basis sets of

triple-zeta, 6-311G* and 6-311+G* gave bond lengths 1.448Å

and 1.446Å respectively. The geometry was also optimized

using with electron correlation using Møller-Plesset

perturbation theory at the second-order MP2 level. This

resulted in bond lengths of 1.483Å,

Table 4.1 Optimized Bond Lengths (angstroms) and Energies (kJ mol⁻¹) for Tetrahedral ClO_4^- and Li^+

Basis Set	Li^+	ClO_4^-	Cl-O
HF/3-21G	-18866.123	-1980731.5	1.851
HF/6-31G	-18993.135	-1990540.8	1.877
HF/6-31+G	-18993.148	-1990625.2	1.893
HF/6-31G*	-18993.283	-1991271.8	1.450
HF/6-31+G*	-18993.283	-1991310.0	1.452
HF/6-311G*	-18994.077	-1991511.1	1.448
HF/6-311+G*	-18994.079	-1991544.4	1.446
MP2/6-31G*	-18993.358	-1991261.4	1.483
MP2/6-31+G*	-18993.283	-1991297.2	1.489
MP2/6-311G*	-18994.077	-1991503.7	1.473
	-18994.079	-1991535.9	MP2/6-311+G*
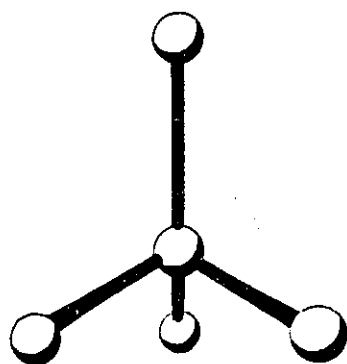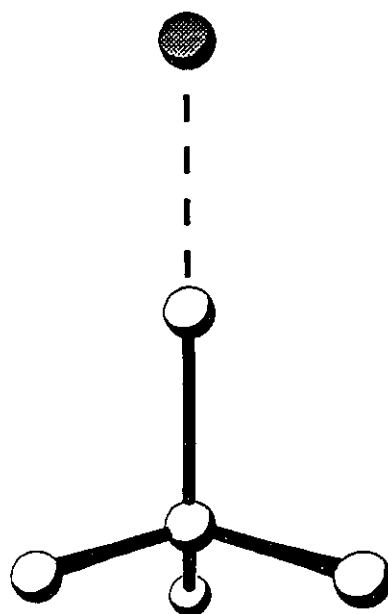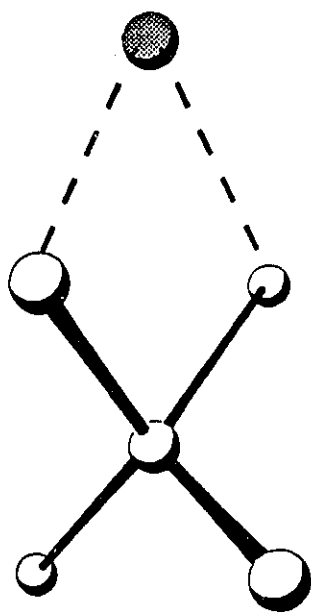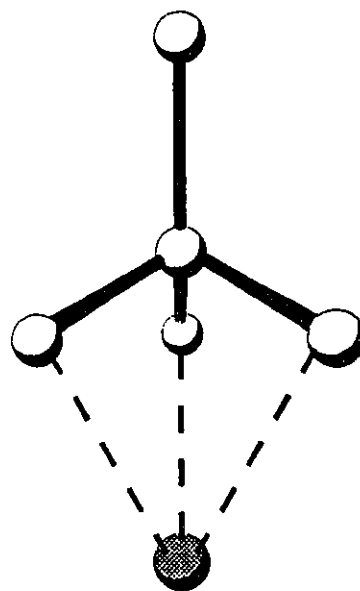
Figure 4.1 Coordination Geometries for $Li^+ClO_4^-$ Ion-Pairs: Monodentate, Bidentate, and Tridentate

Table 4.2 Optimized Geometry for the Monodentate Li⁺ClO₄⁻ ion-pair (O is uncoordinated oxygen and O' is coordinated)

	Li-O'	Cl-O'	Cl-O	O-Cl-O'
HF/3-21G	1.6015	1.6667	1.8999	105.6775
HF/6-31G	1.6653	1.6902	1.9569	105.1504
HF/6-31+G	1.6559	1.6940	1.9712	105.2945
HF/6-31G*	1.6987	1.4978	1.4294	106.6821
HF/6-31+G*	1.6807	1.4953	1.4303	106.7884
HF/6-311G*	1.6702	1.4896	1.4221	106.7136
HF/6-311+G*	1.6705	1.4894	1.4234	106.7684
MP2/6-31G*	1.6936	1.5546	1.4599	106.1205
MP2/6-31+G*	1.6410	1.5534	1.4649	106.2681
MP2/6-311G*	1.6652	1.5423	1.4478	106.1328
MP2/6-311+G*	1.6710	1.5434	1.4511	106.2109

Table 4.3 Optimized Geometry for the Bidentate Li⁺ClO₄⁻ ion-pair (O is uncoordinated oxygen and O' is coordinated)

	Li-O'	Cl-O'	Cl-O	O'-Cl-O'	O-Cl-O
HF/3-21G	1.847	1.836	2.071	93.72	125.82
HF/6-31G	1.911	1.847	2.060	93.64	123.31
HF/6-31+G	1.905	1.847	2.050	93.56	123.24
HF/6-31G*	1.897	1.486	1.421	101.59	113.15
HF/6-31+G*	1.885	1.485	1.422	101.49	112.91
HF/6-311G*	1.883	1.481	1.413	101.32	113.25
HF/6-311+G*	1.881	1.482	1.413	101.41	113.10
MP2/6-31G*	1.909	1.529	1.453	101.91	113.48
MP2/6-31+G*	1.910	1.531	1.456	101.81	113.16
MP2/6-311G*	1.879	1.519	1.439	101.82	113.70
MP2/6-311+G*	1.884	1.522	1.441	101.87	113.41

Table 4.4 Optimized Geometry for the tridentate Li$^+$ClO$_4^-$ ion-pair (O is uncoordinated oxygen and O$'$ is coordinated)

	Li-O$'$	Cl-O$'$	Cl-O	O$'$-Cl-O
HF/3-21G	1.962	1.929	2.435	126.13
HF/6-31G	2.041	1.931	2.490	125.03
HF/6-31+G	2.053	1.921	2.351	124.47
HF/6-31G*	2.160	1.466	1.414	113.76
HF/6-31+G*	2.278	1.465	1.414	113.76
HF/6-311G*	2.268	1.461	1.405	113.84
HF/6-311+G*	2.268	1.460	1.405	113.83
MP2/6-31G*	2.282	1.503	1.447	113.54
MP2/6-31+G*	2.278	1.465	1.414	113.76
MP2/6-311G*	2.268	1.461	1.405	113.84
MP2/6-311+G*	2.268	1.460	1.405	113.83

1.489Å, 1.473Å, and 1.476Å for MP2/6-31G*, MP2/6-31+G*, MP2/6-311G*, and MP2/6-311+G* respectively. From these results, it can be seen that SCF MO calculations at HF/6-31G* provide an adequate geometric optimization of the model systems.

4.4 ION-PAIR GEOMETRIES AND ENERGIES

In analysing ion-pair geometries, it was of interest to follow trends using different basis sets in the calculations. Three different coordination geometries for

$Li^+ClO_4^-$ are considered: monodentate **1**, bidentate **2**, and tridentate **3** as shown in Figure 4.1. fully optimized geometries for all of these configurations are given in Tables 4.2., 4.3, and 4.4. Total energies calculated for the three geometries at the various basis sets are presented in Table 4.5, along with relative energies for the binding of Li^+ to ClO_4^- for the monodentate, bidentate, and tridentate geometries.

The Hartree Fock basis sets 3-21G and 6-31G predicts that the tridentate geometry is the most favourable. Calculated vibrational frequencies at each stationary point resulted in one imaginary frequency in each of the monodentate and bidentate geometries suggesting that these are transition structures and not minimum energy conformations. Where the tridentate geometry is slightly less favourable than bidentate. With the addition of the diffuse function to the double zeta basis set (HF/6-31+G), the bidentate structure becomes slightly more stable than the tridentate structure. Molecules that are poorly represented by normal valence structures are greatly affect by the addition of polarization functions to the basis sets[22]. With the addition of the polarization function (HF/6-31G*), the bidentate geometry energy becomes significantly lower relative to both the monodentate and

Table 4.5 Total Energies and Relative Energies† (kJ mol⁻¹) for Optimized Geometries of Li⁺ClO₄⁻ Ion Pairs

Basis Set	1	2	3
HF/3-21G	-2000196.5	-2000332.5	-2000368.9
	(-598.8)	(-734.8)	(-771.3)
HF/6-31G	-2010048.0	-2010142.7	-2010151.6
	(-514.1)	(-608.7)	(-617.6)
HF/6-31+G	-2010108.0	-2010189.5	-2010189.4
	(-489.6)	(-571.2)	(-571.1)
HF/6-31G*	-2010793.8	-2010862.0	-2010818.2
	(-528.8)	(-597.0)	(-553.1)
HF/6-31+G*	-2010818.6	-2010880.3	-2010835.1
	(-515.3)	(-577.0)	(-531.8)
HF/6-311G*	-2011039.9	-2011096.5	-2011050.3
	(-534.7)	(-591.3)	(-545.1)
HF/6-311+G*	-2011063.2	-2011116.1	-2011068.6
	(-524.7)	(-577.6)	(-530.1)
MP2/6-31G*	-2010779.2	-2010848.9	-2010805.3
	(-524.4)	(-594.2)	(-550.6)
MP2/6-31+G*	-2010801.9	-2010865.3	-2010820.5
	(-511.4)	(-574.8)	(-529.9)
MP2/6-311G*	-2011028.5	-2011086.8	-2011040.9
	(-530.7)	(-589.0)	(-543.1)
MP2/6-311+G*	-2011050.8	-2011105.4	-2011058.3
	(-520.8)	(-575.3)	(-528.3)

† Figure in parentheses is energy for structures relative to the total energy of the combined isolated Li⁺ and ClO₄⁻ species.

tridentate structures. Table 4.6 provides monodentate and

tridentate ion-pair energies relative to

Table 4.6 Energies (kJ mol^{-1}) of structures monodentate (1) and tridentate (3) Relative to bidentate (2) for Ion Pairs Li$^+$ClO$_4^-$.

Basis Set	ΔE (1)	ΔE (3)
HF/6-31G*	68.2	43.9
HF/6-31+G*	61.7	45.2
HF/6-311G*	56.6	46.2
HF/6-311+G*	52.9	47.5
MP2/6-31G*	69.8	43.6
MP2/6-31+G*	63.4	44.9
MP2/6-311G*	58.3	45.9
MP2/6-311+G*	54.5	47.0

the bidentate ion-pair using selected basis sets.

Vibrational frequency calculations show that each of the

bidentate and monodentate structures contain a single

imaginary frequency (bending modes of Cl-O-Li$^+$) which

indicates that the unfavourable monodentate and tridentate

structures are actually not minimum energy structures but

are in fact transition state structures. The bidentate

conformation remains the minimum energy structure when

calculating the energies using HF/6-31+G*, HF/6-311G*, and HF/6-311+G*.

Electron correlation was included by applying Møller-Plesset perturbation theory[23] at the second-order MP2 (full) level, with all the orbitals active in order to provide good estimates of relative energies. The full MP2 method confirms the HF/6-311+G* prediction that the bidentate structure is the most favourable. The energies for the monodentate and tridentate transition structures remain relatively close; ΔE = 7.5 kJ mol^{-1}. There is considerable difference between the bidentate and tridentate geometries (ΔE = 47.0 kJ mol^{-1}) and bidentate and monodenate geometries (ΔE = 54.5 kJ mol^{-1}) for the MP2/6-311+G* basis set. Evidence of the formation of ion-pairs comes from the comparison of the total combined energy of the uncoordinated Li^+ and ClO_4^- ions with the coordinated $Li^+ClO_4^-$ which works out to be -575.3 kJ mol^{-1} as predicted by MP2/6-311+G* this suggests that the formation of ion-pairs is energetically favourable. Explanation as to why the bidentate structure is favoured over the monodentate and tridentate structures can be obtained by examining the population analysis of the MP2/6-311+G* calculation. Electron density between lithium and oxygen (0.19) indicates the formation of a Li^+-O in the monodentate structure. In the bidentate structure, the formation of two Li^+ bonds are almost equal in strength to the monodentate single Li^+-O

bond as indicated by the electron density (0.17) for each Li$^+$-O atom pair. In the tridentate structure, the Li$^+$-O contains only a small amount of electron density (0.01) suggesting only a weak coordination between the lithium anion and the three oxygens.

The ion-pairing has the effect of lengthening the Cl-O' bond distance involving the coordinated O atoms. The amount to which the bond length changes is related to the geometry of the ion pair with the order mondentate>bidentate>tridentate. Conversely, the uncoordinated Cl-O bond length decreases in the order of geometries: monodentate>bidentate>tridentate. Similar trends have been recorded in BF$_4$$^-Li^+$[6] and LiCF$_3SO_3$[24]. This effect has been described as the hyperconjugation model[25,26], caused by partial transfer of electrons from the anion to Li$^+$ where the donation of lone pair electrons of oxygen p-orbitals to unoccupied s orbitals of Li$^+$. In this work, the hyperconjugation effect is thus reflected in the changes in the atomic charges on each atom upon formation of the Li$^+$ClO$_4$$^-$ complex as shown in Table 4.7.

The distance between Li$^+$-O' in the order of geometries is; monodentate>bidentate>monodentate. Experimental distances of 1.82 - 2.02 Å for the Li$^+$-O bond have been observed[18]. A more detailed comparison between the experimental and theoretical results would not prove

Table 4.7 Calculated Atomic Charges for the free anion ClO$_4^-$ and bidentate Li$^+$ClO$_4^-$ ion-pair.

ClO$_4^-$ Free Anion

	Cl	O	O'	Li
HF/3-21G	0.760659	-0.440164	-	-
HF/6-31G	0.878899	-0.469722	-	-
HF/6-31+G	0.212749	-0.303187	-	-
HF/6-31G*	1.855818	-0.713954	-	-
HF/6-31+G*	1.955535	-0.738884	-	-
HF/6-311G*	1.489126	-0.622282	-	-
HF/6-311+G*	0.730974	-0.432743	-	-
MP2/6-31G*	1.882701	-0.720675	-	-
MP2/6-31+G*	1.883632	-0.720908	-	-
MP2/6-311G*	1.471829	-0.617957	-	-
MP2/6-311+G*	0.717809	-0.429452	-	-

Li$^+$ClO$_4^-$ Bidentate

	Cl	O	O'	Li
HF/3-21G	0.529235	-0.162120	-0.413346	0.621697
HF/6-31G	0.700343	-0.216405	-0.536634	0.805735
HF/6-31+G	-0.041893	-0.059954	-0.286208	0.734216
HF/6-31G*	2.073618	-0.606901	-0.778494	0.697173
HF/6-31+G*	2.010190	-0.598930	-0.730517	0.648704
HF/6-311G*	1.527802	-0.505540	-0.645312	0.773904
HF/6-311+G*	0.576495	-0.231112	-0.376169	0.638065
MP2/6-31G*	2.063058	-0.609544	-0.769809	0.695648
MP2/6-31+G*	1.884039	-0.578590	-0.694273	0.661686
MP2/6-311G*	1.498678	-0.499895	-0.634771	0.770653
MP2/6-311+G*	0.541189	-0.226285	-0.354752	0.620886

meaningful, since the experimental distances refers to a solid crystal while the calculated distances are of a single ion-pair complex. Using the MP2/6-311+G* calculation results, a rough estimate can be made for the minimum distance at which Li^+ will have no effect on the ClO_4^- anion. Extrapolation of the MP2/6-311+G* results suggest the distance would converge upon the free anion value for a hypothetical cation of ionic radius of about 2.4 Å.

4.5 VIBRATIONAL FREQUENCIES AND INTENSITIES

As was the case with the calculated geometry, the calculated harmonic vibrational frequencies results from the first three basis sets 3-21G, 6-31G, and 6-31+G gave unrealistic results. With the addition of the polarization function, the values became reasonably close to experiment as shown in Table 4.8. The total irreducible representation of the perchlorate anion, ClO_4^-, with T_d point group symmetry has (3N-6) nine vibrational modes,

$$\Gamma = 1a_1 + 1e + 2f_2$$

a totally symmetric, a double degenerate and two triple degenerate vibrational modes. All of the vibrational modes are Raman active, while only the f_2 modes are IR active.

Experimental results from Raman spectroscopy give the observed vibrational frequencies: $\upsilon_1(a_1)=936$, $\upsilon_2(e)=462$, $\upsilon_3(t_2)=1113$, and $\upsilon_4(t_2)=629$ cm^{-1}. The normal coordinate analysis was performed at the Hartree-Fock level. The calculation at the Hartree-Fock level provided reliable vibrational results and not much would have been gained by employing electron correlation using Møller-Plesset perturbation theory. Application of electron correlation with MP2 would give a better prediction of the upper part of the potential curve which would not effect the fundamental vibrational frequencies. Unscaled frequencies from the normal coordinate calculation of ClO_4^- anion are given in Table 4.8.

The dramatic effect of the addition of the polarization functions is readily apparent when comparing with the experimental values. The HF/6-311+G* gives unscaled values that are the closest to experimental values: $\upsilon_1(a_1)=948$, $\upsilon_2(e)=479$, $\upsilon_3(t_2)=1127$, and $\upsilon_4(t_2)=666$ cm^{-1}, all of the vibrational modes predicted by HF/6-311+G* are slightly overestimated, and would be very similar if anharmonicity corrections were known. It should be pointed out that the basis set HF/6-31G* provides reasonable unscaled values for vibrational frequencies and could potentially be employed for a quick estimation of vibrational frequencies for similar species. The focus of this study is the theoretical

Table 4.8 Calculated vibrational frequencies (cm^{-1}) for the ClO$_4^-$ anion and bidentate Li$^+$ClO$_4^-$ ion-pair, experimental Raman vibrational frequencies are provide in parentheses

	6-31G*	6-31+G*	6-311G*	6-311+G*	Assignment
Anion ClO$_4^-$ (T$_d$)					
ν_1 (a$_1$)	975	957	943	948	sym. str
(936)					
ν_2 (e)	478	474	486	479	sym. str
(462)					
ν_3 (t)	1188	1148	1137	1127	asym. str
(1113)					
ν_4 (t)	668	659	671	666	asym. def
(629)					
Bidentate Li$^+$ClO$_4^-$ (C$_{2v}$)					
ν_1 (a$_1$)	1211	1236	1188	1183	ClO$_4$ antisym str
ν_2 (a$_1$)	947	964	932	932	ClO$_4$ sym str
ν_3 (a$_1$)	719	720	723	717	ClO$_4$ antisym def
ν_4 (a$_1$)	612	603	609	605	LiO sym str
ν_5 (a$_1$)	483	483	488	483	ClO$_4$ sym def
ν_6 (a$_2$)	445	447	454	450	ClO$_2$ twist
ν_7 (b$_1$)	1064	1068	1037	1032	ClO'$_2$ antisym str
ν_8 (b$_1$)	659	661	661	660	ClO$_2$ wag
ν_9 (b$_1$)	401	384	386	386	LiO'Cl bend
ν_{10} (b$_2$)	1290	1320	1267	1259	ClO$_2$ sym str
ν_{11} (b$_2$)	653	655	658	656	ClO$_2$ rock
ν_{12} (b$_2$)	151	148	157	160	LiO.Cl torsion

prediction of Raman spectra, the next step would be to compare the calculated intensities to experimental spectra. The calculated spectra in wavenumbers are plotted with relative intensities in the Y axis and energy on the X axis. An arbitrary band width was given to the lines to give the approximate appearance of broadening. The relative intensities and energies were taken from the HF/6-311+G* calculations. The resulting projected spectrum is shown in Figure 4.2. The experimental Raman spectra of the perchlorate anion and that of the nonaqueous solution are shown in Figure 4.3. Upon inspection, a reasonably good agreement between the experimental and theoretical Raman spectral features is achieved not only for the vibrational frequencies but also for Raman intensities by HF/6-311+G*. The average deviation from the experimental values works out to be an overestimate of 3%. In other words, the calculated vibrational modes can be scaled by a value of 0.97 in order to match the experimental values.

Correlation diagrams for splitting of the vibrational frequencies when going from the T_d point group symmetry of ClO_4^- to the coordinated bidentate C_{2v} point group and tridentate/monodentate C_{3v} point group symmetries are shown in Figure 4.4. The normal coordinate calculation for $Li^+ClO_4^-$ ion pairs indicate the bidentate geometry corresponds to a minimum energy structure, having all real vibrational

ClO_4^- Anion

Wavenumber (cm⁻¹)

$Li^+ClO_4^-$ Bidentate Ion-Pair

Wavenumber (cm⁻¹)
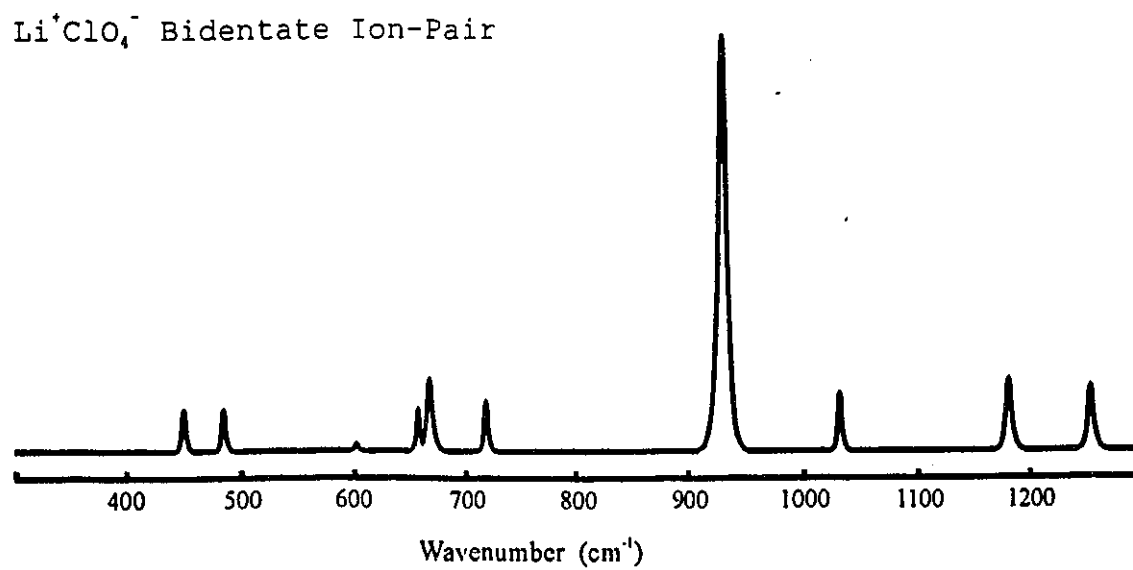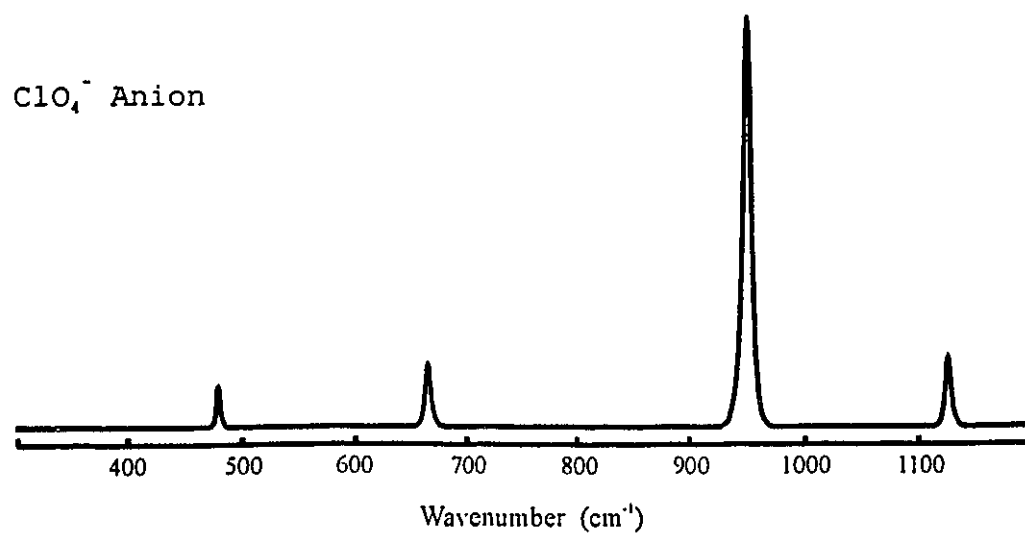
Figure 4.2 Predicted Raman Spectra of ClO_4^- Anion and $Li^+ClO_4^-$ Bidentate Ion-Pair Using HF/6-311+G*
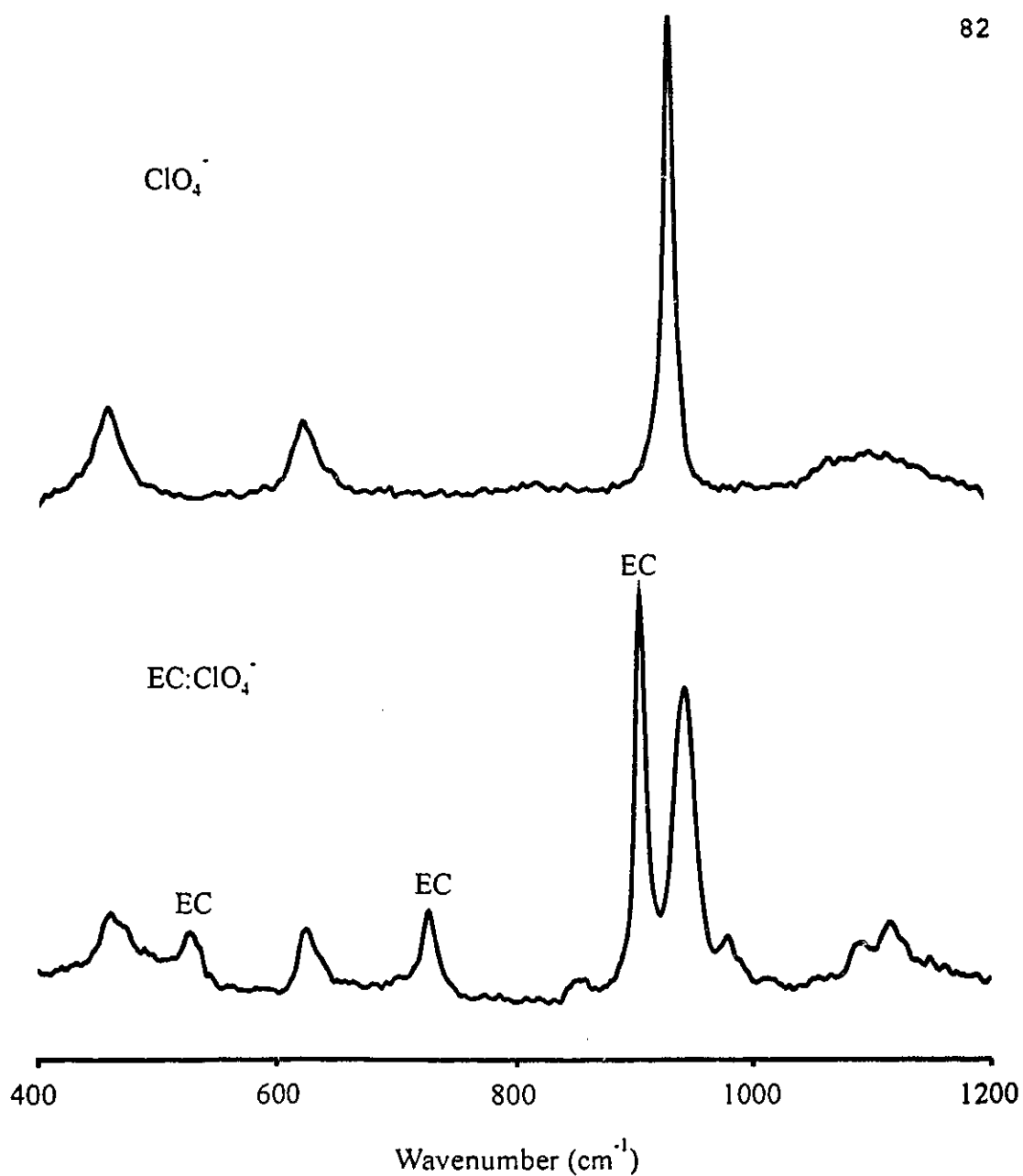
Figure 4.3 Experimental Raman Spectra of ClO_4^- (1.0 M LiClO$_4$ Aqueous Solution) and Raman Spectra of 6.6 M solution in Ethylene Carbonate/Diethyl Carbonate solvent Mixture in the 400-1200 cm^{-1} Spectral Region.

frequencies. The bidentate geometry has C_{2v} point group

symmetry. The 3N-6 = 12 fundamental vibrational modes

produce the total irreducible representation:

$$\Gamma = 5a_1 + 1a_2 + 3b_1 + 3b_2$$

The vibrational frequency used to monitor $Li^+ClO_4^-$ ion-

pairing in electrolyte solutions is the symmetric stretching

a_1 933 cm^{-1} band of the ClO_4^- anion. The HF/6-311+G* basis set

predicts a value of 948 cm^{-1}. With the coordination of

lithium in the bidentate geometry, the band shifts to 932

cm^{-1} a difference of 16 cm^{-1}. In the experimental Raman

spectrum, at high concentrations of lithium perchlorate the

bands that become visible are associated with the formation

of the ion-pair: 944 cm^{-1} and 938 cm^{-1}. The vibrational band

at 944 cm^{-1} will be the result of the formation of contact

ion-pair, while the band that appears at 938 cm^{-1} has been

assigned to the solvent shared ion-pairs[2]. As shown in

Figure 4.2, the results from the HF/6-311+G* frequency

calculation suggest a splitting pattern for the double

degenerate e and two triple degenerate f_2 vibrational modes.

Even though the vibrational modes of the perchlorate anion

are clearly seen in the Raman spectrum, the relative

intensity of the band associated with the ion-pair at 944

cm^{-1} and the 938 cm^{-1} compared to the intensity of the a_1 band
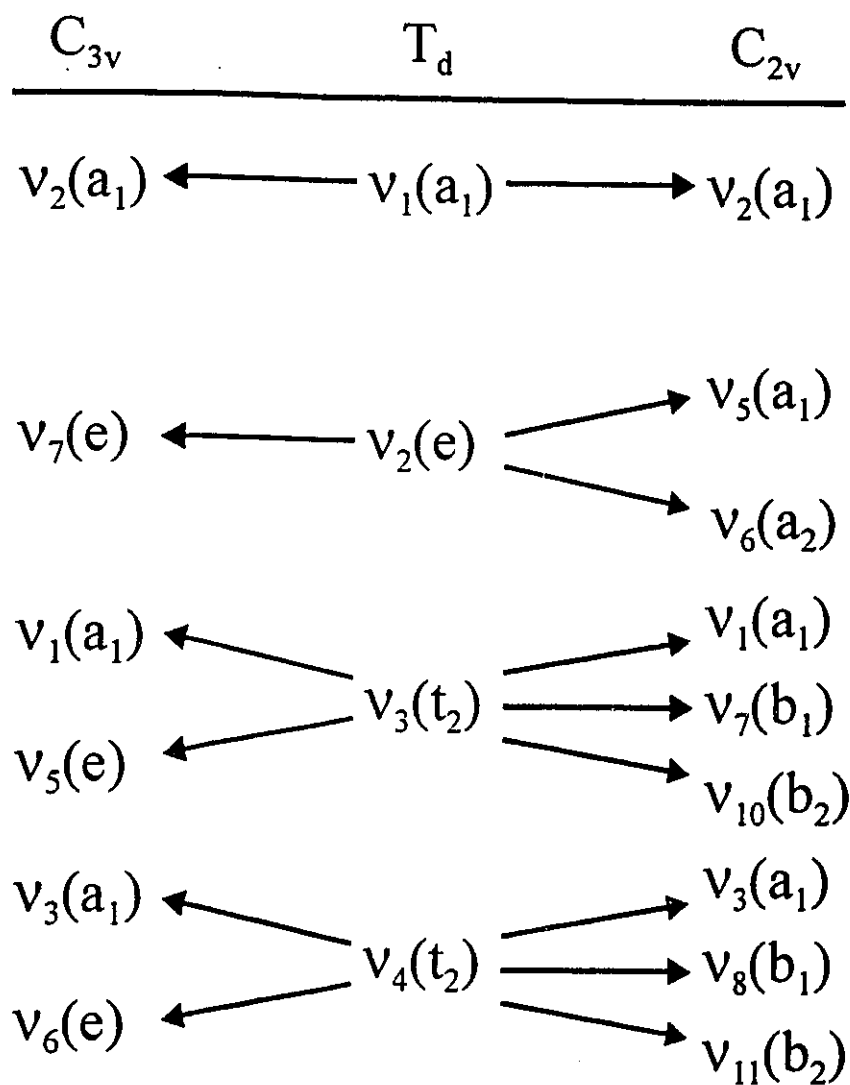
Figure 4.4 Correlation Diagram for the Splitting of the Vibrational Modes of ClO_4^-

1.

2.

350   450   550   650

Wavenumber (cm⁻¹)
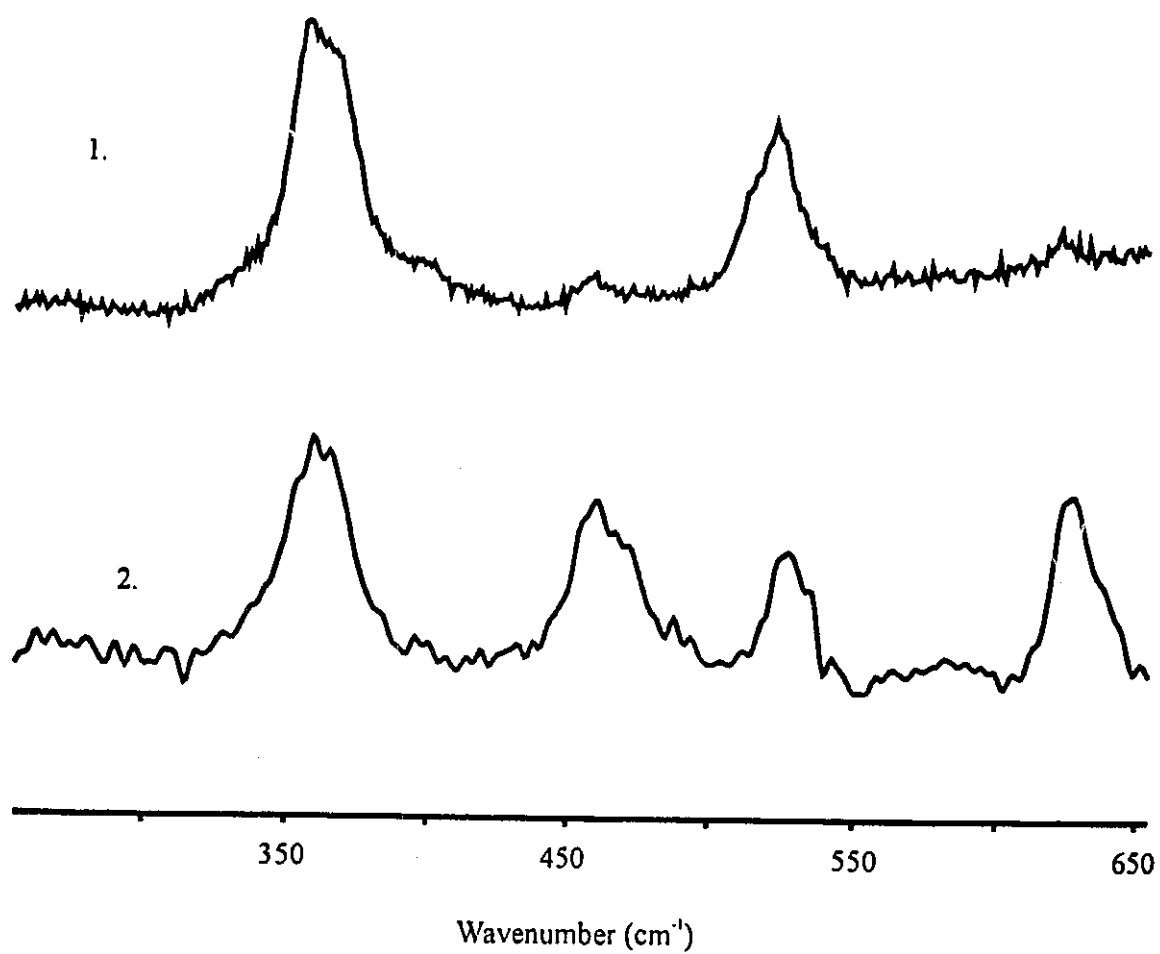
Figure 4.5 Raman spectra of binary solvent solutions
EC/DEC and LiClO₄ concentrations 1. 0.3 M;
2 6.6 M. over the region 300 cm⁻¹ to 700cm⁻¹

at 933 cm^{-1} suggests that the bands resulting from the splitting of the e and f_2 will be very weak and difficult to detect. Furthermore the high ionic strength of the solution will decrease the intensity of the inelastic light scattering. However, there is some evidence of the splitting predicted for the bidentate ion-pair in the 400-500 cm^{-1} region and the 600-700 cm^{-1} spectral region. In Figure 4.5, the Raman spectra for the 6.6 M lithium perchlorate in ethylene carbonate/diethyl carbonate solution mixture is given. The bands at 462 cm^{-1} and 629 cm^{-1} are broad and clearly indicate the presence of more than one component under the observed envelope. Two components under the 462 cm^{-1} envelope would support the C_{2v} symmetry of the ion-pair at higher concentration of electrolyte.

4.6 CONCLUSIONS

The trend in the formation of energetically favourable configurations in the $Li^+ClO_4^-$ ion-pair according to *ab-initio* calculations was studied. It was found that the bidentate structure having C_{2v} point group symmetry for the ion-pair is preferred over the monodentate and tridentate geometries. The vibrational spectrum and the Raman intensities were calculated using the Hartree-Fock Hamiltonian with basis sets containing polarization

functions 6-31G*, 6-31+G*, 6-311G*, and 6-311+G*. The vibrational spectrum is reasonably well predicted by all these basis sets where the HF/6-311+G* gives the most accurate results. The splitting of the e species by the correlation for descent in symmetry from T_d of the free anion to the C_{2v} of the bidentate ion-pair, was calculated to be 33 cm^{-1}. A broad band with at least two components was observed in the Raman spectrum of concentrated electrolyte that could be assigned to the a_1 and a_2 species of the bidentate C_{2v} ion-pair. The existence of ion-pairing has been established experimentally and further insight is obtained through quantum mechanical calculations. A complete modelling of the potential energy surface would be useful, however, the basic results presented here are not likely to be changed.

REFERENCES

1. Nazri, G. A.; MacArthur, D. M.; O'Gara, J. F.; Aroca, R. In *Materials Research Society Symposium Proceedings*; Nazri, G. A.; Shriver, D. F.; Huggins, R. A.; Balkanski, M., Eds.; Materials Research Society: Pittsburg, 1990; Vol. 210, p 163.

2. Battisti, D.; Nazri, G. A.; Klassen, B.; Aroca, R. *J. Phys. Chem.* **1993**, *97*, 5826.

3. Ratcliffe, C. I.; Irish, D. E. *Can. J. Chem.* **1984**, *62*, 1134.

4. Irish, D. E.; Ozeki, T. *Analytical Raman Spectroscopy*, Grasselli, J. G., Bulkin, B. J. ed. **1991**, *114*, 59.

5. Izatt, R. M.; Pawlak, K.; Bradshaw, J. S. *Chem. Rev.* **1995**, *95*, 2529.

6. Bencini, A.; Bianchi, A.; Bazzicalupi, C.; Ciampolini, M.; Dapporto, P.; Fusi, V.; Micheloni, M.; Nardi, N.; Paoli, P.; Valtancoli, B. *J. Chem. Soc., Perkin Trans. 2* **1993**, 115.

7. Bencini, A.; Bianchi, A.; Bazzicalupi, C.; Ciampolini, M.; Dapporto, P.; Fusi, V.; Micheloni, M.; Nardi, N.; Paoli, P.; Valtancoli, B. *J. Chem. Soc., Perkin Trans. 2* **1993**, 715.

8. Bencini, A.; Bianchi, A.; Bazzicalupi, C.; Ciampolini, M.; Dapporto, P.; Fusi, V.; Micheloni, M.; Nardi, N.; Paoli, P.; Valtancoli, B. *Inorg. Chem.* **1991**, *30*, 3687.

9. Zazulak, W.; Chapoteau, E.; Czech, B. P.; Kumar, A. *J. Org. Chem.* **1992**, *57*, 6720.

10. Gejji, S. P.; Hermansson, K.; Tegen, J.; Lindgren, J. *J. Phys. Chem.* **1993**, *97*, 11402.

11. Gaussian 92, Revision G.1, M. J. Frisch, G. W. Truck, M. Head-Gordon, P. M. W. Gill, M. W. Wong, J. B. Forseman, B. G. Johnson, H. B. Schegel, M. A. Robb, E. S. Replogle, R. Gomperts, J. L. Martin, D. J. Fox, D. J. Defrees, J. Baker, J. J. P. Stewart, and J. A. Pople, Gaussian, Inc., Pittsburg PA, 1992.

12. Schlegel, H. B. *J. Comput. Chem.* **1982**, *3*, 214.

13. Binkley, J. S.; Pople, J. A.; Hehre, W. J. *J. Am. Chem. Soc.* **1980**, *102*, 939.

14. Dill, J. D.; Pople, J. A. *J. Am. Chem.* **1975**, *62*, 2921.

15. Clark, T.; Chandrasekhar, J.; Spitznagel, G. W.; Schleyer, P. v. R *J. Comput. Chem.* **1983**, *4*, 294.

16. Binkley, J. S.; Pople, J. A. *J. Chem. Phys.* **1977**, *66*, 879.

17. Krishnan, R.; Binkley, J. S.; Pople, J. A. *J. Chem. Phys.* **1980**, *72*, 650.

18. Krishnan, R.; Pople, J. A. *Int. J. Quantum Chem. Symp.* **1980**, *14*, 91.

19. Williams, I. H. *Chem. Phys. Lett.* **1982**, *J. Mol. Struct.* **1983**, *94*, 275.

20. R. J. Gillespie, *Molecular Geometry*, Van Nostrand Reinhold Company ltd, 1972, p 161.

21. A. Szabo and N. S. Ostund, *Modern Quantum Chemistry*, McGraw-Hill, 1982, p 189.

22. Hehre, W. J. Radom, L.; Schleyer, P. v. R.; Pople, J. A. *Ab-initio Molecular Orbital Theory*, Wiley-International, New York, 1988, pp. 189.

23. Krishnan, R.; Pople, J. A. *Int. J. Quantum Chem. Symp*, **1980**, *14*, 91.

24. Gejji, S. P.; Hermansson, K.; Tegenfeldt, J.; Lindgren, J. *J. Phys. Chem.* **1993**, *97*, 11402.

25. Schleyer, P. von R.; Kos, A. J. *Tetrahedron*, **1983**, *39*, 1141.

26. Francisco, J. S.; William, I. H. *Chem. Phys.* **1985**, *98*, 105.

CHAPTER 5

STRUCTURE AND RAMAN SPECTRA OF CARBONATE SOLVENTS

5.1 INTRODUCTION

Components of a conducting electrolyte solution for a nonaqueous lithium battery consists of a lithium salt dissolved in an organic solvent, or a mixture of solvents, as in the case of binary electrolyte solutions. The salt component, lithium perchlorate for the binary nonaqueous electrolyte solutions, was discussed in detail in Chapter 4. This leads to the solvent components that were used in the makeup of the organic solutions. This chapter is devoted to the structure and characterization of the individual organic carbonates that are incorporated in these binary organic solvents. The problem is approached the same way as was the case for lithium perchlorate. Where the experimental results are used in conjunction with theoretical methods to develop a model to better understand the observed characteristics.

The four solvents that were used in the preparation of the binary organic electrolytes were: ethylene carbonate (EC), propylene carbonate (PC), diethyl carbonate (DEC), and dimethyl carbonate (DMC). Ethylene carbonate was incorporated in all of the solvents since it has the property of having the highest dielectric constant. However, EC has a melting point of 36°C and is therefore a solid at room temperature. The addition to EC of a solvent with low melting point, low viscosity, and relatively high dielectric

constant is required to take full advantage of the properties of EC while lowering the melting point for practical applications.

All of the solvents and resulting electrolyte solutions are studied by Raman spectroscopy. The vibrational bands are assigned using previously published spectra, our own experimental data, and *ab-initio* quantum chemical calculations. Knowledge of the vibrational modes associated with each solvent is important when determining the structure of the electrolyte solution upon the addition of lithium perchlorate salt.

5.2 METHODS

The Raman spectra of all four solvents where obtained by the procedure described in Chapter 2. Ethylene carbonate (EC), propylene carbonate (PC), diethyl carbonate (DEC), and dimethyl carbonate (DMC) were purchased from Fluka and treated according to the procedure described in Chapter 2.

As was the case with the lithium perchlorate salt calculations, all calculations were performed on an IBM RISC6000 computer. *Ab-initio* SCF molecular orbital calculations were performed with the program Gaussian92[1]. Full geometry optimization was performed according to Schegel's method[2]. Employing analytical gradients, to better

than 10^{-3} Å for bond lengths and 10^{-2} for angles. The basis set utilized used are as described in Chapter 4 with the following exceptions. The double-zeta basis functions with diffuse functions (6-31+G) and/or polarizations functions (6-31G*, 6-31+G*) for the perchlorate anion and ion-pair calculations meant that diffuse functions were added only to atomic numbers larger than hydrogen (anything larger than hydrogen are considered to be "heavy atoms") and d-orbitals, or polarization functions added to heavy atoms only. The solvents, EC, PC, DMC, and DEC all contain hydrogens, this requires that separate diffusion functions must be added for hydrogens along with p-orbitals or polarizations functions for all of the hydrogens in the solvent molecules. The basis functions for the triple-zeta basis functions would thus be 6-311G** and 6-311++G**.

5.3 ETHYLENE CARBONATE STRUCTURE AND VIBRATIONAL ASSIGNMENT

The structure of EC is depicted in Figure 5.1, a five membered ring containing two oxygen atoms with a carbonyl group located at the apex. A detailed description of the structure of EC is provided by QM SCF calculations. The resulting geometrical optimization is given in Table 5.1, and compares very well with the published crystal structure[3], where it was determined that the structure of EC

Table 5.1 Optimized geometry of ethylene carbonate using various basis sets.

	3-21G	6-31G	6-31+G	6-31G*
O1-C2	1.183	1.191	1.192	1.173
C2-O3	1.363	1.359	1.355	1.330
O3-C5	1.451	1.448	1.450	1.410
O1-C2-O3	125.446	125.631	125.430	124.896
C2-O3-C5	112.232	112.343	112.151	111.658

	6-31+G*	6-311G	6-311G**	6-311++G**
O1-C2	1.175	1.175	1.191	1.168
C2-O3	1.329	1.330	1.359	1.327
O3-C5	1.411	1.412	1.455	1.410
O1-C2-O3	124.887	124.887	125.631	124.831
C2-O3-C5	111.677	111.677	112.566	111.621

Ethylene carbonate
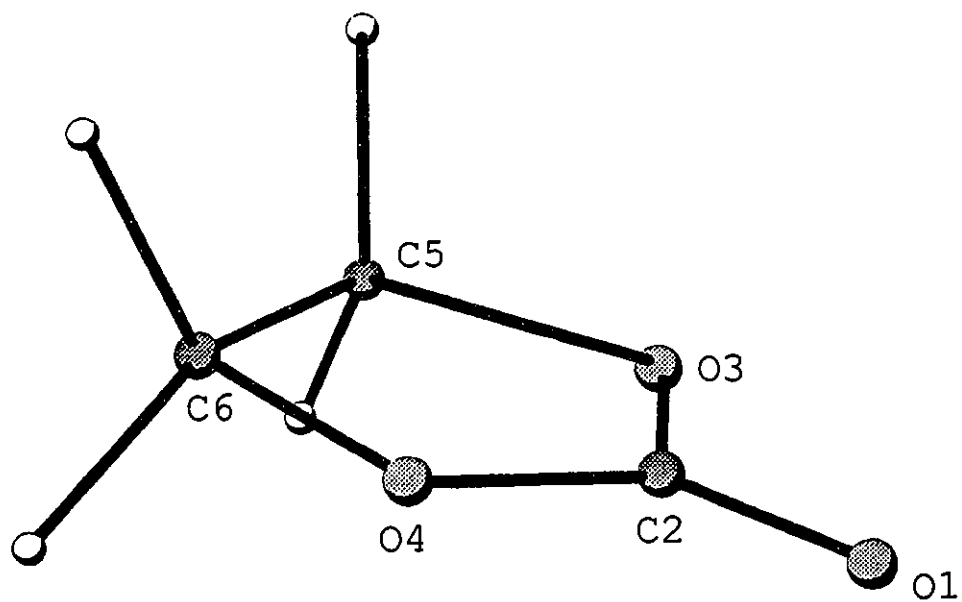
Propylene carbonate
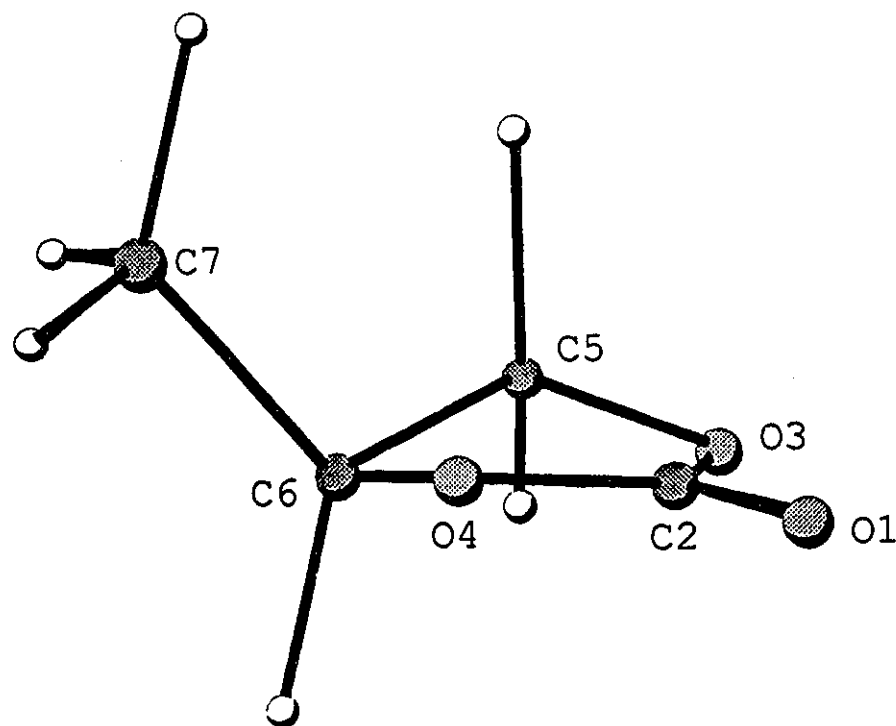
Figure 5.1 Optimized geometry of EC (top) and PC (bottom) using HF/6-311++G** basis set.

Pure EC
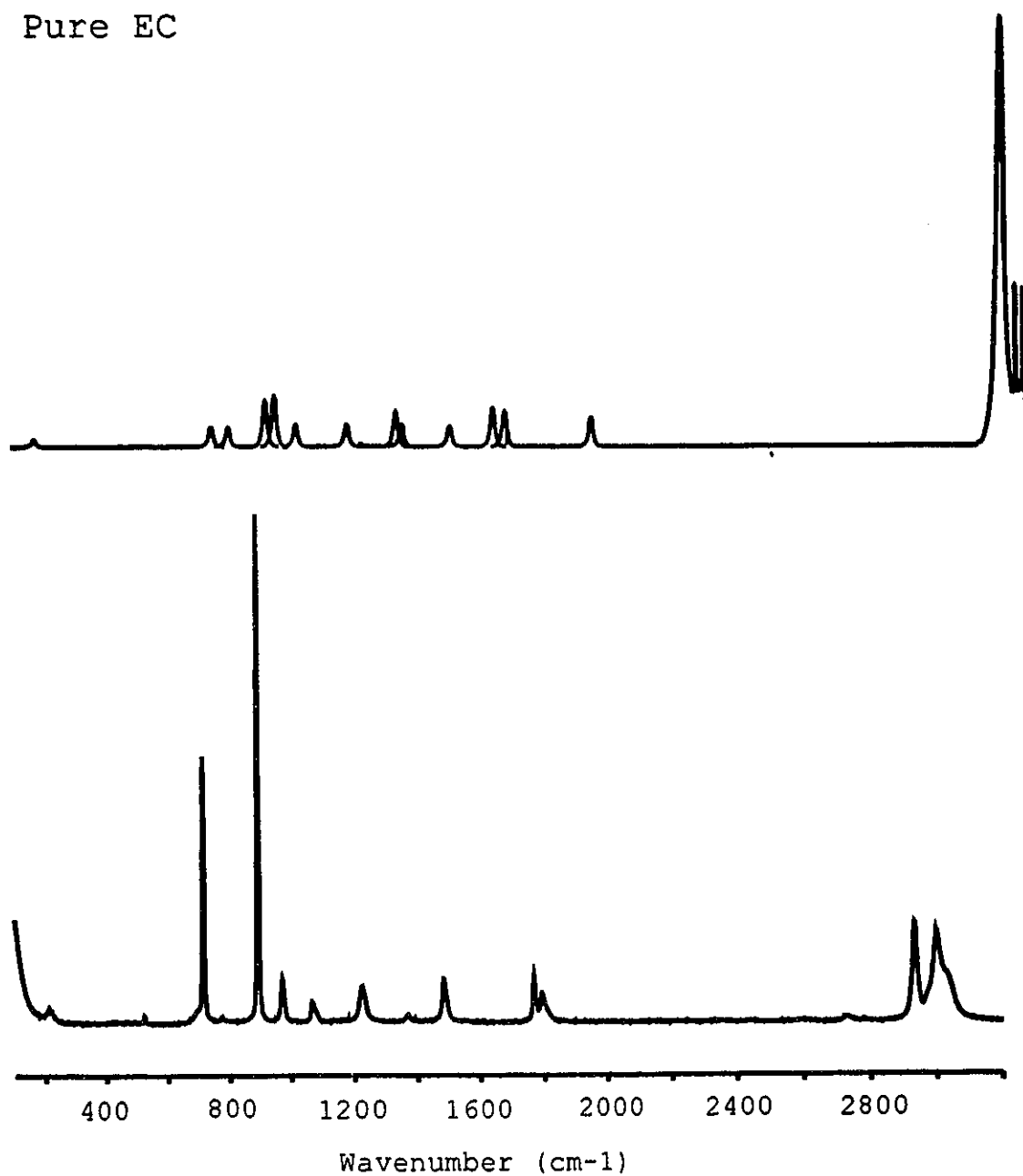
Figure 5.2: Raman spectrum of EC. Below, experimental and above, calculated using HF/6-311++G**

is not planar. However, the structure has been shown to be planar in a gaseous or liquid form[4]. Recent calculations using HF/D95V** basis set agrees with the conclusion that EC has a planar ring structure[5]. There have been multiple studies of EC, including FTIR and Raman spectroscopy[6,7]. However, a complete vibrational assignment using both spectroscopic and quantum chemical methods has not been performed. The Raman spectrum is given in Figure 5.2. The experimental spectra is supplemented by quantum chemical SCF calculation.

The symmetry of EC is assumed to be C_{2v} with the ring being planar. EC has 24 fundamental vibrational modes. According to group theory[5] the number of vibrations of each irreducible representation is:

$$\Gamma = 8a_1 + 4a_2 + 5b_1 + 7b_2$$

All of the vibrational modes are Raman active according to selection rules. The experimental and calculated harmonic vibrational frequency energies are listed in Table 5.2. There are four hydrogen-carbon (H-C) stretching modes observed between the 3028 cm^{-1} and 2931 cm^{-1} region. QM SCF calculations predict the H-C harmonic vibrations to occur from 3293 cm^{-1} to 3229 cm^{-1}. The carbonyl stretching mode shows up at 1794 cm^{-1} in the experimental Raman spectrum,

while the calculated value is 2062 cm^{-1} at the highest level
of theory used(6-311++G**). The carbon-carbon stretching,
carbon-oxygen, and various hydrogen-carbon bending modes
(scissor, twist, wag) show up between 1481 cm^{-1} and 970 cm^{-1}
in the experimental Raman spectrum. An intense mode occurs
at 891 cm^{-1}, which is attributed to the symmetric ring
breathing mode. The calculated value is 926 cm^{-1}(6-311G),
991 cm^{-1}(6-311G**), and 989 cm^{-1} (6-311++G**). The ring
breathing mode of EC is an important frequency for
understanding the effects of salt solvation and will be
dealt with in detail in the next chapter. The calculations
provide atom based Cartesian displacements which were
transferred to a dynamic display program mentioned in
chapter two (the original program code is provided in
appendix one) to graphically observe each normal mode on an
IBM PC. The graphic display for the atomic displacements
resulting from the ring breathing mode at 891 cm^{-1} is shown
in Figure 5.3. The remaining vibrational frequencies that
can be resolved experimentally range between 714 cm^{-1} and
214 cm^{-1} and are attributed to ring bending and carbonyl
bending modes.
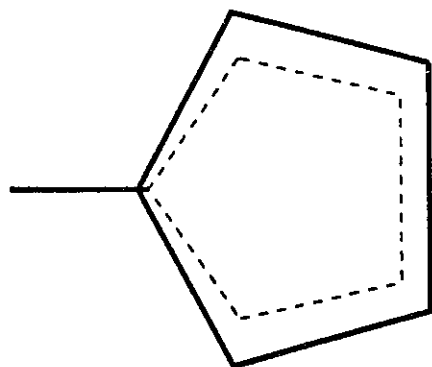
$\nu_7(a_1) = 891 \text{ cm}^{-1}$
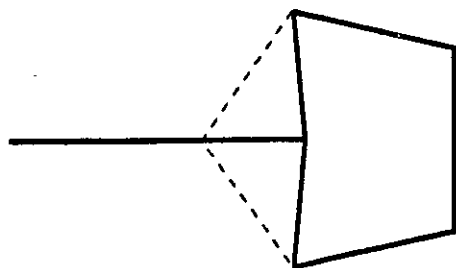
$\nu_2(a_2) = 1794 \text{ cm}^{-1}$

Figure 5.3 Calculated normal mode vibrations at 894, and 1794 cm-1. The dashed line represents the equilibrium geometry and the solid line represents calculated atomic displacements using HF/6–311++G** basis set.

Table 5.2 Calculated frequencies (cm^{-1}) for ethylene carbonate (Raman activity), and experimental Raman frequencies (infrared provided in parentheses).

Mode	6-311G	6-311G**	6-311++G**	Exp. Raman	Assign.'
$v_1(a_1)$	3266(186)	3239(195)	3239(208)	2931(s) (2926)	H-C str
$v_2(a_1)$	1962(9.0)	2083(7.2)	2062(11.7)	1794(m) (1797)	C=O str
$v_3(a_1)$	1690(6.0)	1673(4.1)	1672(2.8)	1481(m) (1486)	C5-C6 str. H_2-C sci
$v_4(a_1)$	1506(6.3)	1528(3.1)	1526(3.4)	(1392)	H_2C wag
$v_5(a_1)$	1188(3.7)	1272(2.3)	1268(2.2)	1080(sh) (1070)	C5-C6, O-C str
$v_6(a_1)$	1026(8.2)	1058(5.9)	1058(5.7)	970(m) (969)	C2-O_2, C5-C6 str
$v_7(a_1)$	926(19.3)	991(16.0)	989(17.8)	891(vs) (891)	ring breathing
$v_8(a_1)$	756(5.7)	789(3.9)	787(4.1)	695(sh)	i.p. ring dist
$v_9(a_2)$	3307(62.6)	3269(67.3)	3269(59.2)	3003(s)	H-C str
$v_{10}(a_2)$	1362(7.9)	1354(5.4)	1352(5.2)	1232(sh)	H_2-twist
$v_{11}(a_2)$	1248(0.2)	1260(0.0)	1260(0.0)		H_2-C rock, o.p. ring bend
$v_{12}(a_2)$	80(0.0)	117(0.0)	124(0.0)		ring tor
$v_{13}(b_1)$	3330(60.5)	3293(65.1)	3293(64.2)	3028(sh) (3040)	H-C str

$\nu_{14}(b_1)$	1335(12.0)	1351(8.3)	1348(6.9)	1220(m) (1218)	H_2-C rock
$\nu_{15}(b_1)$	1127(0.3)	917(0.2)	916(0.2)	(769)	H_2-C rock
$\nu_{16}(b_1)$	929(0.2)	879(1.2)	877(1.2)	714(s)	o.p. C=O-ring bend
$\nu_{17}(b_1)$	186(1.9)	187(3.4)	184(0.2)		o.p. ring bend
$\nu_{18}(b_2)$	3255(20.2)	3229(28.5)	3229(32.2)	2975(m) (2960)	H-C str
$\nu_{19}(b_2)$	1679(13.8)	1658(9.9)	1658(8.5)	(1472)	H_2-C sci
$\nu_{20}(b_2)$	1538(0.2)	1560(0.8)	1558(8.5)	(1419)	H_2-C wag, C2-O str
$\nu_{21}(b_2)$	1230(1.3)	1304(0.9)	1302(1.0)		H_2-C wag, C2-O str
$\nu_{22}(b_2)$	803(1.3)	1199(0.3)	1195(0.4)	1097(m)	O3-C5, O4-C6 str
$\nu_{23}(b_2)$	809(6.6)	828(4.1)	827(3.4)	(754)	i.p. ring dist
$\nu_{24}(b_2)$	542(0.7)	581(0.5)	578(0.4)		i.p. ring-C=O bend

†Abbreviations used: Exp. = experimental, Assign. = assignment, str = stretch, sci = scissor, i.p. = in plane, o.p. = out of plane, dist = distortion, and tor = torsion.

5.4 PROPYLENE CARBONATE STRUCTURE AND VIBRATIONAL ASSIGNMENT

The structure of PC is similar to that of EC, the difference being the addition of a methyl group in the place of one hydrogen on one of the carbon atoms as depicted in Figure 5.1. As mentioned above, EC had C_{2v} and symmetry constraints could be applied to the z-matrix simplifying the calculation and thus reducing the computation time. PC, on the other hand does not have any symmetry elements giving it C_1 symmetry which resulted in having to optimize all the parameters separately which increased the computation time considerably.

Optimized bond lengths, bond angles, and dihedral angles with various basis sets are given in Table 5.3. There are structural differences that are immediately apparent when compared to EC. The result of the additional methyl group causes the ring to twist out of the molecular plane by a certain amount compared to the hypothetical planar structure. The degree to which the ring twists is obtained by the amount the dihedral angle deviates from 180 degrees which is summarized in Table 5.3. The values for the ring twist range from 6.1° to 9.7°, at the highest level of theory used (HF/6-311++G**) the ring twist value is 8.0°. Therefore, the symmetry of PC is C_1 with the ring

Table 5.3 Optimized geometry of propylene carbonate using various basis sets

	3-21G	6-31G	6-31+G	6-31G*
O1-C2	1.183	1.192	1.193	1.173
C2-O3	1.364	1.358	1.354	1.33
C2-O4	1.366	1.361	1.358	1.332
O3-C5	1.462	1.46	1.461	1.42
O4-C6	1.455	1.449	1.45	1.411
C5-C7	1.52	1.51	1.509	1.513
O1-C2-O3	125.79	125.897	125.713	125.132
O1-C2-O4	125.515	125.535	125.342	124.915
C2-O3-C5	110.557	111.859	111.671	110.84
C2-O4-C6	110.338	111.36	111.147	110.35
O3-C5-C7	108.675	109.3	109.445	110.222
Ring twist	9.7°	6.7	6.1	7.7

	6-31+G*	6-311G	6-311G**	6-311++G**
O1-C2	1.175	1.189	1.167	1.168
C2-O3	1.33	1.353	1.328	1.328
C2-O4	1.332	1.356	1.33	1.33
O3-C5	1.422	1.456	1.419	1.42
O4-C6	1.413	1.445	1.41	1.411
C5-C7	1.512	1.508	1.511	1.511
O1-C2-O3	125.132	125.831	125.129	125.12
O1-C2-O4	124.9	125.447	124.87	124.855
C2-O3-C5	110.816	111.524	110.82	110.751
C2-O4-C6	110.346	111.017	110.318	110.256
O3-C5-C7	110.357	109.605	110.405	110.519
Ring twist	7.9	7.5	7.7	8

pure PC

Wavenumber (cm^{-1})
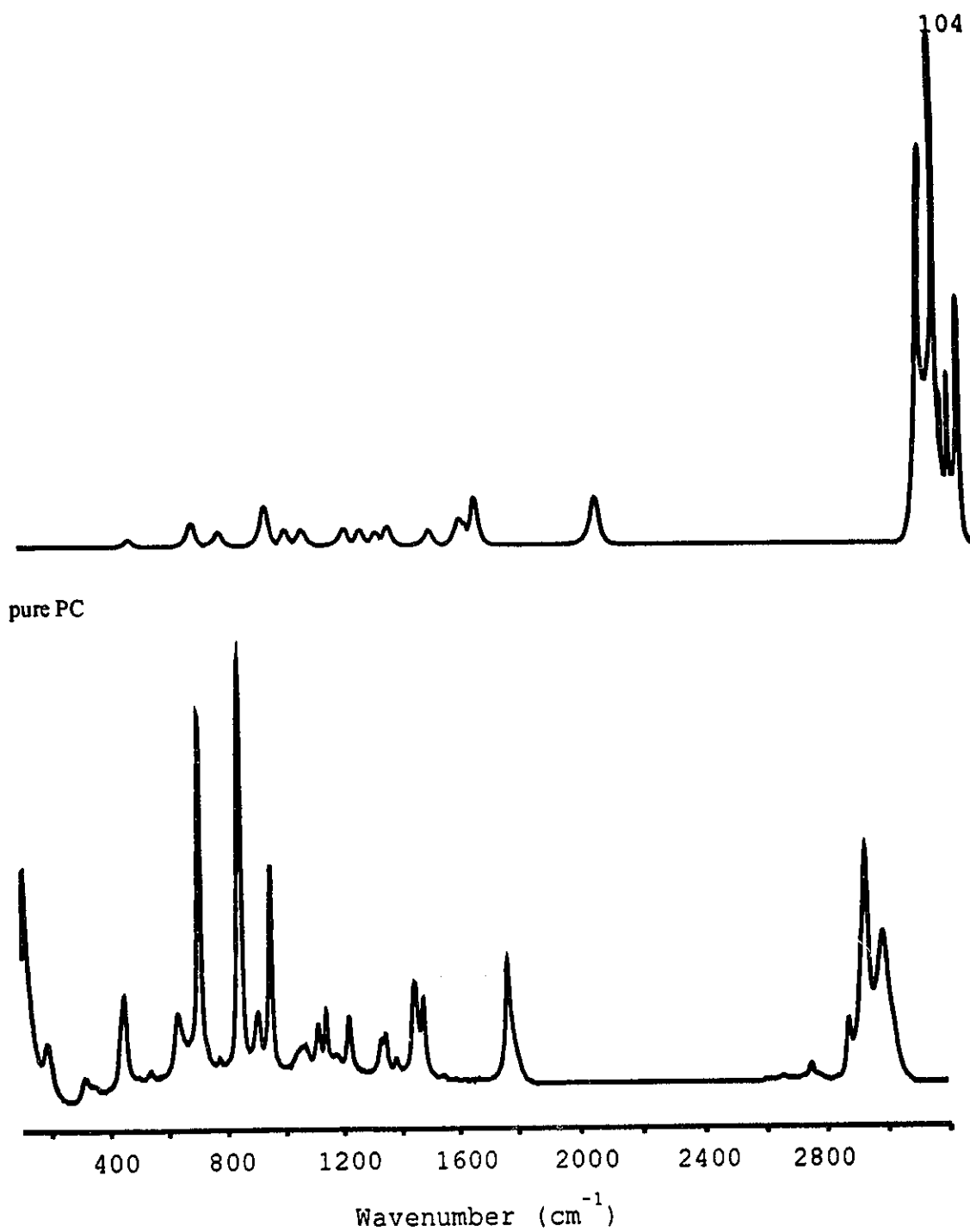
Figure 5.4: Experimental Raman spectrum of PC (bottom).
Predicted Raman spectrum using HF/6-311++G**
basis set(top).

being twisted out of plane by about 8 degrees. All of the 33 vibrational modes are Raman active according to selection rules. The experimental and calculated harmonic vibrational frequency energies are listed in Table 5.4. The experimental Raman spectrum along with the predicted Raman spectrum using the HF/6-311++G** basis is shown in Figure 5.4. There have been previous infrared and Raman investigations of PC[9] - [11], however, a detailed vibrational analysis has not been carried out. There are six hydrogen-carbon (H-C) stretching modes observed between 3020 cm^{-1} and 2882 cm^{-1}. QM SCF calculations predict the H-C harmonic vibrations to occur from 3287 cm^{-1} to 3172 cm^{-1}. The carbonyl stretching mode appears at 1781 cm^{-1} in the experimental Raman spectrum, while the calculated value is 2062 cm^{-1} at the highest level of theory used(6-311++G**). The carbon-carbon stretching, carbon-oxygen, and various hydrogen-carbon bending modes (scissor, twist, wag) show up between 1483 cm^{-1} and 911 cm^{-1} in the experimental Raman spectrum, the calculated values are over-estimated by a factor of 1.08 ($\approx$8%). An intense mode occurs at 849 cm^{-1}. One would be tempted to attribute the band as being a ring breathing mode as was the case with the Raman spectrum of EC. However, one would more likely describe the vibration at 849 cm^{-1} as a ring distortion. The calculated

$\nu_7 = 1781\ cm^{-1}$

$\nu_{26} = 712\ cm^{-1}$

$\nu_{24} = 849\ cm^{-1}$
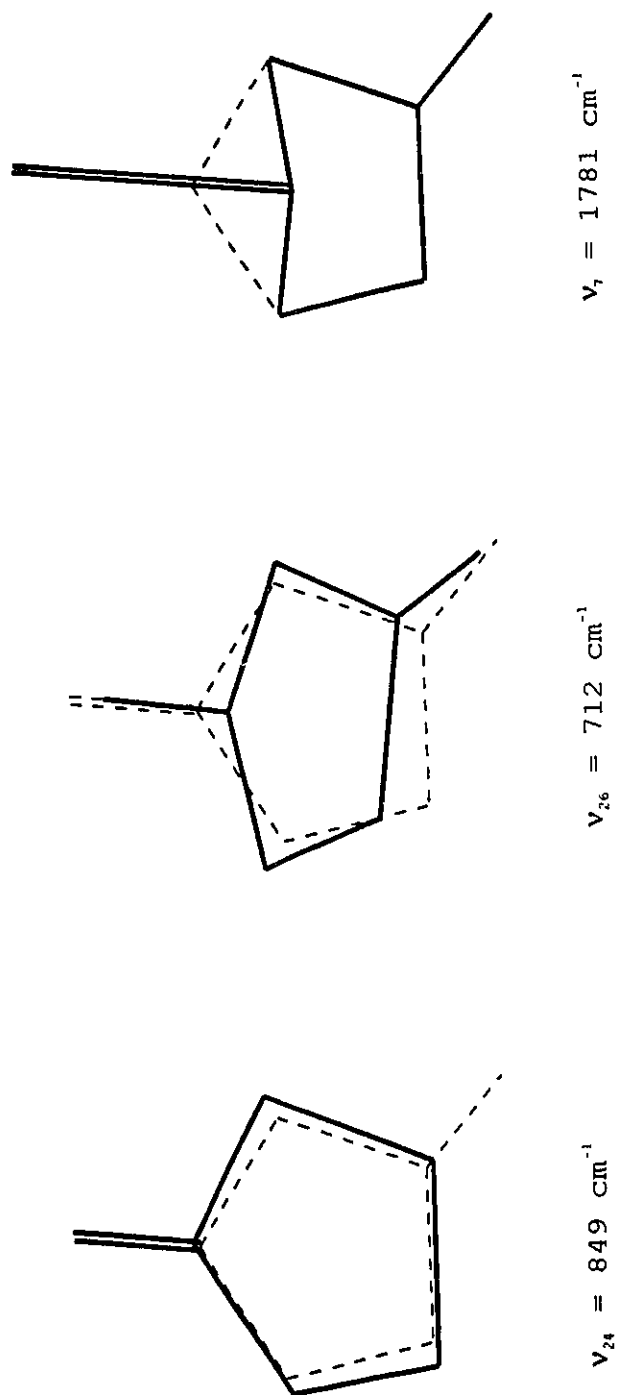
Figure 5.5: Calculated normal mode vibrations at 712, 849, and 1781 cm-1. The dashed line represents the equilibrium geometry and the solid line represents calculated atomic displacements using HF/6-311++G** basis set.

value is 910 cm^{-1}(6-311G), 942 cm^{-1}(6-311G**), and 941 cm^{-1} (6-311++G**). Another relatively intense band appears at 712 cm^{-1} in the experimental spectrum, *ab-initio* results suggests that this is another ring distortion mode with a calculated value of 757 cm^{-1} (6-311G), 786 cm^{-1} (6-311++G), and 784 cm^{-1} (6-311++G**). The graphical representation of the carbonyl and the two ring distortion modes are depicted in Figure 5.5. The remaining vibrational frequencies that can be resolved experimentally range between 633 cm^{-1} and 186 cm^{-1} and are attributed to ring bending and carbonyl bending modes.

Table 5.4 Calculated frequencies(cm^{-1})(Raman activities), experimental Raman frequencies, and assignment for propylene carbonate (infrared frequencies in parentheses.

Mode	6-311G	6-311G**	6-311++G**	Exp. Raman	Assign.'
v_1	3322(69.2)	3288(76.3)	3287(75.7)	3022(s)	H_2-C str
v_2	3270(47.9)	3260(57.4)	3259(52.3)	2995(s)	H_3-C str
v_3	3249(40.6)	3242(50.3)	3240(46.7)	2982(sh) (2987)	H_3-C str
v_4	3242(88.0)	3213(62.1)	3213(72.2)	2942(s)	H_2-C str
v_5	3233(137)	3206(161)	3204(158)	2928(sh) (2924)	H-C str
v_6	3174(114)	3173(104)	3172(123)	2884(m) (2880)	H_3-C str
v_7	1960(9.1)	2082(7.5)	2062(12.1)	1781(s) (1780)	C=O str
v_8	1677(9.5)	1657(6.5)	1656(5.3)	1485(m) (1484)	H_2-C sci
v_9	1648(12.7)	1616(8.1)	1616(6.3)	1466(sh) (1473)	H_3-C sci
v_{10}	1634(13.1)	1603(8.8)	1604(6.9)	1454(m) (1451)	H_3-C bend, H-C bend
v_{11}	1581(1.5)	1570(0.1)	1569(0.2)		H_2-C, H_3-C, H-C bend
v_{12}	1551(1.7)	1546(0.8)	1545(0.4)	1393(w) (1387)	H_2-C, H_3-C sci
v_{13}	1511(4.7)	1515(4.1)	1512(0.4)		H_3-C umb, H-C bend

v_{14}	1492(4.5)	1496(3.1)	1495(3.0)	1356(m) (1353)	H2-C, H3-C sci, H-C bend
v_{15}	1354(7.1)	1357(5.5)	1356(4.8)	1226(m) (1223)	H_2-C bend
v_{16}	1284(3.3)	1321(2.6)	1318(2.4)		C-C=O, H-C, H_2-C bend
v_{17}	1273(5.2)	1271(2.0)	1269(2.1)	1150(m) (1162)	H_3-C, H_2-C bend
v_{18}	1221(2.3)	1263(3.1)	1261(3.2)	1122(m) (1118)	C-O str, CH_3 rock
v_{19}	1195(3.0)	1231(1.0)	1227(0.9)	(1033)	C-O str, CH_3 rock
v_{20}	1165(3.0)	1210(3.1)	1209(3.1)	1072(m) (1063)	ring str H_2-C bend
v_{21}	1061(1.3)	1072(3.3)	1070(3.4)	957(s) (957)	H-C, H_2-C, H_3-C bend
v_{22}	1037(3.0)	1037(0.9)	1037(1.0)	(945)	H-C, H_2-C, H_3-C bend
v_{23}	982(3.6)	1013(3.4)	1012(3.1)	913(m) (916)	C2-O3, C2-O4 str
v_{24}	910(15.5)	942(10.0)	941(10.8)	849(vs) (849)	ring breathing
v_{25}	814(1.6)	889(1.1)	888(1.1)	(776)	C=O-ring bend
v_{26}	757(6.2)	786(4.2)	784(4.0)	712(s) (712)	ring dist

v_{27}	690(7.9)	697(5.4)	694(5.4)	633(m)	ring bend, CH$_2$ rock
v_{28}	566(0.4)	601(0.3)	600(0.3)	540(w)	C=O-ring bend, dist
v_{29}	478(1.8)	483(1.5)	483(1.6)	447(m)	ring twist
v_{30}	326(0.7)	327(0.6)	325(0.5)	186(m)	CH$_3$-C-C bend
v_{31}	244(0.1)	252(0.1)	251(0.1)		CH$_3$ twist
v_{32}	180(0.4)	185(0.3)	186(0.3)		molecular tor
v_{33}	99(0.3)	108(0.2)	113(0.3)		molecular tor

†Abbreviations used: Exp. = experimental, Assign. = assignment, str = stretch, sci = scissor, i.p. = in plane, o.p. = out of plane, dist = distortion, and tor = torsion.

5.5 DIMETHYL CARBONATE STRUCTURE AND VIBRATIONAL ASSIGNMENT

Figure 5.6 illustrates the structure of dimethyl carbonate (DMC). Unlike EC and PC discussed so far which have a ring structure, the structure of DMC has a methyl group attached on each side of the carbonate O-CO-O framework in an open linear chain. The symmetry of DMC was belongs to the C_{2v} point group symmetry in the QM calculations, however, there is evidence that there is internal rotation around the oxygen and methyl-carbon group[12]. A summary of the calculation results for the geometry optimization using various basis sets are presented in Table 5.5.

The solvent DMC belongs to the C_{2v} point group symmetry and has a total of 30 fundamental vibrations. From group theory[13] the symmetry of the vibrations works out to be:

$$\Gamma = 10a_1 + 5a_2 + 6b_1 + 9b_2$$

According to the selections rules, all of the vibrational modes are Raman active. The experimental and calculated harmonic vibrational frequency energies are listed in Table 5.6. The experimental and predicted Raman spectra are illustrated in Figure 5.7. There are six hydrogen-carbon (H-C) stretching modes observed between 3045 cm^{-1} and 2963 cm^{-1}.

QM SCF calculations predict the H-C harmonic

Table 5.5 Optimized geometry of dimethyl carbonate using Hartree-Fock theory.

	3-21G	6-31G	6-31+G	6-31G*
O1-C2	1.206	1.217	1.219	1.190
C2-O3	1.332	1.328	1.325	1.313
O3-C5	1.455	1.449	1.450	1.417
O1-C2-O3	124.994	124.772	124.640	125.436
C2-O3-C5	117.304	119.182	119.415	116.404

	6-31+G*	6-311G	6-311G**	6-311++G**
O1-C2	1.192	1.213	1.184	1.186
C2-O3	1.312	1.325	1.310	1.309
O3-C5	1.419	1.445	1.417	1.417
O1-C2-O3	125.311	124.810	125.449	125.372
C2-O3-C5	116.807	118.971	116.596	116.851

Diemethyl carbonate
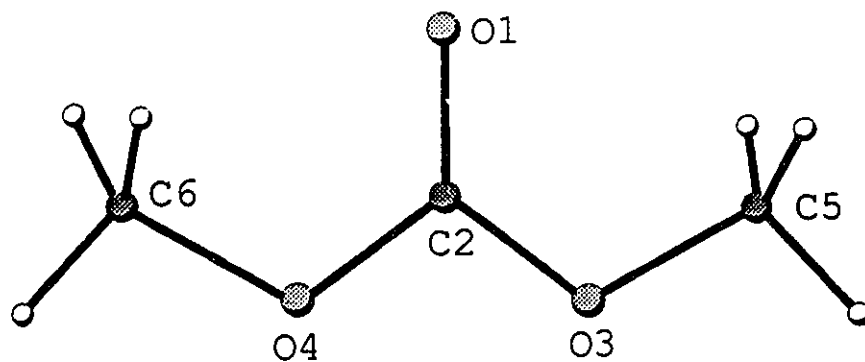
Diethyl carbonate
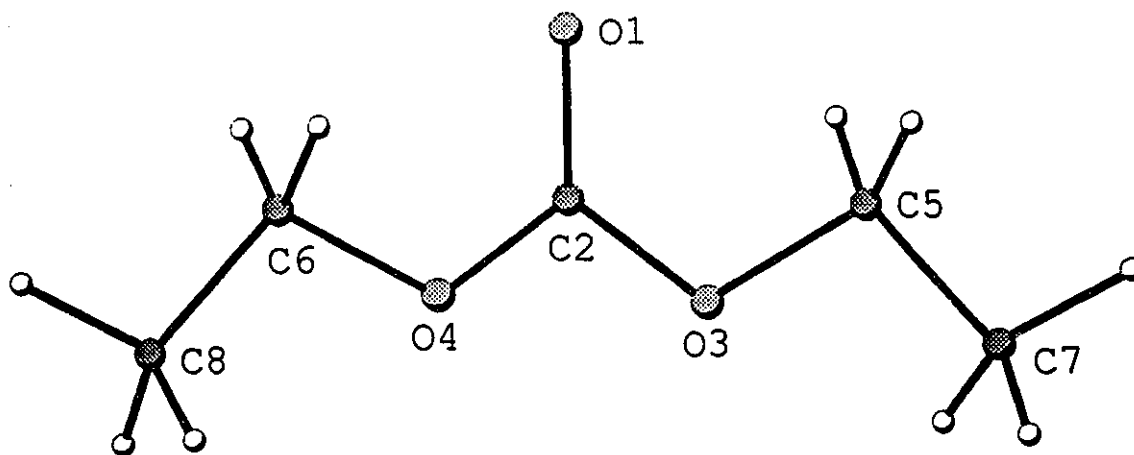
Figure 5.6: Optimized geometry of DMC (top) and DEC (bottom) using HF/6-311++G** basis set.

Dimethyl carbonate

114

Wavenumber (cm^{-1})
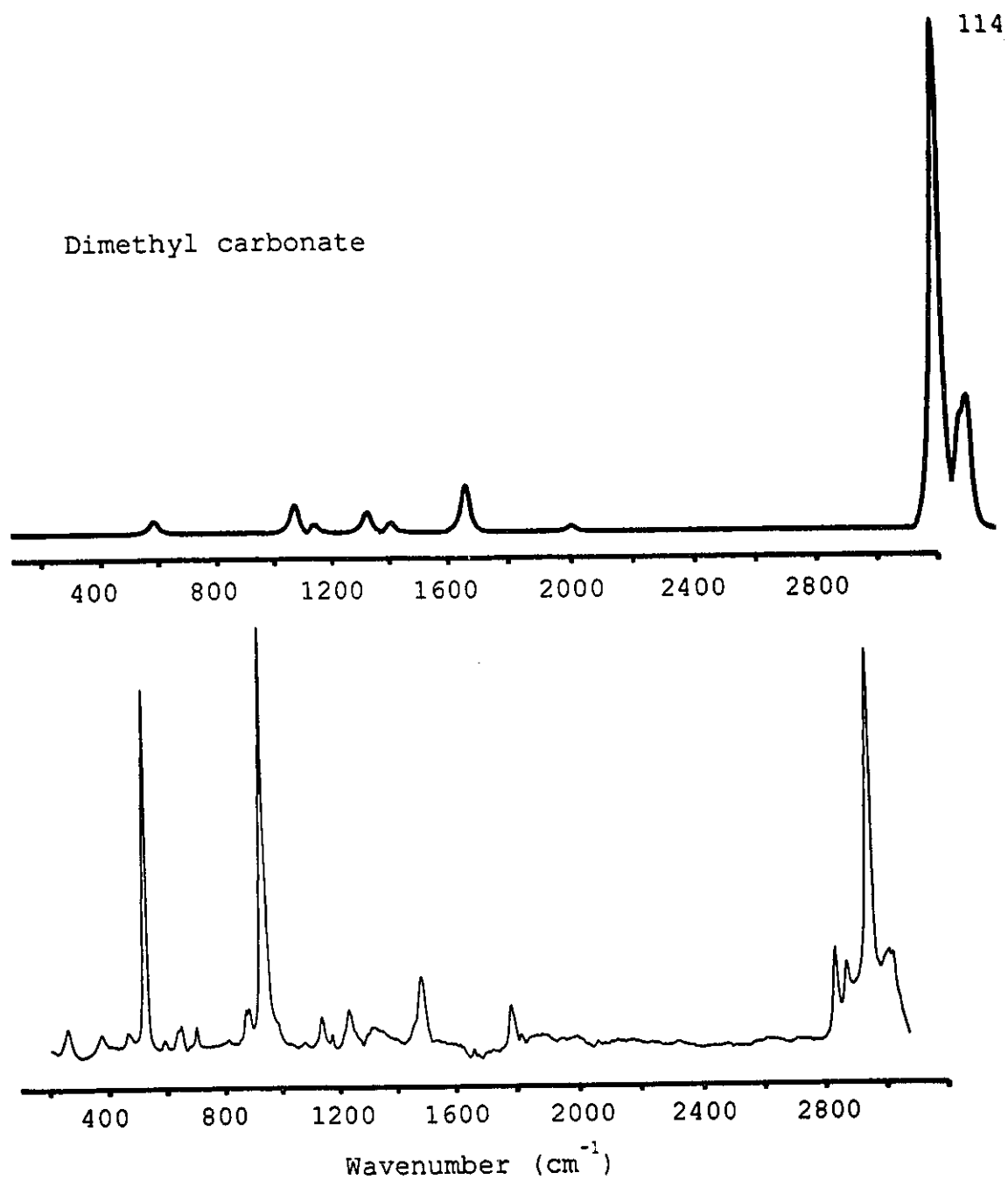
Figure 5.7   Experimental Raman spectrum of DMC (bottom).
Predicted Raman spectrum using HF/6-311++G**
basis set(top).

vibrations to occur from 3310 cm^{-1} to 3208 cm^{-1}. The carbonyl stretching mode shows up at 1754 cm^{-1} in the experimental Raman spectrum, while the calculated value is 1959 cm^{-1} at the highest level of theory used(6-311++G**). Bending modes (sci, umb, rock) of hydrogen-carbon (C-H$_3$), some of which are coupled with carbon-oxygen stretching modes appearing experimentally between 1460 cm^{-1} and 1114 cm^{-1}. The calculated values are over estimated by a factor of 1.08 (≈8%) causing the values to be between 1624 cm^{-1} and 1278 cm^{-1}. An intense mode occurs at 913 cm^{-1}, which is attributed to the symmetric O-CO-O bending mode, the calculated value is 1032 cm^{-1} at the highest level of theory(6-311++G**). The graphical representation of the carbonyl and the O-CO-O bending modes are depicted in Figure 5.8. The vibrational frequencies experimentally observed between 633 cm^{-1} and 186 cm^{-1}, are attributed to ring bending and carbonyl bending modes. The graphical representation of the vibrational normal modes of carbonyl stretch 1754 cm^{-1}, and the symmetric bending mode at 913 cm^{-1} are represented in Figure 5.8.

913 cm^{-1}

1754 cm^{-1}

903 cm^{-1}
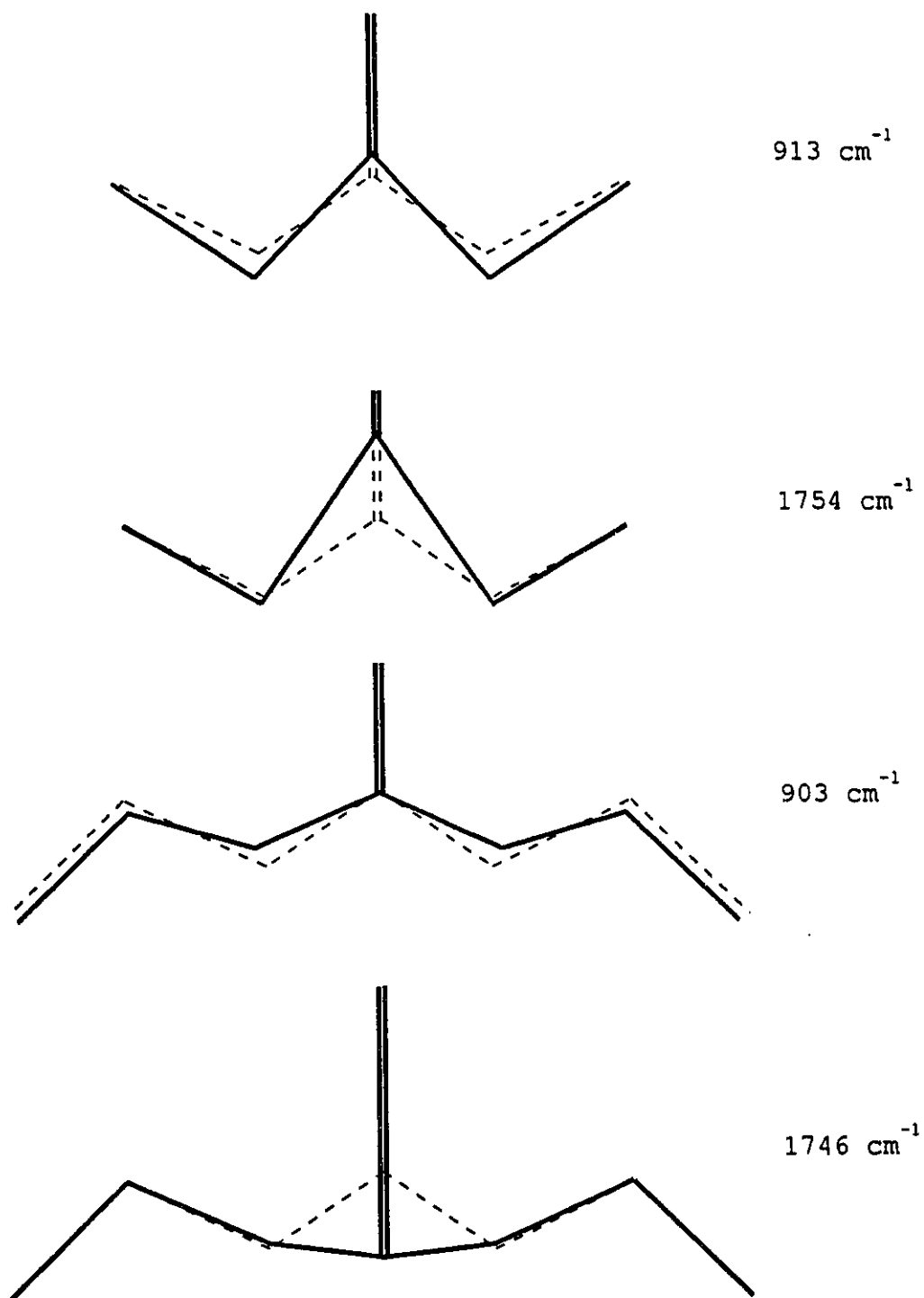
1746 cm^{-1}

Figure 5.8: Calculated normal mode vibrations: 913, and 1745, and 1781 cm-1 for DMC, 903 and 1746 cm-1 for DEC. The dashed line represents the equilibrium geometry and the solid line represents calculated atomic displacements using HF/6-311++G** basis set.

Table 5.6 Calculated frequencies (cm⁻¹) for dimethyl carbonate (Raman activity) and experimental Raman frequencies (infrared are in parentheses)

Mode	6-311G	6-311G**	6-311++G**	Exp. Raman	Assign.'
$v_1(a_1)$	3339(65.0)	3311(66.5)	3310(63.2)	3045(m) (3032)	C-H$_3$ str
$v_2(a_1)$	3216(215)	3209(228)	3209(262)	2963(vs) (2961)	C-H$_3$ str
$v_3(a_1)$	1828(0.2)	1980(0.6)	1959(1.6)	1754(w) (1758)	C=O str
$v_4(a_1)$	1654(15.0)	1627(9.6)	1624(6.9)	1460(m)	C-H$_3$ sci
$v_5(a_1)$	1605(7.4)	1600(5.3)	1598(2.4)	1437(sh)	C-H$_3$ umb
$v_6(a_1)$	1334(6.2)	1359(4.2)	1356(3.5)		C-H$_3$ rock
$v_7(a_1)$	1233(8.0)	1281(6.1)	1278(5.6)	1114(w)	O-C str
$v_8(a_1)$	967(19.3)	1035(11.3)	1032(11.0)	913(s) (915)	i.p. O-C2-O-C bend
$v_9(a_1)$	530(5.7)	555(3.7)	551(4.1)	517(m)	O-C2-O bend
$v_{10}(a_1)$	233(0.3)	250(0.2)	254(0.3)		i.p. C2-O-C bend
$v_{11}(a_2)$	3297(19.6)	3284(70.7)	3286(17.7)	3023(m)	C-H$_3$ str
$v_{12}(a_2)$	1641(33.5)	1613(23.5)	1612(20.1)	1440(m)	C-H$_3$ bend
$v_{13}(a_2)$	1280(8.7)	1290(4.2)	1288(3.9)		CH$_3$ rock
$v_{14}(a_2)$	212(0.2)	220(0.1)	219(0.4)		o.p. mol tor
$v_{15}(a_2)$	111(0.1)	142(0.1)	142(0.1)		o.p. mol tor
$v_{16}(b_1)$	3298(64.4)	3285(70.7)	3287(61.5)	3024(m) (3011)	C-H$_3$ str
$v_{17}(b_1)$	1642(1.5)	1613(0.3)	1613(0.1)		C-H$_3$ bend
$v_{18}(b_1)$	1282(2.3)	1292(1.5)	1290(1.4)	1153(w)	CH$_3$ rock

$\nu_{19}(b_1)$	842(0.8)	913(0.6)	915(0.7)	(795)	o.p. O=C-O$_2$ bend
$\nu_{20}(b_1)$	136(0.0)	165(0.0)	167(0.0)		CH$_3$ twist
$\nu_{21}(b_1)$	115(0.0)	124(0.0)	123(0.0)		mol tor
$\nu_{22}(b_2)$	3338(77.8)	3310(79.5)	3310(69.9)	3045(m) (3032)	C-H$_3$ str
$\nu_{23}(b_2)$	3215(0.3)	3208(1.0)	3208(1.1)		C-H$_3$ str
$\nu_{24}(b_2)$	1653(9.2)	1636(4.0)	1632(3.0)	1437(sh)	C-H$_3$ umb, C2-O str
$\nu_{25}(b_2)$	1634(0.8)	1621(2.5)	1619(1.5)		C-H$_3$ bend
$\nu_{26}(b_2)$	1471(1.1)	1477(0.8)	1474(0.6)	(1284)	C2-O str, C-H$_3$ umb
$\nu_{27}(b_2)$	1314(5.9)	1325(2.1)	1322(2.3)	1210(w) (1207)	CH$_3$ rock
$\nu_{28}(b_2)$	1036(2.1)	1102(1.7)	1096(1.8)	967(sh) (971)	O-C str
$\nu_{29}(b_2)$	735(1.8)	776(1.4)	773(1.1)	696(w)	i.p. C-O-C bend
$\nu_{30}(b_2)$	346(0.7)	380(0.3)	378(0.2)	257(w)	i.p. O=C-O-C bend

†Abbreviations used: Exp. = experimental, Assign. = assignment, str = stretch, sci = scissor, i.p. = in plane, o.p. = out of plane, dist = distortion, and tor = torsion.

5.6 DIETHYL CARBONATE STRUCTURE AND VIBRATIONAL ASSIGNMENT

The structure of the solvent DEC is similar to that of DMC as shown in Figure 5.6, with two the methyl groups replaced with two ethyl groups. The geometry optimization was given the same treatment as DMC with the added complication of two extra carbon atoms that resulted in increased computational time. Results from the *ab-initio* QM calculations of DEC are summarised in Table 5.7.

The vibrational characterization of DEC is similar to that of DMC. The solvent DEC vibrational spectrum contains 48 fundamental vibrational modes. DEC is assumed to have C_{2v} symmetry giving the total irreducible representation:

$$\Gamma = 15a_1 + 9a_2 + 10b_1 + 14b_2$$

According to the selection rules, all of the vibrational modes are Raman active. The experimental and calculated harmonic vibrational frequency energies are listed in Table 5.8. The experimental and predicted Raman spectra are illustrated in Figure 5.9. There are eight hydrogen-carbon (H-C) stretching modes are observed between 3009 cm^{-1} and

Table 5.7 Optimized geometry of diethyl carbonate using Hartree-Fock theory

	3-21G	6-31G	6-31+G	6-31G*
O1-C2	1.207	1.218	1.220	1.190
C2-O3	1.332	1.328	1.325	1.313
O3-C5	1.463	1.459	1.461	1.425
C5-C7	1.520	1.510	1.510	1.513
O1-C2-O3	124.901	124.702	124.558	125.424
C2-O3-C5	117.777	119.637	119.756	116.895
O3-C5-C7	105.681	106.361	106.353	107.204
	6-31+G*	6-311G	6-311G**	6-311++G**
O1-C2	1.192	1.214	1.184	1.186
C2-O3	1.312	1.326	1.310	1.310
O3-C5	1.427	1.455	1.424	1.425
C5-C7	1.513	1.508	1.512	1.512
O1-C2-O3	125.293	124.760	125.445	125.363
C2-O3-C5	117.223	119.368	117.066	117.284
O3-C5-C7	107.282	106.687	107.373	107.438
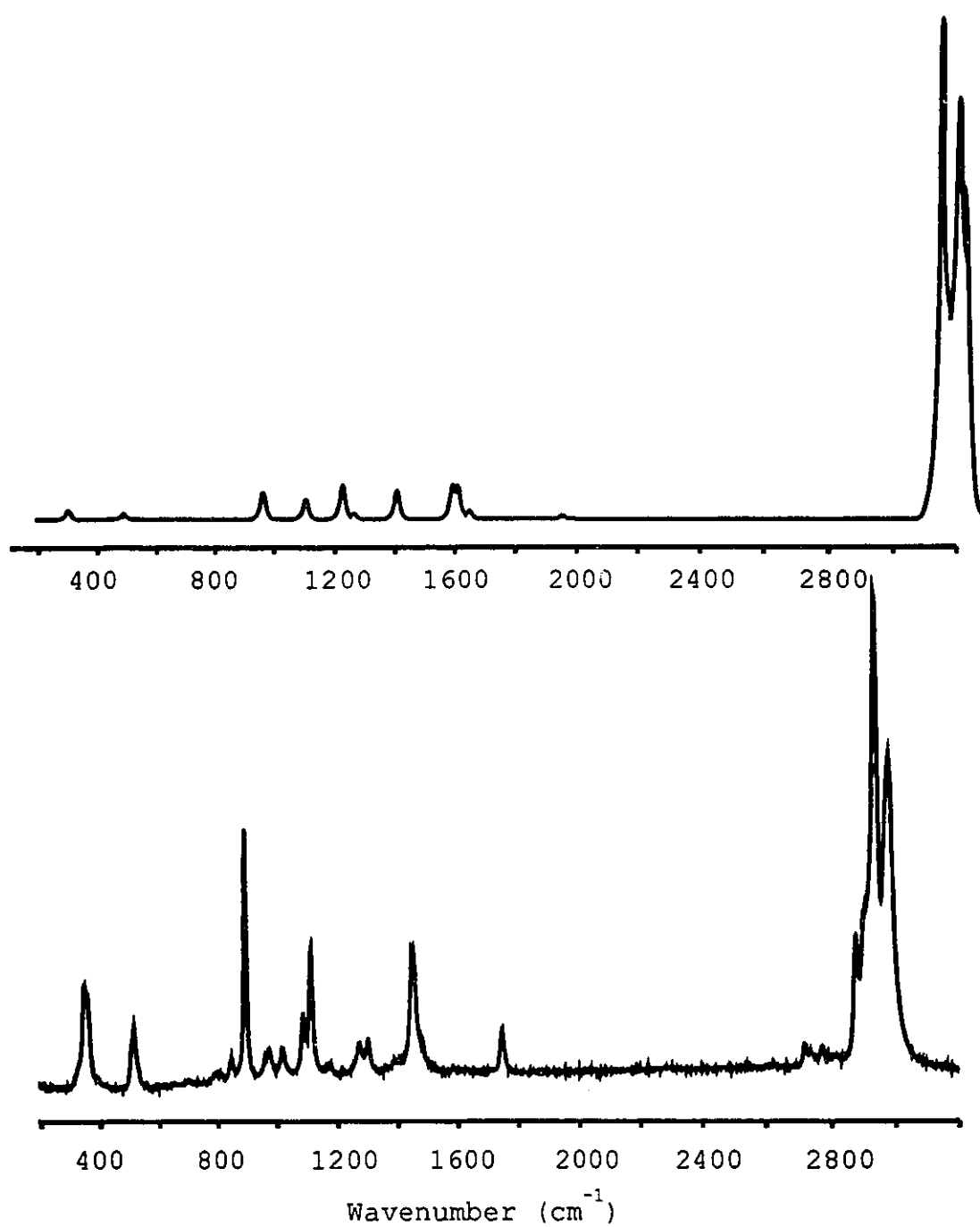
Figure 5.9: Experimental Raman spectrum of DEC (bottom).
Predicted Raman spectrum using HF/6-311++G**
basis set(top).

2880 cm^{-1} region. QM SCF calculations predict the H-C

harmonic vibrations to occur from 3271 cm^{-1} to 3173 cm^{-1}

(HF/6-311++g**). The carbonyl stretching mode shows up at

1746 cm^{-1} in the experimental Raman spectrum, while the

calculated value is 1951 cm^{-1} at the highest level of theory

used(6-311++G**). Bending modes (sci, umb, rock) of

hydrogen-carbon (C-H$_3$, C-H$_2$), some of which are coupled with

carbon-oxygen and carbon-carbon stretching modes appearing

experimentally between 1482 cm^{-1} and 1023 cm^{-1}. The

calculated values are over estimated by a factor of 1.08

($\approx$8%) causing the values to be between 1601 cm^{-1} and 1093 cm^{-1}. The equivalent symmetric O-CO-O bending mode is located

at 903 cm^{-1} and the calculated value is 1001 cm^{-1} (6-311++G**). The graphical representation of the carbonyl and

the O-CO-O bending modes are depicted in Figure 5.8.

Vibrational frequencies observed experimentally between 814

cm^{-1} and 362 cm^{-1} are assigned to ring bending and carbonyl

bending modes.

As expected, a comparison of the Raman spectra of DMC

and DEC reveal distinct differences. The normal modes which

are seen in the DEC spectrum but not the DMC spectrum

include: two bands occurring at 1306, 1276 cm^{-1}, a strong

band at 1120 cm^{-1}, a medium intensity band located at 1023

cm^{-1}, and a strong intensity band located at 362 cm^{-1}. The

two bands located at 1306 and 1276 cm^{-1} have calculated

values of 1455 and 1276 cm^{-1} respectively which are attributed to C-H$_2$ wag and C-H$_2$ twist. The strong intensity band occurring at 1023 cm^{-1} is calculated at 1093 cm^{-1} and attributed to C-C stretching coupled with a O=C-O bending mode. Lastly, the strong intensity band at 362 cm^{-1} has a calculated value of 420 cm^{-1} and described as a O-C-C bending mode.

The SCF QM accurately predicts shifts of frequencies resulting from the additional carbon atom on DEC. For example, the H-C stretch range 3009 cm^{-1} and 2880 cm^{-1} region for DEC. QM SCF calculations predict the H-C harmonic vibrations of DEC to occur from 3271 cm^{-1} to 3173 cm^{-1}. The H-C stretching vibrations of DMC are located between 3045 cm^{-1} and 2963 cm^{-1} giving a relative increase of 36 cm^{-1}. While QM SCF calculations predict the DMC H-C harmonic vibrations to occur from 3310 cm^{-1} to 3208 cm^{-1}, a relative increase of 39 cm^{-1}.

Table 5.8 Calculated frequencies (cm⁻¹) for diethyl carbonate (Raman activities) and experimental Raman frequencies.

Mode	6-311G	6-311G**	6-311++G**	Exp. Raman	Assign.'
$v_1(a_1)$	3245(101)	3242(104)	3240(96.0)	2982(s)	C-H$_3$, C-H$_2$ str
$v_2(a_1)$	3221(238)	3217(224)	3216(238)	2939(vs)	C-H$_3$, C-H$_2$ str
$v_3(a_1)$	3175(233)	3174(239)	3173(283)	2880(m)	C-H$_3$ str
$v_4(a_1)$	1815(0.5)	1972(0.4)	1951(1.4)	1746(w)	C=O str
$v_5(a_1)$	1680(7.2)	1652(4.6)	1649(4.3)		C-H$_2$, C-H$_3$ sci
$v_6(a_1)$	1652(33.9)	1617(23.7)	1616(18.1)	1454(m)	C-H$_2$, C-H$_3$ sci
$v_7(a_1)$	1580(1.4)	1565(4.2)	1563(3.3)	1394(w)	C-H$_3$ umb, C-H$_2$ wag
$v_8(a_1)$	1546(1.8)	1518(0.5)	1517(0.3)	1365(w)	C-H$_3$ umb, C-H$_2$ wag
$v_9(a_1)$	1249(16.5)	1285(4.5)	1282(3.6)	1179(w)	O-C5, O-C6 str
$v_{10}(a_1)$	1233(7.7)	1247(16.0)	1245(17.2)	1120(s)	CH$_3$ rock, C-O-C bend
$v_{11}(a_1)$	1080(0.5)	1094(0.6)	1093(0.4)	1023(m)	C-C str, O=C-O$_2$ bend
$v_{12}(a_1)$	972(21.7)	1002(11.2)	1001(11.4)	903(vs)	CH$_3$ rock, C-O-C bend
$v_{13}(a_1)$	526(3.6)	549(2.1)	548(2.0)	524(m)	i.p. O-C-O bend
$v_{14}(a_1)$	364(4.6)	373(3.4)	372(3.9)	362(m)	i.p. O-C-C bend
$v_{15}(a_1)$	124(0.2)	134(0.3)	133(0.3)		i.p. mol bend
$v_{16}(a_2)$	3280(4.6)	3271(4.8)	3271(9.3)	3009(sh)	C-H$_3$, C-H$_2$ str

$v_{17}(a_2)$	3250(0.8)	3240(0.0)	3239(0.0)		C-H$_3$, C-H$_2$ str
$v_{18}(a_2)$	1636(33.7)	1600(22.4)	1601(17.8)	1454(m)	C-H$_3$ bend
$v_{19}(a_2)$	1421(25.7)	1417(16.2)	1417(15.7)	1276(m)	CH$_2$ twist
$v_{20}(a_2)$	1300(1.8)	1287(0.3)	1285(0.3)	1179(w)	CH$_2$ wag
$v_{21}(a_2)$	897(0.0)	875(0.0)	874(0.1)		CH$_3$ twist, CH$_2$ rock
$v_{22}(a_2)$	276(0.0)	290(0.0)	289(0.0)		CH$_3$ twist
$v_{23}(a_2)$	174(0.1)	178(0.1)	176(0.1)		o.p. C-O-C bend
$v_{24}(a_2)$	51(0.2)	66(0.1)	67(0.0)		o.p. mol tor
$v_{25}(b_1)$	3281(4.6)	3271(9.4)	3271(9.3)		C-H$_3$, C-H$_3$ str
$v_{26}(b_1)$	3250(206)	3240(209)	3239(187)	2982(s)	C-H$_3$, C-H$_2$ str
$v_{27}(b_1)$	1636(1.2)	1600(0.5)	1601(0.6)	1454(m)	C-H$_3$ bend
$v_{28}(b_1)$	1422(0.4)	1419(0.0)	1418(0.0)		CH$_2$ twist
$v_{29}(b_1)$	1301(1.2)	1289(0.4)	1287(0.4)		C-H$_3$ bend, CH$_2$ wag
$v_{30}(b_1)$	899(0.5)	917(0.6)	919(0.7)	814(w)	o.p. O=C-O bend
$v_{31}(b_1)$	838(0.5)	870(0.1)	870(0.1)	793(w)	CH$_3$ twist, CH$_2$ rock
$v_{32}(b_1)$	266(0.0)	280(0.0)	279(0.0)		CH$_3$ twist
$v_{33}(b_1)$	104(0.0)	113(0.0)	111(0.0)		o.p. mol tor
$v_{34}(b_1)$	56(0.1)	66(0.0)	67(0.0)		o.p. mol tor
$v_{35}(b_2)$	3245(17.8)	3242(25.8)	3239(23.6)	2982(s)	C-H$_3$, C-H$_2$ str
$v_{36}(b_2)$	3221(1.1)	3216(0.2)	3215(0.1)		C-H$_3$, C-H$_2$ str
$v_{37}(b_2)$	3175(5.9)	3174(4.7)	3173(3.8)		C-H$_3$ str
$v_{38}(b_2)$	1681(4.6)	1655(2.9)	1652(2.7)	1482(w)	C-H$_3$, C-H$_2$ sci

$v_{39}(b_2)$	1651(3.8)	1617(1.4)	1616(1.2)		C-H$_3$, C-H$_2$ sci
$v_{40}(b_2)$	1588(4.6)	1584(1.0)	1580(0.9)	1394(w)	C-H$_3$ umb, C-H$_2$ wag
$v_{41}(b_2)$	1570(0.2)	1533(0.1)	1532(0.1)	1314(m)	C-H$_3$ umb, C-H$_2$ wag
$v_{42}(b_2)$	1446(4.0)	1457(1.4)	1455(1.9)	1306(m)	C-H$_2$ wag, C2-O str
$v_{43}(b_2)$	1242(0.1)	1229(0.1)	1227(0.2)		C-H$_3$ rock, O-C-C bend
$v_{44}(b_2)$	1120(10.0)	1134(8.1)	1132(8.4)	1093(m)	C-C str C5-O, C6-O str
$v_{45}(b_2)$	922(0.4)	952(1.1)	950(1.0)	854(w)	CH$_3$, CH$_2$ rock
$v_{46}(b_2)$	791(0.4)	827(0.3)	824(0.2)	710(w)	i.p. C-O-C bend
$v_{47}(b_2)$	405(1.7)	421(1.2)	420(0.9)	362(m)	i.p. O-C-C bend
$v_{48}(b_2)$	257(0.1)	256(0.0)	275(0.0)		i.p. O=C-O-C bend

[†]Abbreviations used: Exp. = experimental, Assign. = assignment, str = stretch, sci = scissor, i.p. = in plane, o.p. = out of plane, dist = distortion, and tor = torsion.

REFERENCES

1. Gaussian 92, Revision G.1, M. J. Frisch, G. W. Truck, M. Head-Gordon, P. M. W. Gill, M. W. Wong, J. B. Forseman, B. G. Johnson, H. B. Schegel, M. A. Robb, E. S. Replogle, R. Gomperts, J. L. Martin, D. J. Fox, D. J. Defrees, J. Baker, J. J. P. Stewart, and J. A. Pople, Gaussian, Inc., Pittsburgh PA, 1992.

2. Schegel, H. B. *J. Compt. Chem.* **1985**, *3*, 214.

3. Brown, C. J. *Acta Cryst.*, **1954**, 7, 92.

4. Angell, C. L. *Trans. Faraday Soc.*, **1956**, *52*, 1178.

5. Blint, R. J. *J. Electrochem. Soc.* **1995**, *142*, 696.

6. Nazri, M. M.Sc. Thesis, Oakland University, 1995.

7. Hydodo, S.; Okabayashi, K. *Electrochim. Acta* **1989**, *34*, 1551.

8. Wilson Jr., E. B.;Decius, J. C.; Cross, P. C. *Molecular Vibrations*, Dover, New York, 1955.

9. Janz, G. J.; Ambrose, J.; Coutts, J. W.; Downey, J. R. Jr. *Spectrochim. Acta.*, **1979**, *35A*, 175.

10. Pethrick, R. A.; Wilson, A. D. *Spectrochim. Acta*, **1974**, *30A*, 1073.

11. Durig, J. R.; Coulter, C. L.; Wertz, D. W. *J. Mol. Spectrosc.*, **1968**, *27*, 285.

12. Evens, M. W.; Afsar, M. N.; Davies, G. J.; Ménard, C.; Goulon *Chem. Phys. Let.* **1977**, *52*, 388.

13. Wilson Jr., E. B.;Decius, J. C.; Cross, P. C. *Molecular Vibrations*, Dover, New york, 1955.

CHAPTER 6

BINARY SOLVENT ELECTROLYTE SOLUTIONS

6.1 INTRODUCTION

The concept of combining high dielectric ester, such as EC, with low viscous ether or ester to obtain the best conducting electrolyte solution has received much attention[1,2,3]. Electrolytic properties of ethylene carbonate based solutions and the charge-discharge cycling behaviour of lithium in the these solutions have been studied[4-7]. From these studies EC has been established as an important electrolyte component with the desired properties for use in lithium secondary batteries.

The structural changes that occur at the molecular level by mixing EC with other solvents have not been discussed in detail. The system is complicated by the addition of a salt to the binary solvent mixture, which influences the molecular arrangements. Structural changes are reflected in the spectroscopy, conductivity, and viscosity behaviour of EC based binary solvent electrolytes. With these considerations in mind, the spectroscopic, conductivity, and viscosity studies of EC based binary electrolytes were performed. The work was complimented by quantum chemical *ab-intio* calculations, which is a powerful method to provide insight into molecular structure.

6.2 METHODS

Spectroscopic measurements were performed on the prepared electrolyte solutions previously described. The 514.5 nm excitation line from a Spectra Physics model 164 Ar^+ laser was used for Raman scattering of the solutions contained in glass capillaries. A polarization rotator (Spectra-Physics Model 1310-21) was mounted on the laser to produce S-polarized (TE) incident light. Raman shifts were measured with a SPEX-1403 double spectrometer. The spectral bandpass and laser power was 2 cm^{-1} and 50 mW respectively. All Raman spectra were acquired in steps of 0.5 cm^{-1} with a delay of 2 seconds per step over the range 200 cm^{-1} to 3200 cm^{-1}. Raman files were imported into Spectra-Calc™ (Galactic Industries Corp.) software for data manipulation and spectral plotting.

6.3 RAMAN SPECTRA OF EC/PC/LiClO₄ ELECTROLYTE SOLUTION

The Raman spectra of EC/PC solutions containing variable lithium perchlorate concentrations are presented in Figures 6.1 to 6.5. Molar ratios range from 20/20/1 (EC/PC/LiClO₄) to 1/1/1 (0.3 M to 6.6 M lithium perchlorate). The relative intensities are adjusted to an internal standard, which is a vibrational band that remains unaffected by the addition of lithium perchlorate. Several

Figure 6.1: Raman spectra of EC/PC/LiClO$_4$ electrolyte
solutions with varying concentrations of
lithium perchlorate over the range 250-750 cm^{-1}

EC/PC/LiClO$_4$ = 10/10/1

EC/PC/LiClO$_4$ = 5/5/1

EC/PC/LiClO$_4$ = 3/3/1

EC/PC/LiClO$_4$ = 2/2/1

EC/PC/LiClO$_4$ = 1/1/1

760   800   840   880   920   960   1000

Wavenumber (cm-1)

Figure 6.2: Raman spectra of EC/PC/LiClO$_4$ electrolyte
solutions with varying concentrations of
lithium perchlorate over the range 750-1000 cm^{-1}

EC/PC/LiClO$_4$ = 10/10/1

EC/PC/LiClO$_4$ = 5/5/1

EC/PC/LiClO$_4$ = 3/3/1

EC/PC/LiClO$_4$ = 2/2/1

EC/PC/LiClO$_4$ = 1/1/1

Wavenumber (cm^{-1})
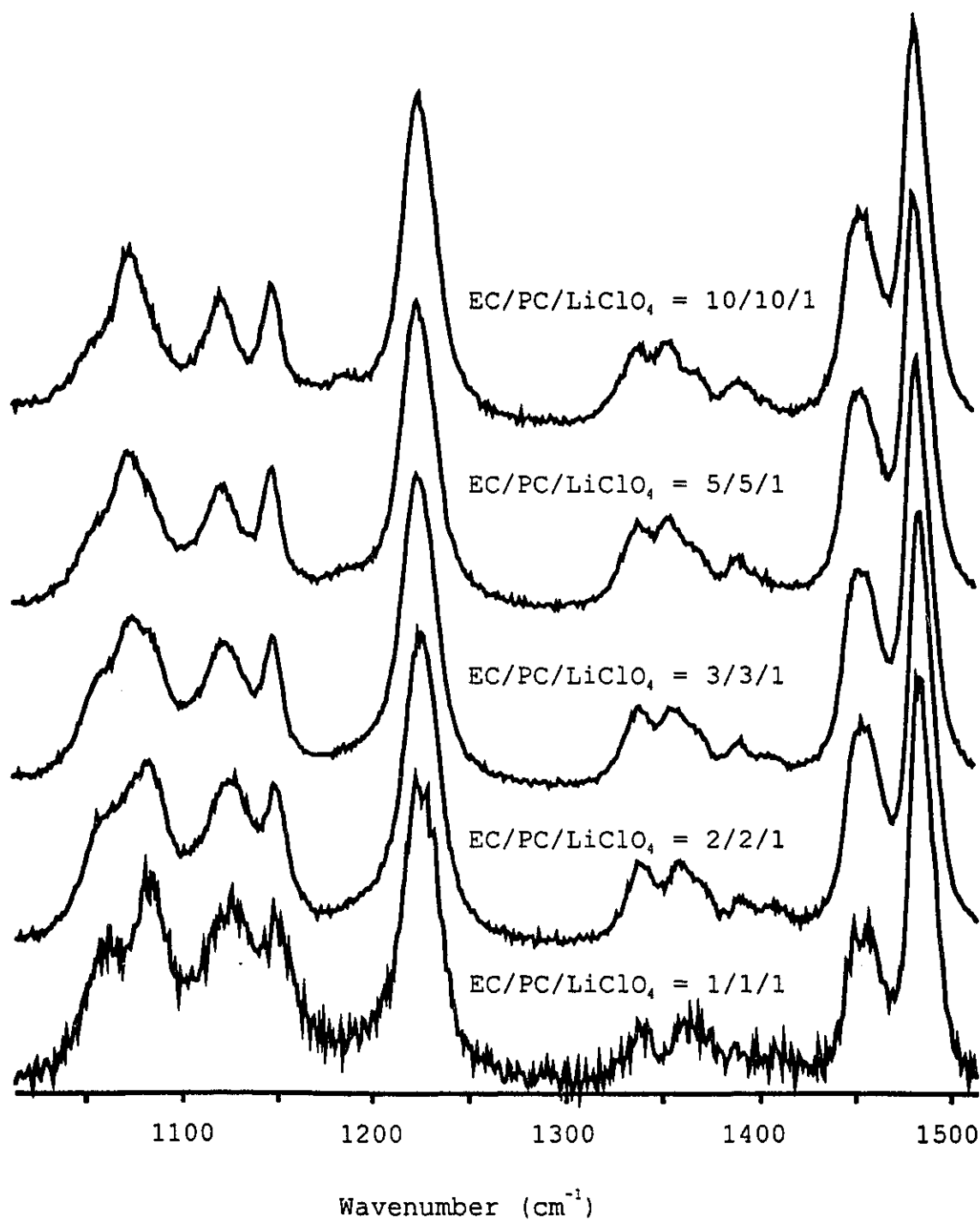
Figure 6.3: Raman spectra of EC/PC/LiClO$_4$ electrolyte
solutions with varying concentrations of
lithium perchlorate over the range
1000-1500 cm-1

EC/PC/LiClO$_4$ = 10/10/1

EC/PC/LiClO$_4$ = 5/5/1

EC/PC/LiClO$_4$ = 3/3/1

EC/PC/LiClO$_4$ = 2/2/1

EC/PC/LiClO$_4$ = 1/1/1

1600   1700   1800   1900   2000

Wavenumber (cm^{-1})
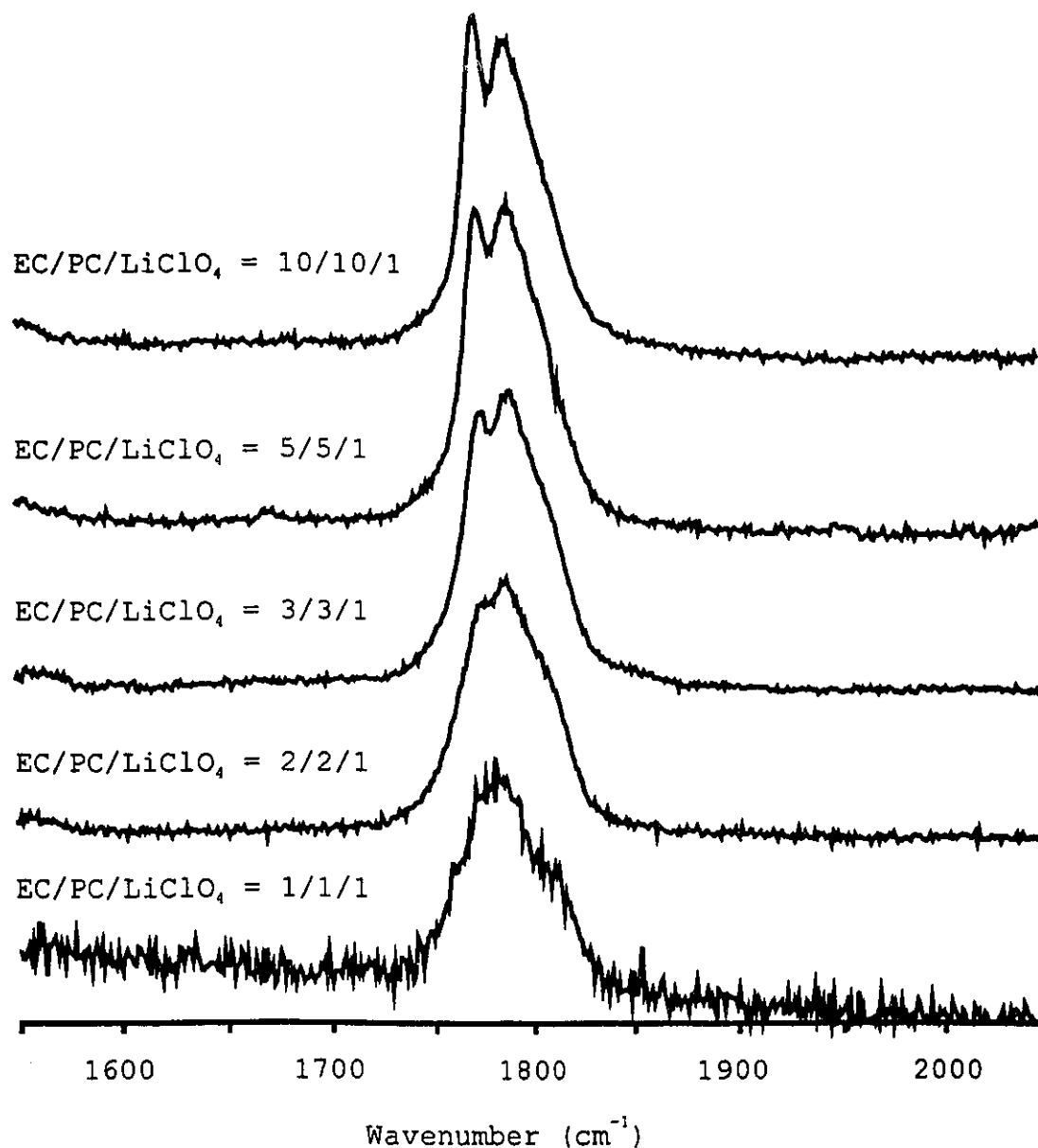
Figure 6.4: Raman spectra of EC/PC/LiClO$_4$ electrolyte
solutions with varying concentrations of
lithium perchlorate over the range
1500-2000 cm^{-1}

EC/PC/LiClO$_4$ = 10/10/1

EC/PC/LiClO$_4$ = 5/5/1

EC/PC/LiClO$_4$ = 3/3/1

EC/PC/LiClO$_4$ = 2/2/1

EC/PC/LiClO$_4$ = 1/1/1

Wavenumber (cm^{-1})
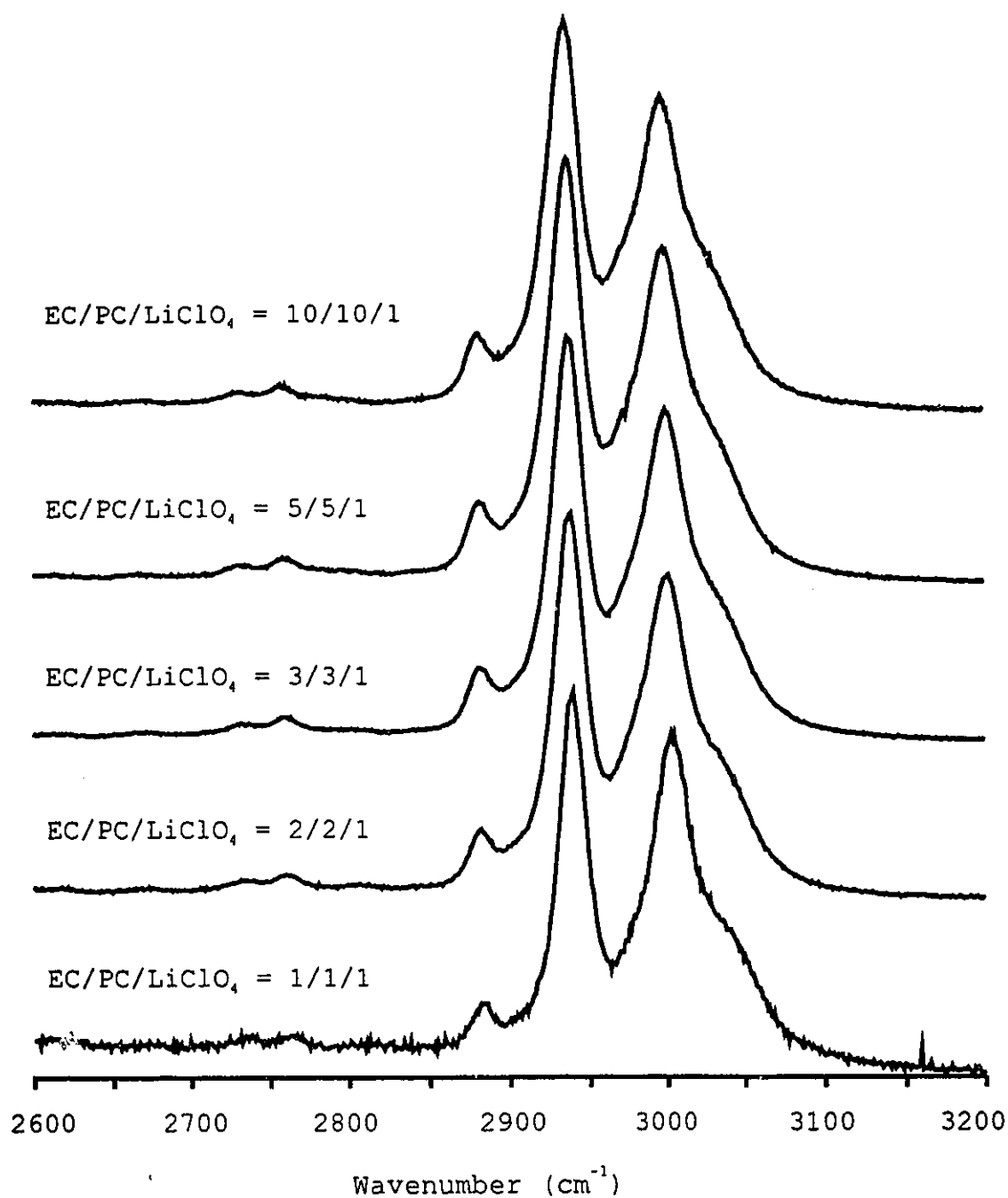
Figure 6.5: Raman spectra of EC/PC/LiClO$_4$ electrolyte
solutions with varying concentrations of
lithium perchlorate over the range
2600- 3200cm^{-1}

bands do not change in relative intensity. Therefore, the vibration chosen in this case is the C-H bending mode located at 1224 cm^{-1}. The spectra are presented so that the bands affected by the addition of lithium perchlorate can be viewed in detail. There have been some discussion on the behaviour of band shifts in EC/PC binary solvent electrolytes[8,9]. The vibrational assignment of observed frequencies for EC, PC and $LiClO_4$ have been discussed in previous Chapters, so that we can focus on the changes in the spectra of the electrolytes. The areas of interest in the Raman spectral regions are those which showed dynamic changes due to solvent-solute interactions with an increase in lithium perchlorate concentration. Intuitively one would expect that the lithium cation would attach itself to the most electronegative part of the solvent molecules. In the case of EC and PC, the carbonyl oxygen would be the most likely position for the lithium atom. This would result in vibrational changes in the carbonyl end of the molecules while the hydrogen related vibrations should therefore be unaffected.

The first significant dynamical change that occurs in the Raman spectra include an increase in a broadening of the band located at 457 cm^{-1}, Figure 6.1 which is attributed to both the ring twisting mode of PC and the perchlorate $v_2(e)$ band. The intensity increase of the band at 629 cm^{-1}

assigned to the perchlorate $\nu_4(f)$ vibration can be seen in Figure 6.1. At same time the relative intensity of the shoulder at 633 cm^{-1}, a coupled ring bending mode and CH$_2$ twist, is unaffected. The band centered at 714 cm^{-1} shows a significant decrease in intensity as the concentration of lithium perchlorate increases while the opposite trend in intensity is observed for the 724 cm^{-1} band with increasing salt concentration. According to the assignments, the 714 cm^{-1} is a combination of an out of plane EC O=C-ring bending mode (714 cm^{-1}) and the PC ring breathing mode (712 cm^{-1}). The new band at 724 cm^{-1} then can be considered to be the above frequencies undergoing a shift of 10 cm^{-1}. The intense band located at 891 cm^{-1}, Figure 6.2, belongs to the symmetric ring breathing mode of EC, as depicted in Figure 5.3, and is shifted by 10 cm^{-1} to 904 cm^{-1} with the addition of lithium perchlorate. The symmetric stretch $\nu_1(a_1)$ of the perchlorate anion is observed at 933 cm^{-1} along with the vibrational bands that include the solvent-shared ion-pairs (938 cm^{-1}) and contact ion-pairs (944 cm^{-1}) which appears in the most concentrated solutions as discussed in detail in Chapter 4. The region between 1040 and 1100 cm^{-1} contains the ring C-O stretching vibrations of EC and PC as shown in Figure 6.3 and are affected by the increase in lithium perchlorate concentration. The vibrations observed between 1200 - 1500 cm^{-1} are various hydrogen-carbon bending modes

of both EC and PC which are unaffected by the addition of lithium perchlorate. It is important to point out the change in the band shape of the carbonyl stretches located at 1781(PC) and 1794(EC), that also takes place due to increase concentration of lithium perchlorate as seen in Figure 6.4.

6.4 RAMAN SPECTRA OF EC/DEC/LiClO₄ ELECTROLYTE SOLUTIONS

Raman spectra of the EC/DEC/LiClO₄ electrolyte solutions with varying molar ratios ranging from 20/20/1 to 1/1/1 (0.3M to 6.6 M lithium perchlorate concentrations) are presented in Figures 6.6 - 6.10. As in the Raman spectra of the EC/PC/LiClO₃ electrolyte solutions, the relative intensities are adjusted to an internal standard. The chosen vibrational band that is unaffected by the addition of lithium perchlorate in case is located at 1224 cm⁻¹ which is attributed to the C-H bending mode of EC.

Considering the electrolyte solution contains EC, the vibrational band shifts due to EC should occur in EC/DEC/LiClO₄ as in the electrolyte solution EC/PC/LiClO₄. The differences between the Raman spectra of pure EC and DEC were discussed in the previous chapter. Figure 6.6 demonstrates that the 714 cm⁻¹ (o.p. C=O-ring bending) EC vibrational band undergoes dynamical changes due to the

EC/PC/LiClO$_4$ = 20/20/1

EC/PC/LiClO$_4$ = 10/10/1

EC/PC/LiClO$_4$ = 5/5/1

EC/PC/LiClO$_4$ = 3/3/1

EC/PC/LiClO$_4$ = 2/2/1

EC/PC/LiClO$_4$ = 1/1/1

300   400   500   600   700

Wavenumber (cm^{-1})
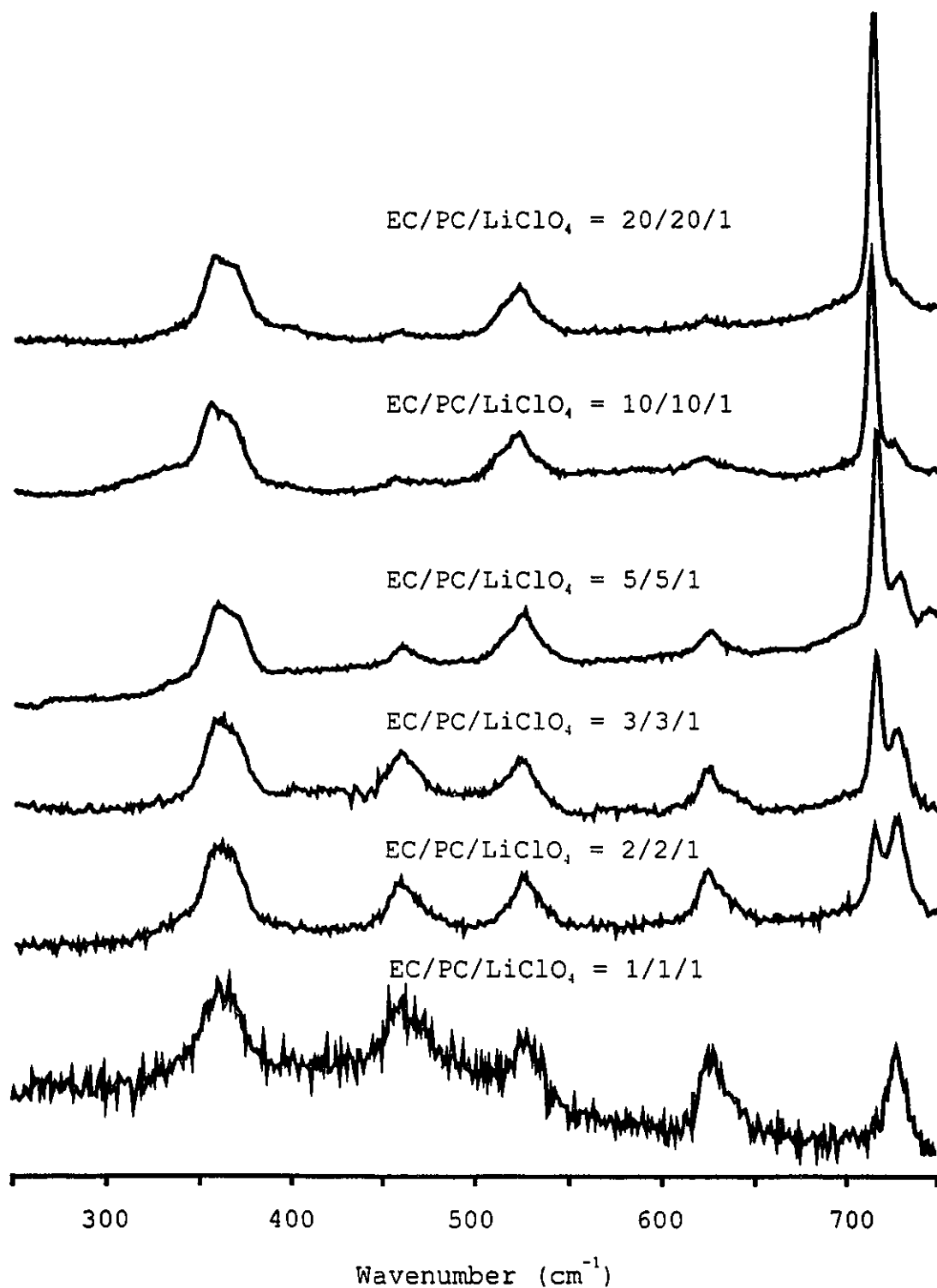
Figure 6.6: Raman spectra of EC/DEC/LiClO$_4$ electrolyte
solutions with varying concentrations of
lithium perchlorate over the range 250-750 cm^{-1}

EC/DEC/LiClO₄ = 10/10/1

EC/DEC/LiClO₄ = 5/5/1

EC/DEC/LiClO₄ = 3/3/1

EC/DEC/LiClO₄ = 2/2/1

EC/DEC/LiClO₄ = 1/1/1

Wavenumber (cm^{-1})
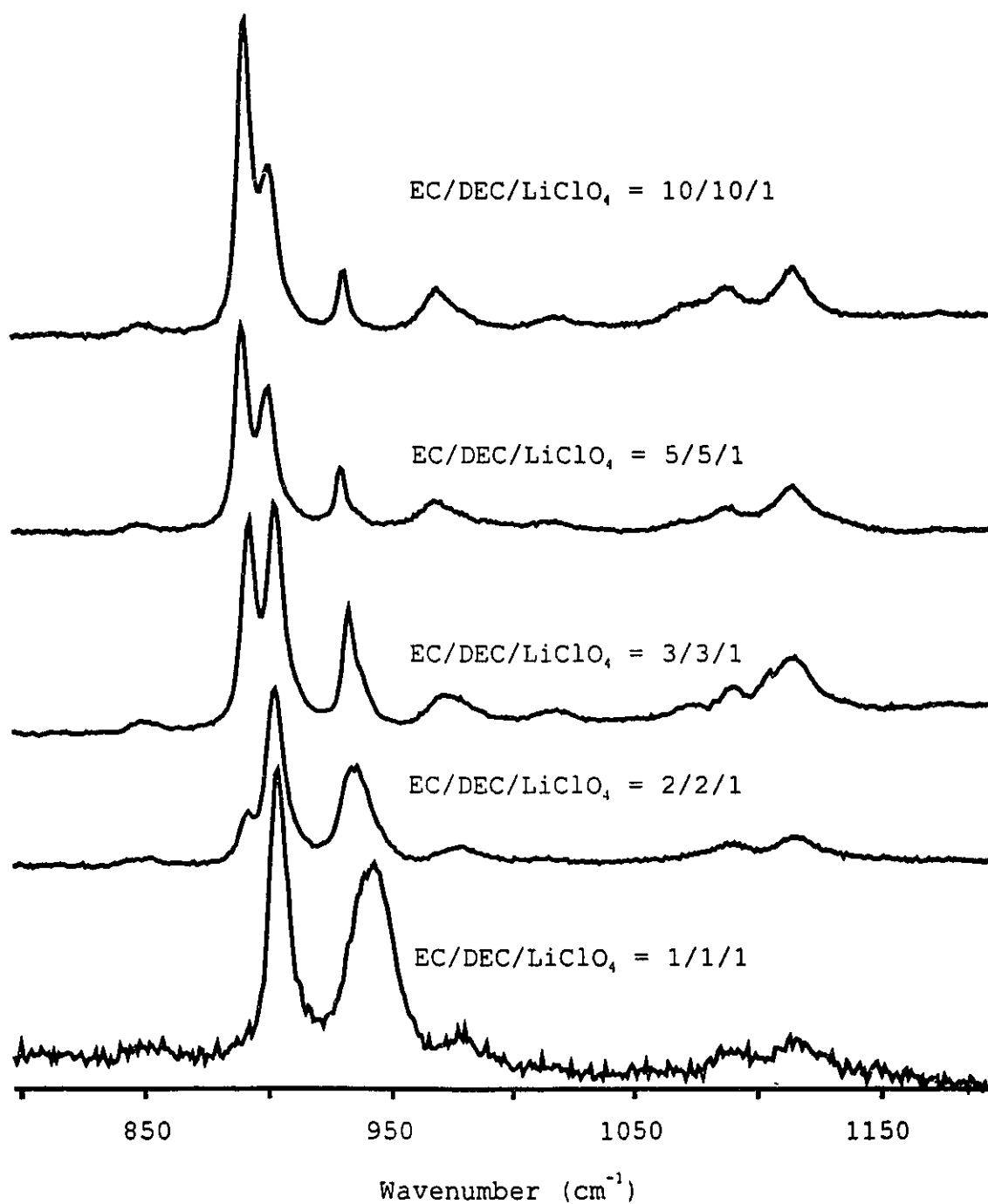
Figure 6.7: Raman spectra of EC/DEC/LiClO₄ electrolyte solutions with varying concentrations of lithium perchlorate over the range 800-1200 cm^{-1}

EC/DEC/LiClO$_4$ = 10/10/1

EC/DEC/LiClO$_4$ = 5/5/1

EC/DEC/LiClO$_4$ = 3/3/1

EC/DEC/LiClO$_4$ = 2/2/1

EC/DEC/LiClO$_4$ = 1/1/1

1200   1300   1400   1600   1800

Wavenumber (cm^{-1})
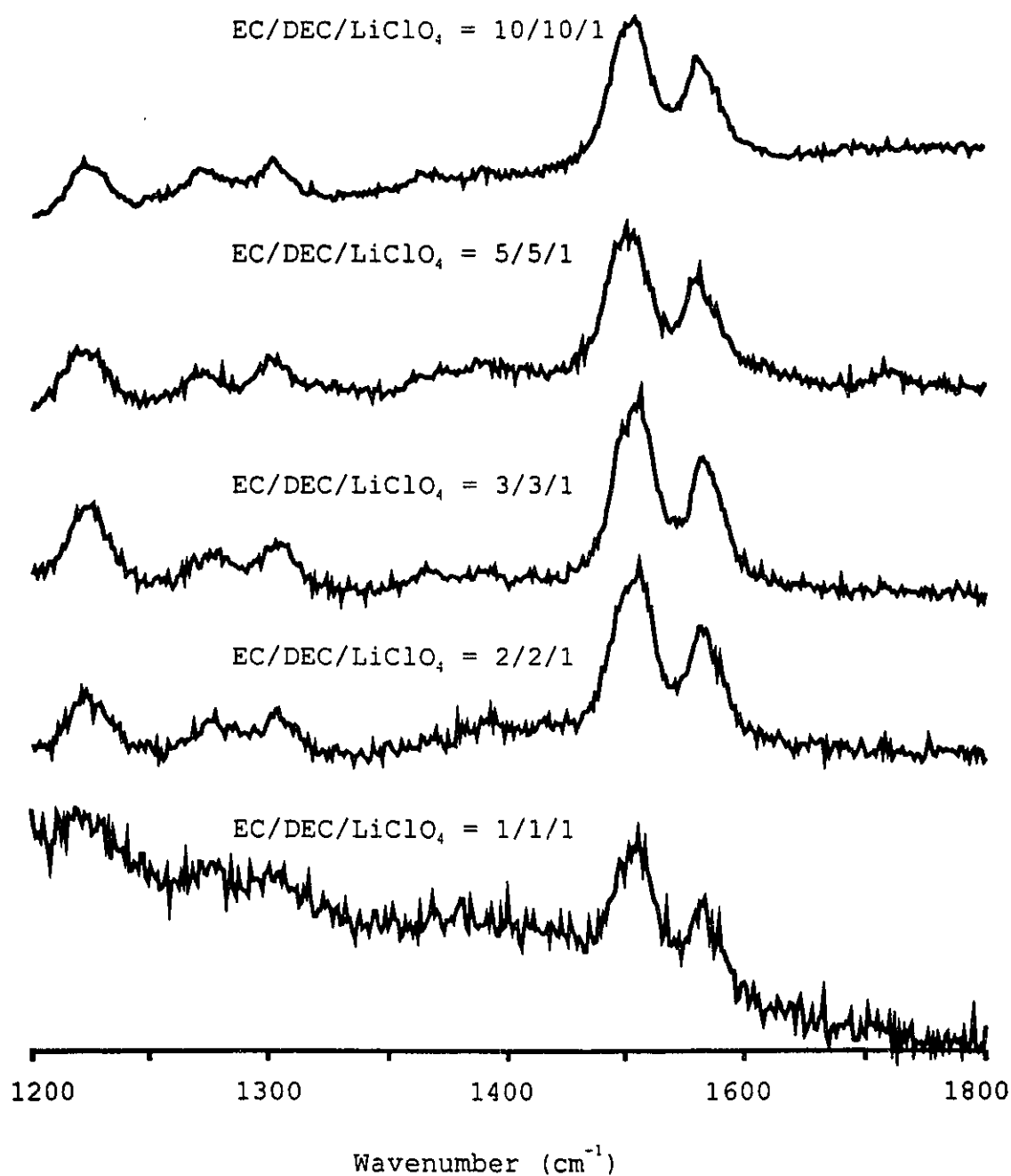
Figure 6.8: Raman spectra of EC/DEC/LiClO$_4$ electrolyte
solutions with varying concentrations of
lithium perchlorate over the range 1200-1800 cm^{-1}

EC/DEC/LiClO$_4$ = 10/10/1

EC/DEC/LiClO$_4$ = 5/5/1

EC/DEC/LiClO$_4$ = 3/3/1

EC/DEC/LiClO$_4$ = 2/2/1

EC/DEC/LiClO$_4$ = 1/1/1

1620   1700   1780   1860

Wavenumber (cm^{-1})
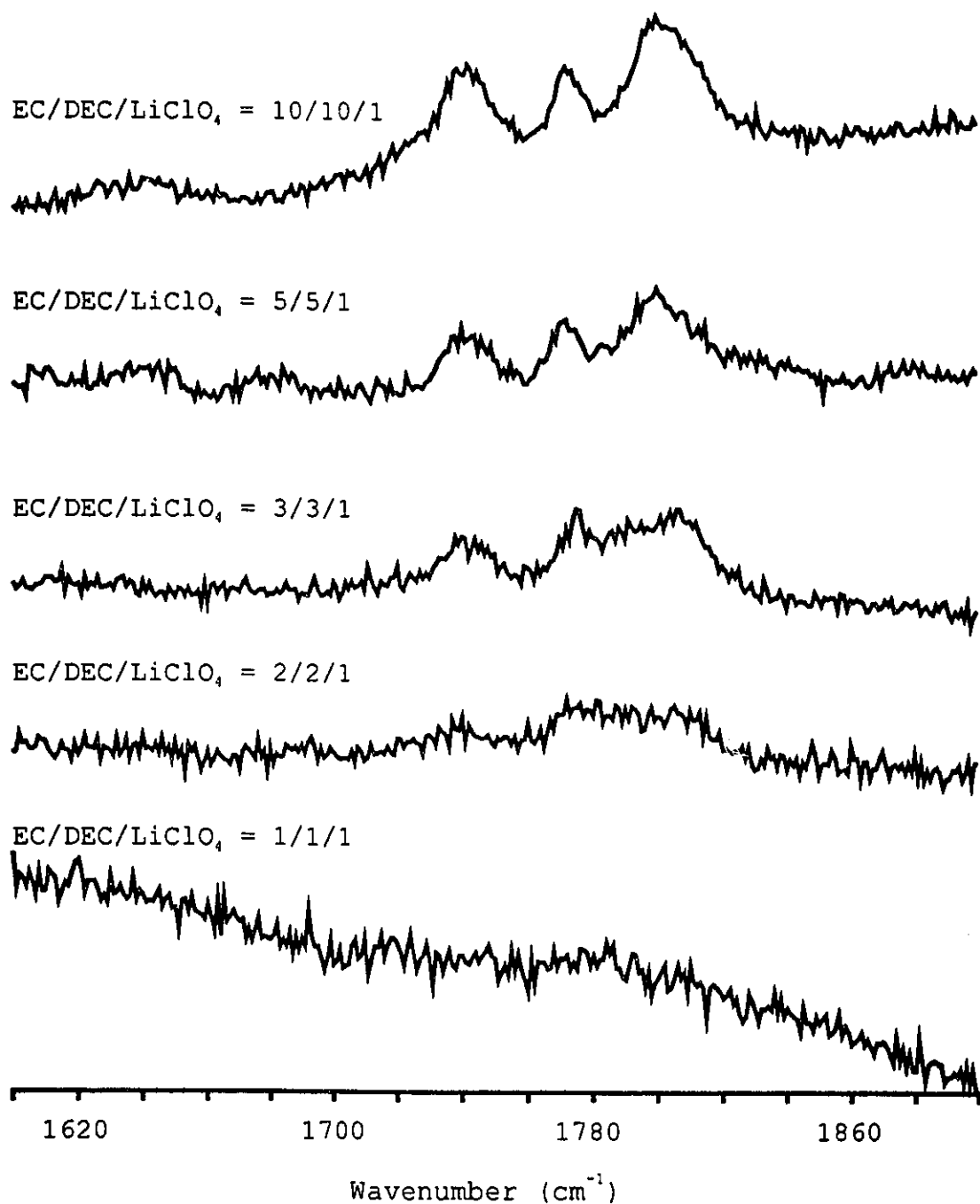
Figure 6.9: Raman spectra of EC/DEC/LiClO$_4$ electrolyte solutions with varying concentrations of lithium perchlorate over the range 1600-1900 cm^{-1}

EC/DEC/LiClO$_4$ = 10/10/1

EC/DEC/LiClO$_4$ = 5/5/1

EC/DEC/LiClO$_4$ = 3/3/1

EC/DEC/LiClO$_4$ = 2/2/1

EC/DEC/LiClO$_4$ = 1/1/1

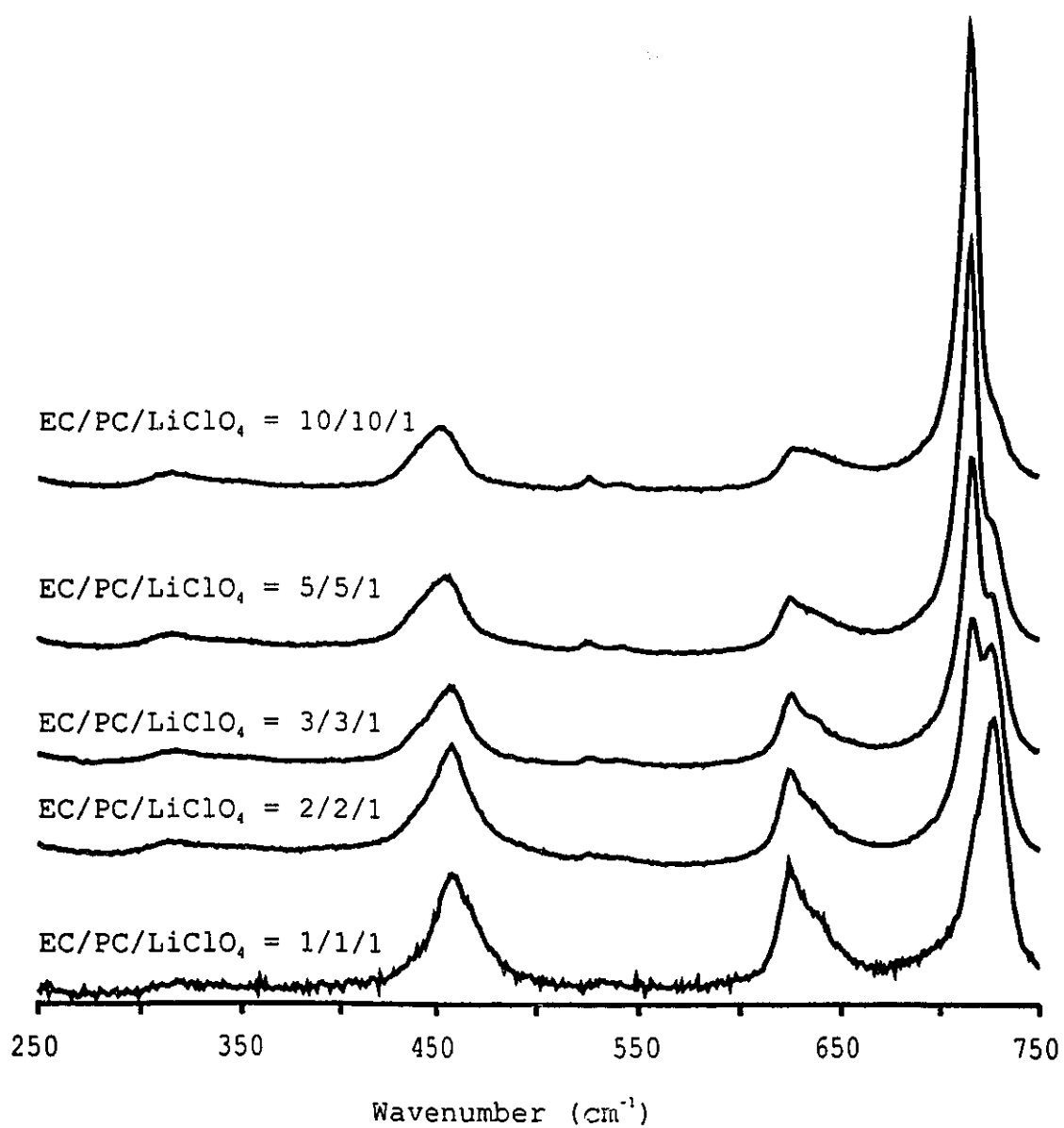2600   2700   2800   2900   3000   3100   3200

Wavenumber (cm-1)
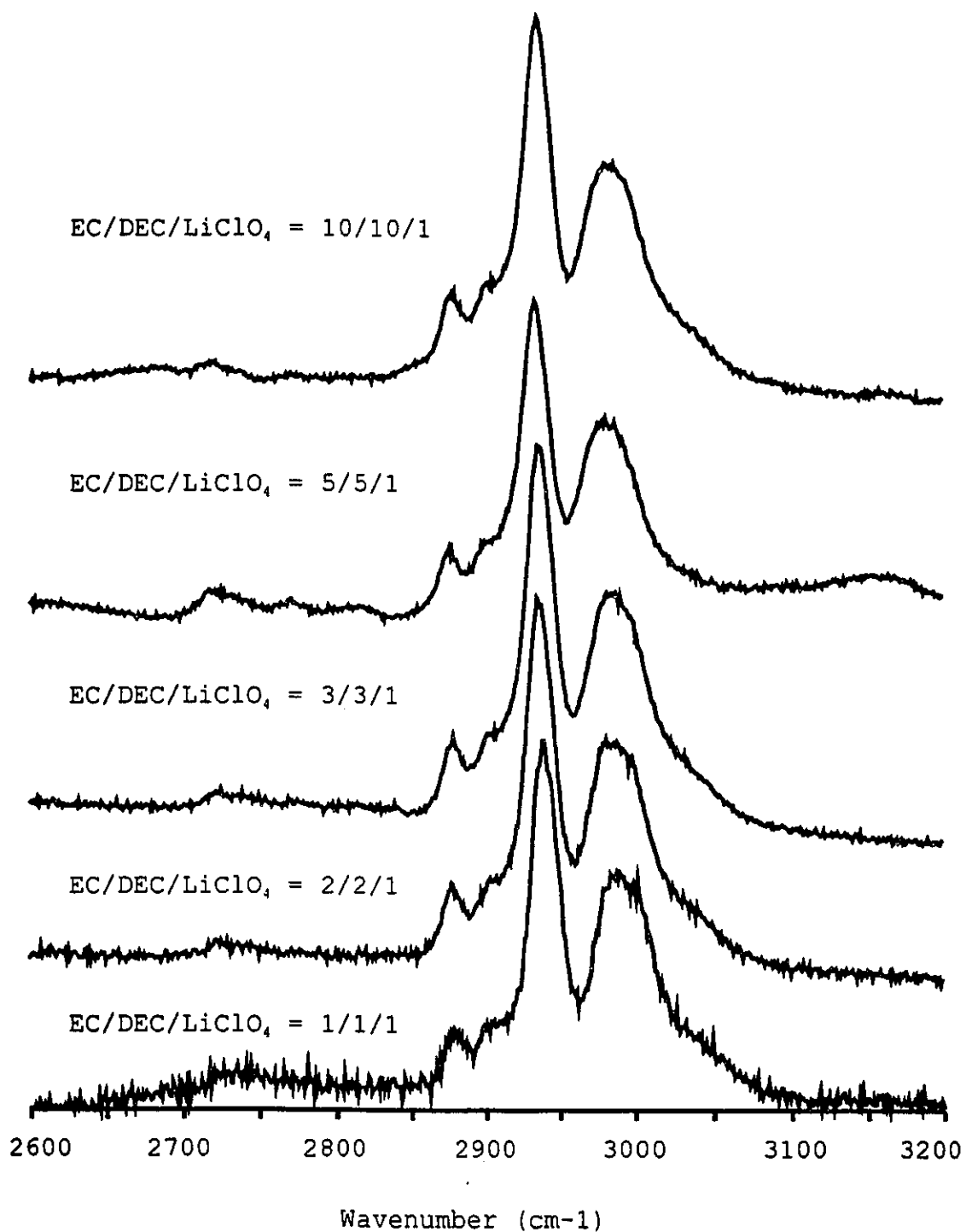
Figure 6.10: Raman spectra of EC/DEC/LiClO$_4$ electrolyte solutions with varying concentrations of lithium perchlorate over the range 2600-3200 cm^{-1}
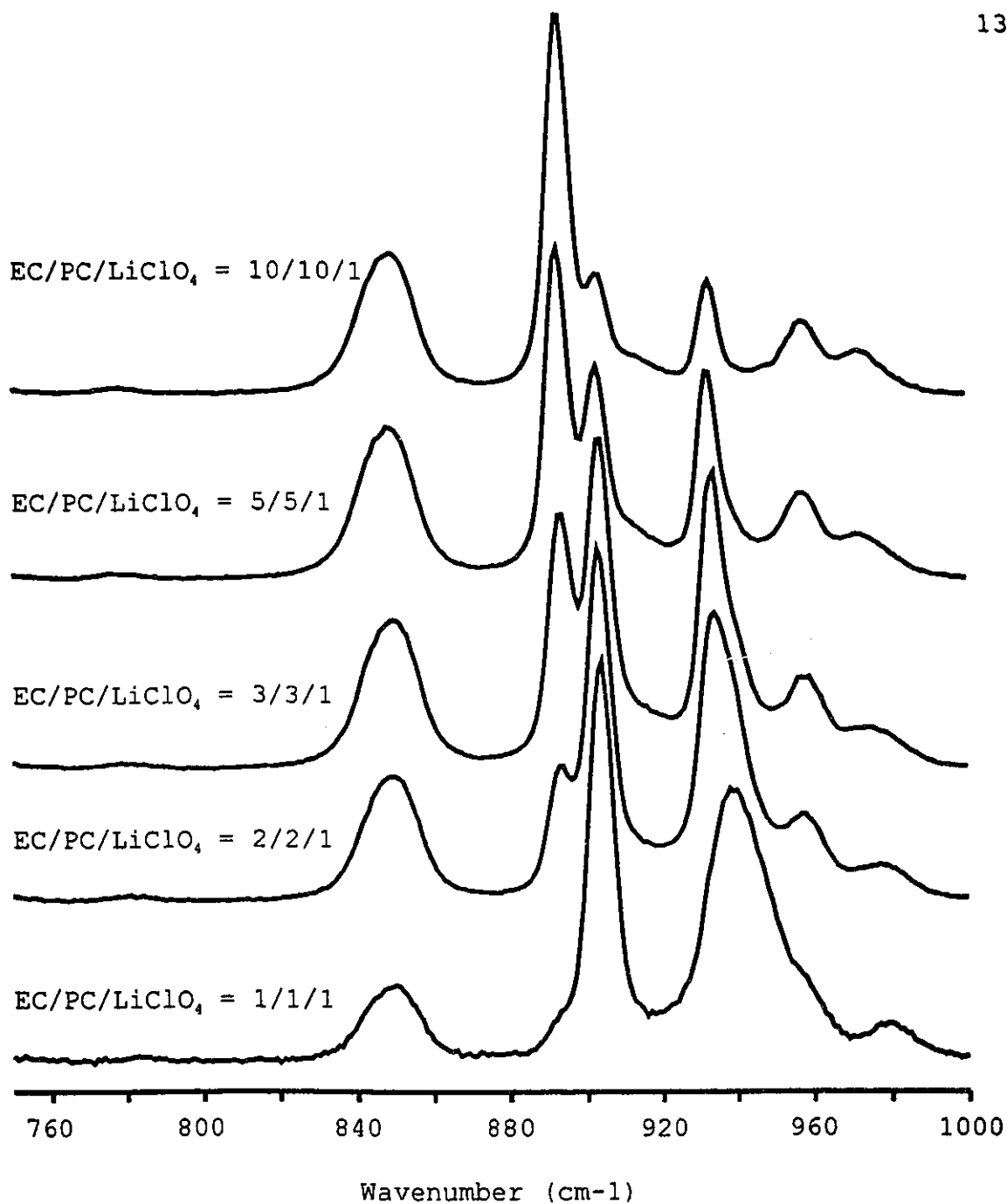
increase in lithium perchlorate concentration. This band is solely associated with EC since there are no bands belonging to DEC in this region. The band at 714 cm^{-1} shows a significant decrease in intensity as the concentration of lithium perchlorate increases while at the same time a band at 724 cm^{-1} becomes more intense with increasing salt concentration, however, the 724 cm^{-1} band in the EC/DEC/LiClO$_4$ does not become as intense as the 724 cm^{-1} band in the EC/PC/LiClO$_4$ spectra. There are two intense bands located at 894 cm^{-1} (EC ring breathing), Figure 6.7, and a band located at 903 cm^{-1} which is primarily a C-O-C bend of DEC. The symmetric stretch $v_1(a_1)$ of the perchlorate anion is as expected at 933 cm^{-1} along with the formation of bands that include the solvent-shared ion-pairs (938 cm^{-1}) and contact ion-pairs (944 cm^{-1}) at higher electrolyte concentrations, as discussed in detail in Chapter 4. The dynamic changes of the carbonyl stretches that occur in the Raman spectra with increasing lithium perchlorate concentration is the in the band shapes, Figure 6.9, frequencies at 1746(DEC) and 1794(EC). In fact, the carbonyl bands almost completely disappear at the highest concentration of lithium perchlorate salt. The observed vibrational frequencies in the region 2850-3100 cm^{-1}, Figure 6.10, are all H-C stretching modes. All of the H-C stretching modes are unaffected by the addition of lithium

perchlorate which is expected considering that the H-C bending modes were unaffected as well.

6.5 ELECTROLYTE SOLUTION STRUCTURAL CONCLUSIONS FROM THE RAMAN SPECTRA

The fact that the vibrational band shape of the hydrogen-carbon stretching modes in the region 2800-3200 cm^{-1}, do not change even at the highest concentration of lithium perchlorate indicates that the solvent-ion interaction is highly localized on the oxygen atoms. It can be said that there is no hydrogen bonding between the perchlorate anion oxygens and hydrogens of the solvent molecules. This is supported by the fact that hydrogen-carbon bending modes, in the region 1200-1300 cm^{-1}, are also unaffected by increase in lithium perchlorate concentration. In summary, the lithium cation is coordinating to the carbonyl oxygen. Consider for instance, the O=C-ring bending mode of EC located at 714 cm^{-1}, which clearly decreases in intensity with increasing lithium perchlorate concentration as the new band of the associated solvent molecule at 724 cm^{-1} gains in intensity. As the lithium perchlorate concentration increases, there are more cations available to which the oxygen can coordinate with. Therefore, as the salt concentration increases, the number of coordinated solvent

molecules that exist in the electrolyte increases. So that the bands attributed to the coordinated solvent-cation species increases in intensity at the expense of the uncoordinated solvent species.

REFERENCES

1. Morita, M.; Tachihara, F.; Matsuda, Y. *Electrochim. Acta,* **1988,** *33,* 239.

2. Tobishima, S.; Arakawa, M.; Yamaki, J. *Electrochim. Acta,* **1988,** *33,* 317.

3. Tobishima, S.; Okada, T. *J. Appl. Electrochim.,* **1985,** *15,* 467.

4. Tobishima, S.; Yamaji, A. *Electrochim. Acta,* **1985,** *29,* 267.

5. Tobishima, S.; Yamaji, A.; Okada, T. *Electrochim. Acta,* **1984,** *29,* 1471.

6. Tobishima, S.; Okada, T. *Electrochim. Acta,* **1984,** *30,* 1715.

7. Arakawa, M.; Tobishima, S.; Hirai, T.; Yamaji, J. *J. Power Sources,* 1987, *20,* 293.

8. Hyodo, S.; Okabayashi, K. *Electrochim. Acta,* **1989,** *11,* 1551.

9. Hyodo, S.; Okabayashi, K. *Ibid.* 1557.

CHAPTER 7

LITHIUM CATION COORDINATION NUMBER AND TRANSPORT

PROPERTIES

7.1 SOLVATION NUMBER OF THE LITHIUM CATION

In the electrolyte solutions discussed, each lithium cation (Li^+) will be surrounded by multiple solvent molecules. An important consequence of solvation number is that the power of a lithium battery depends on the mobility of the lithium cation. The lithium cation binds to the components of the electrolyte solution so that the conductivity of an electrolyte solution is affected by the binding strength of the lithium cation to solvent molecules, or as discussed in Chapter 4, the binding to the anion forming ion-pairs. The number and position of solvent molecules around the lithium cation will depend upon steric or van der Waals interactions between the solvent molecules that will minimize the interaction between the solvent molecules. Considering that each solvent molecule will be competing for charge around the cation, carbonyl-cation binding strength per molecule is reduced as each additional solvent is added. In an electrolyte solution, the measured coordination number will be the average of a statistical distribution of complexes with different coordination numbers which occur in solution at any moment in time. The orientation of the solvent molecules will depend upon the temperature and density of the solvent and the attraction to Li^+.
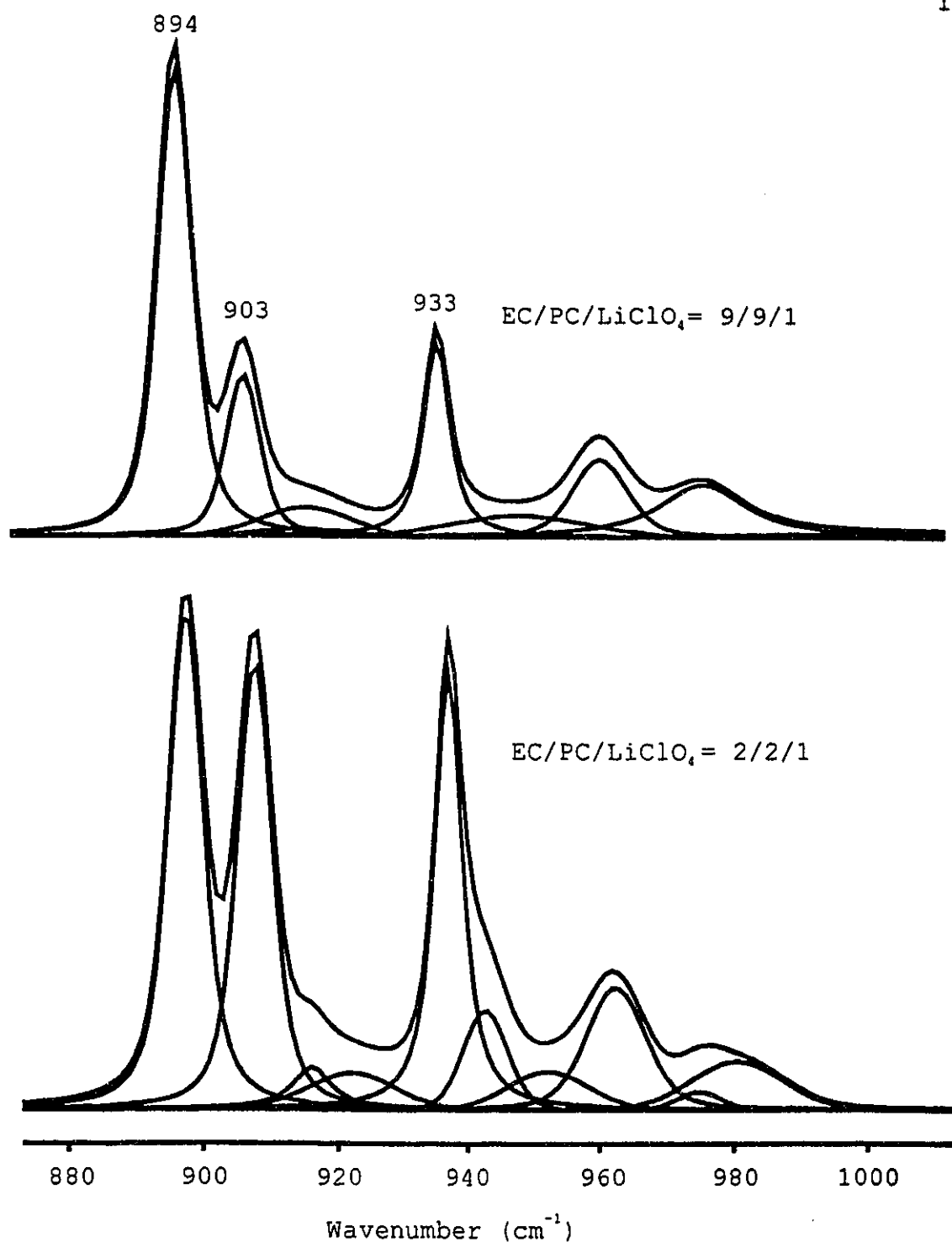
Figure 7.1 Band analysis using the Voigt curve fitting routine over the spectral region 850-1050 cm^{-1} for the binary-solvent solutions EC/PC/LiClO$_4$ = 2/2/1 and EC/PC/LiClO$_4$ = 9/9/1

The band analysis of the experimental Raman spectra was carried out using the Voigt curve fitting routine from the program Spectra Calc, and an example is shown in Figure 7.1. The program provided band deconvolution and integrated intensities. The coordination number of the lithium cation was calculated by two different methods: First, using integrated intensities following the method described by Irish *et. al.*[1,2], then by using *ab-initio* quantum mechanical method.

The procedure to calculate solvation number using experimental Raman spectra requires an internal intensity standard, i.e., a Raman band whose intensity and shape remains unaffected by the addition of salt. Ideally, the Raman band should be in a separate spectral window, clearly isolated from the bands of interest. A band at 1224 cm^{-1} (C-C stretching mode of EC) of EC was found to fulfill the above requirements. The 1224 cm^{-1} band is relatively isolated from the rest of the bands in the spectrum. Upon the addition of $LiClO_4$ to the solvent system, the reference band retained a symmetric, single band profile even when the concentration of $Li^+ClO_4^-$ exceeded 6M (a solvent/solvent/salt ratio of 1/1/1).

The relative integrated intensities I_{894}/I_{1224}, I_{903}/I_{1224}, and I_{total}/I_{1224} (total = 894+903) are plotted *vs.*
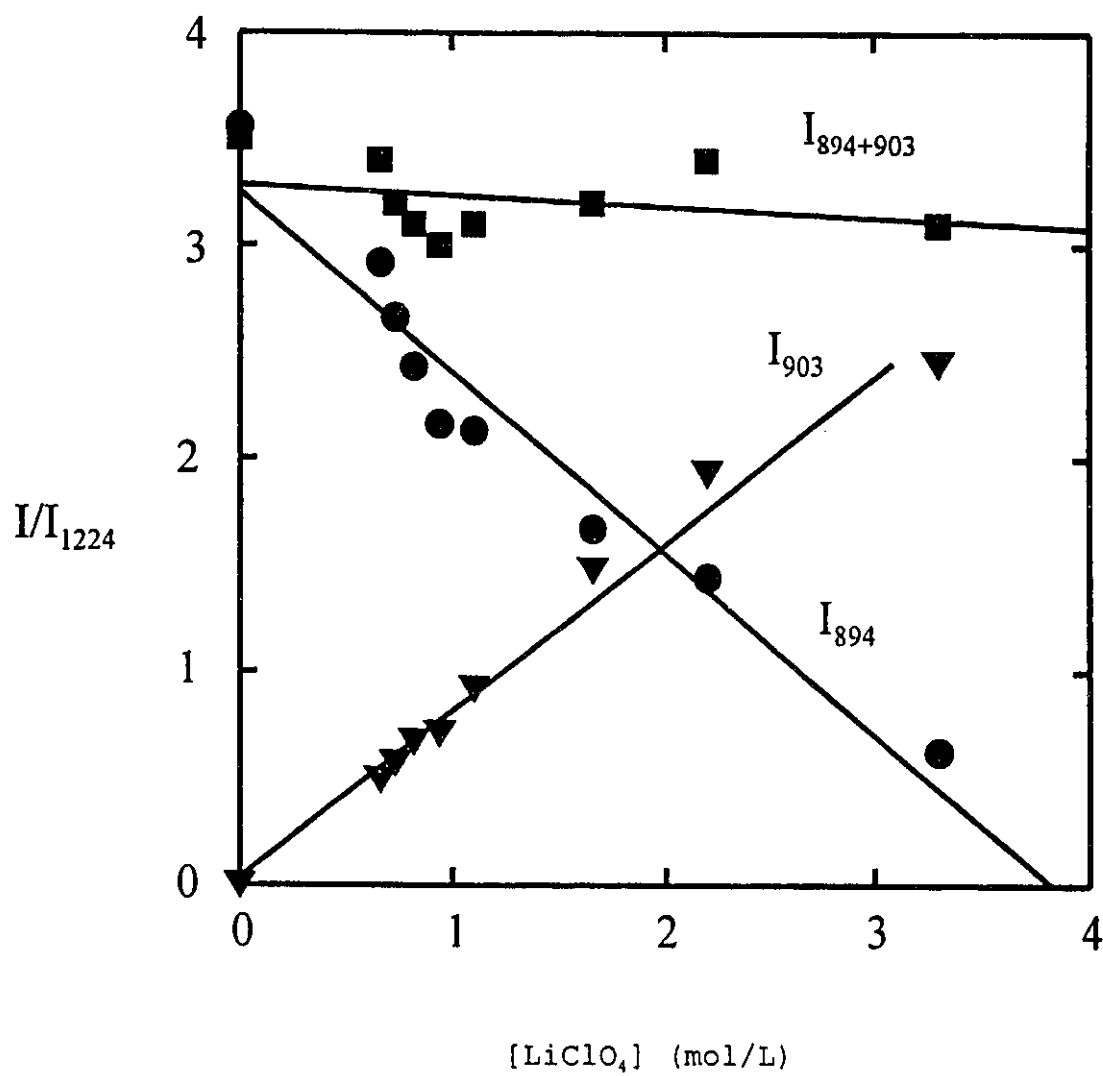
Figure 7.2 Relative integrated intensity ratios: I_{894}/I_{1224}, I_{903}/I_{1224} and I_{total}/I_{1224} plotted vs $LiClO_4$ concentration

concentration of LiClO$_4$ as shown in Figure 6.12. The
intensity of the 894 cm^{-1} band decreases while a new band at
903 cm^{-1} increases as LiClO$_4$ concentration increases as shown
in Figure 7.2. The assignment of the bands correspond to the
free solvent and the coordinated solvent molecules. The
total intensity, I_{total}/I_{1224} decreases slightly with
increasing salt concentration.

Relative integrated intensity data of the bands gave
the equation

$$I_T = 0.1437 I_b - 3.055$$

so that (where the J terms are defined by Irish et. al.[1,2])
J_f = 0.1347, J_b = 0.1573 and C$_{EC}$ 22.68 mol/kg. The
coordination number of the lithium cation which is
equivalent to the average ligand number of lithium, or n_s,
is defined as

$$n_s = C_b/C_{Li} = I_b/(C_{Li} J_b)$$

A coordination number from 4.5 to 6.2 is suggested as
tabulated in Table 7.1.

Table 7.1 Calculation of solvation number on Li$^+$

LiClO$_4$ mol/kg	I_b	I_T	C_b/mol/kg	$\bar{n}_s$
0.52	0.49	3.41	3.11	5
0.58	0.57	3.24	3.60	5
0.66	0.67	3.10	4.22	5
0.75	0.71	2.87	4.50	5
0.88	0.92	3.13	5.81	6·
1.05	1.17	3.45	7.45	6
1.31	1.48	3.15	9.45	6
1.75	1.93	3.37	12.25	6
2.63	2.45	3.07	15.52	5
5.26	3.80	3.80	24.20	4

The binding of ethers and acetaldehyde to the lithium cation have been studied using *ab-initio* methods with the D95V** basis set and Hartree-Fock theory, a coordination number of between 4 and 6 was calculated[3]. In this work the calculation of the solvation number of EC around Li$^+$ was accomplished by using the Hartree-Fock 6-31G basis set.

The first step was to decide upon the position of the lithium cation with respect to EC. Intuitively, the lithium cation would expected to be coordinated to the carbonyl oxygen. To support these assumptions, the calculated charges

are listed in Table 7.2 for the atoms of EC.

Table 7.2 Calculated charges of EC using various basis sets at the Hartree-Fock level of theory. Geometry based upon Figure 5.1.

Basis set	O1	C2	O3	C5	H7
6-31G	-0.50	1.04	-0.68	-0.02	0.22
6-31+G	-0.54	0.84	-0.47	-0.14	0.23
6-31G*	-0.55	1.03	-0.60	-0.04	0.20
6-31+G*	-0.59	1.00	-0.51	-0.13	0.21
6-311G	-0.45	0.90	-0.59	-0.06	0.21
6-311G**	-0.43	0.68	-0.40	-0.05	0.12
6-311++G**	-0.44	0.55	-0.22	-0.16	0.16

According to the calculated charges, it appears in some cases that the ring oxygen is the more electronegative of the atoms in EC. However, the highest level of theory used (HF/6-311++G**) predicts the carbonyl oxygen to be the most electronegative. According to the results from the 6-311++G** basis set, the position of the lithium cation was assumed to be on the carbonyl oxygen. The minimum energy structure corresponds to the lithium cation bound to the carbonyl oxygen. To confirm these conclusions, calculations were performed with the Li⁺ attached to one of the ring

oxygens and the carbonyl oxygen in a bidentate planar coordination geometry. This resulted in a much higher energy structure. The last possible coordination geometry, where the Li$^+$ is located above the EC molecular plane and in the centre of the three oxygens. Calculations of the latter resulted in an optimization that did not converge and can be disregarded.

The primary solvation shell around the EC molecules usually includes as many as six or more ligands. The number of EC molecules which can coordinate the lithium cation will be determined using an approximate enthalpy of reaction for coordination.

$$\Delta H_r = E[Li^+(EC)_n] - E[Li^+(EC)_{n-1}] - E(EC)$$

Where E represents the ground state calculated energies, n is the number of solvent molecules, and ΔH_r is the enthalpy of the coordination reaction. The coordination reaction that corresponds to the enthalpy of reaction can be written as:

$$Li^+(EC)_{n-1} + EC \rightarrow Li^+(EC)_n$$
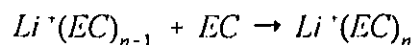
For the coordination calculations, specific symmetries were imposed. For Li$^+$(EC)$_2$ the EC ligands were positioned 180° from each other. For Li$^+$(EC)$_3$ the EC molecules form a trigonal planar; tetrahedral for Li$^+$(EC)$_4$, trigonal bipyramidal for Li$^+$(EC)$_5$, and octahedral for Li$^+$(EC)$_6$. The

orientation of the molecules in each of the coordinated systems was selected to give the highest symmetry. Results for the calculated heats of formation for complexes of EC with Li$^+$ are presented in Table 7.3.

Table 7.3 Calculated heats of formation for the coordination of EC to Li$^+$ using the HF/6-31G basis set.

Reactions	ΔH(kJ/mol)	Li$^+$-O distance
Li$^+$ + (EC) $\rightarrow$ Li$^+$(EC)	-247.9	1.74
Li$^+$(EC) + (EC) $\rightarrow$ Li$^+$(EC)$_2$	-190.1	1.78
Li$^+$(EC)$_2$ + (EC) $\rightarrow$ Li$^+$(EC)$_3$	-112.2	1.85
Li$^+$(EC)$_3$ + (EC) $\rightarrow$ Li$^+$(EC)$_4$	-62.0	1.93
Li$^+$(EC)$_4$ + (EC) $\rightarrow$ Li$^+$(EC)$_5$	7.9	2.07
Li$^+$(EC)$_5$ + (EC) $\rightarrow$ Li$^+$(EC)$_6$	2.5	2.16
Li$^+$(EC)$_6$ + (EC) $\rightarrow$ Li$^+$(EC)$_7$	154.1	

The calculations on the complexes were carried out for complexes containing up to seven EC ligands. The heat of formation of the first four complexes result in negative energy values suggesting that the formation of Li$^+$(EC)$_4$ is favourable. The calculations of the formation of the complex containing five and more EC ligands becomes energetically unfavourable. These results suggest that a coordination

number of four is preferred. This corresponds well with the conclusions derived from Raman experimental evidence described earlier as well as other published Raman, and infrared spectroscopy results which have found coordination numbers between four and five[1,4].

7.2 SELECTIVE SOLVATION IN BINARY SOLVENT ELECTROLYTE SOLUTIONS

The problem of the local structure around the lithium cation in of mixed solvent electrolyte solutions is not well understood. When dealing with electrolyte solutions comprised of two solvents, selective solvation of the lithium cation may occur. The study performed by Hyodo and Okabayashi[8,9] concluded that selective solvation was not confirmed in the EC/PC/LiClO$_4$ binary solvent solution. Once again the problem can be approached using quantum chemical *ab-initio* calculations to provide insight into the selective solvation problem.

The calculations were performed on the four solvent molecules studies: EC, PC, DMC, and DEC. Calculations were approached by taking the results from the *ab-initio* calculations that were performed on the solvent molecules in Chapter 5. The starting geometry used was the results from the geometry optimizations from the HF/6-311++G** basis set.

The lithium cation was positioned in a 180º geometry with respect to the carbonyl group of each solvent molecule. Upon performing a full optimization, the lithium cation was allowed to move, in other words, the parameters for the bond length, angle, and dihedral angle were set as variables. Binding energies were calculated by subtracting the ground state energies of free solvent and free lithium cation from the singly coordinated Li⁺-solvent. Results from the calculations are presented in Table 7.4.

Table 7.4 Ground State energies (kJ mol⁻¹) calculations using HF/6-311++G** basis set, the Li⁺ energy (HF/6-311+G*) is calculated to be -18998.1672.

Solvent	Pure Solvent	Solvent + Li⁺	Solvation Energy
EC	-894337.9663	-913560.7960	-224.66251
PC	-996901.2550	-1016098.899	-199.47706
DEC	-1102467.818	-1121667.579	-201.59281
DMC	-897413.4443	-916602.0379	-190.42641

Experimentally, the binding of Li⁺ to water has been studied by high pressure mass spectroscopy[5] and to O(CH₃)₂ and formaldehyde by ion cyclotron resonance[6]. Blint found that the experimental results agreed closely to the calculated results with the HF/D95V** basis set for the binding energies of Li⁺ to water and O(CH₃)₂ and at the most

disagreed by 2 kcal/mol (8 kJ/mol). Using HF/D95V** basis set[4], the binding energy of Li⁺ to EC was calculated to be -52.0 kcal (-217.7 kJ/mol), while the calculation using the basis set HF/6-311++G** resulted in a binding energy of -53.6 kcal/mol(224.4 kJ/mol). The application of HF/6-311++G** should give satisfactory results for the relative binding energies of the solvents in this study. Results from the HF/6-311++G** calculations show that the single coordination of EC to Li⁺ is favoured over that of Li⁺ coordinating to PC by the amount of about 26 kJ/mol.

7.3 EXPERIMENTAL FOR CONDUCTIVITY AND VISCOSITY STUDIES

High Purity Lithium perchlorate, ethylene carbonate(EC), propylene carbonate(PC), diethyl carbonate(DEC), and dimethyl carbonate(DMC) were obtained from Fluka and used without further purification. The binary solvent mixtures containing equal molar amounts of EC/PC, EC/DEC, and EC/DMC were prepared. As all of these solvents are highly hydroscopic, they were stored over molecular sieves in an argon atmosphere dry box. Lithium perchlorate (Fluka) was dried at 160º under vacuum for 24h. In the dry box, the oxygen and moisture contents were less than 1 ppm. Electrolytes were prepared using the binary solvent mixtures with concentrations ranging from 0.3 mol/l of solvent

mixture to 6.0 mol/l. The resulting binary solvent mixture concentrations were chosen such that the molar amounts in each electrolyte worked out to be the ratios 1/1/1, 2/2/1, 3/3/1, 4/4/1, 5/5/1, 6/6/1, 8/8/1, 10/10/1, and 20/20/1 (solvent/solvent/lithium salt). This presentation of the binary solvent electrolyte concentrations serve to ease the interpretation of the results.

Conductivity measurements were recorded at 1000 Hz and 25°C with a Digibridge (GenRad Model 1658) having cell constant of 1. Viscosity measurements were carried out using a Brookfield model LVT dial viscometer. All measurements were recorded at constant temperature of 25 °C. The solutions with concentrations from 0.3 to 6.0 mol/l $LiClO_4$ were measured with the UL (ultra low) viscosity adapter at shear rates from 36.69 sec^{-1}. to 1.83 sec^{-1} depending on the viscosity of the electrolyte. A liquid is considered to be a Newtonian liquid when the viscosity is not affected by different shear rates. The solutions studied behaved as non-Newtonian liquids, this can be illustrated by the results obtained at different shear rates for a single solution. For instance, for the 1.05 mol/kg solution, when shear rates of 36.69 sec^{-1} and 14.68 sec^{-1} were applied, viscosities of 7.72 cP and 8.00 cP were measured respectively. The dependence of conductivity and viscosity on temperature was studied using the dial viscometer with a water jacket around

the sample chamber, the temperature was controlled with a Haake circulating bath. These measurements were carried out for the most efficient electrolyte only, which in this case is the 8/8/1 electrolyte or 0.8 M of $LiClO_4$. All of the conductivity and viscosity measured were measured in an argon environment as described in Chapter 2.

7.4 LITHIUM PERCHLORATE CONCENTRATION DEPENDENCE OF VISCOSITY AND CONDUCTIVITY IN BINARY-SOLVENT ELECTROLYTE SOLUTIONS

Viscosity and conductivity results for the binary-solvent electrolyte solution $EC/PC/LiClO_4$, where the molar ratio of EC and PC are 1:1, as a function of lithium perchlorate concentration are presented in Figures 7.3 and 7.4. Figures 7.5 and 7.6 (viscosity and conductivity data for the binary-solvent electrolyte solution $EC/DEC/LiClO_4$ where the molar ratio of EC and DEC are 1:1). Viscosity for the $EC/PC/LiClO_4$ electrolyte is observed to increase with increase in lithium perchlorate concentration. For lithium perchlorate concentrations from 0.33 M ($EC/PC/LiClO_4$ = 20/20/1) to 3.3 M ($EC/PC/LiClO_4$ = 2/2/1), viscosity changes from 3.82 cP to 147 cP. The electrolyte having $EC/PC/LiClO_4$ = 1/1/1 molar ratio (6.6 M) was a solid at room temperature thus viscosity data could not be collected at this high
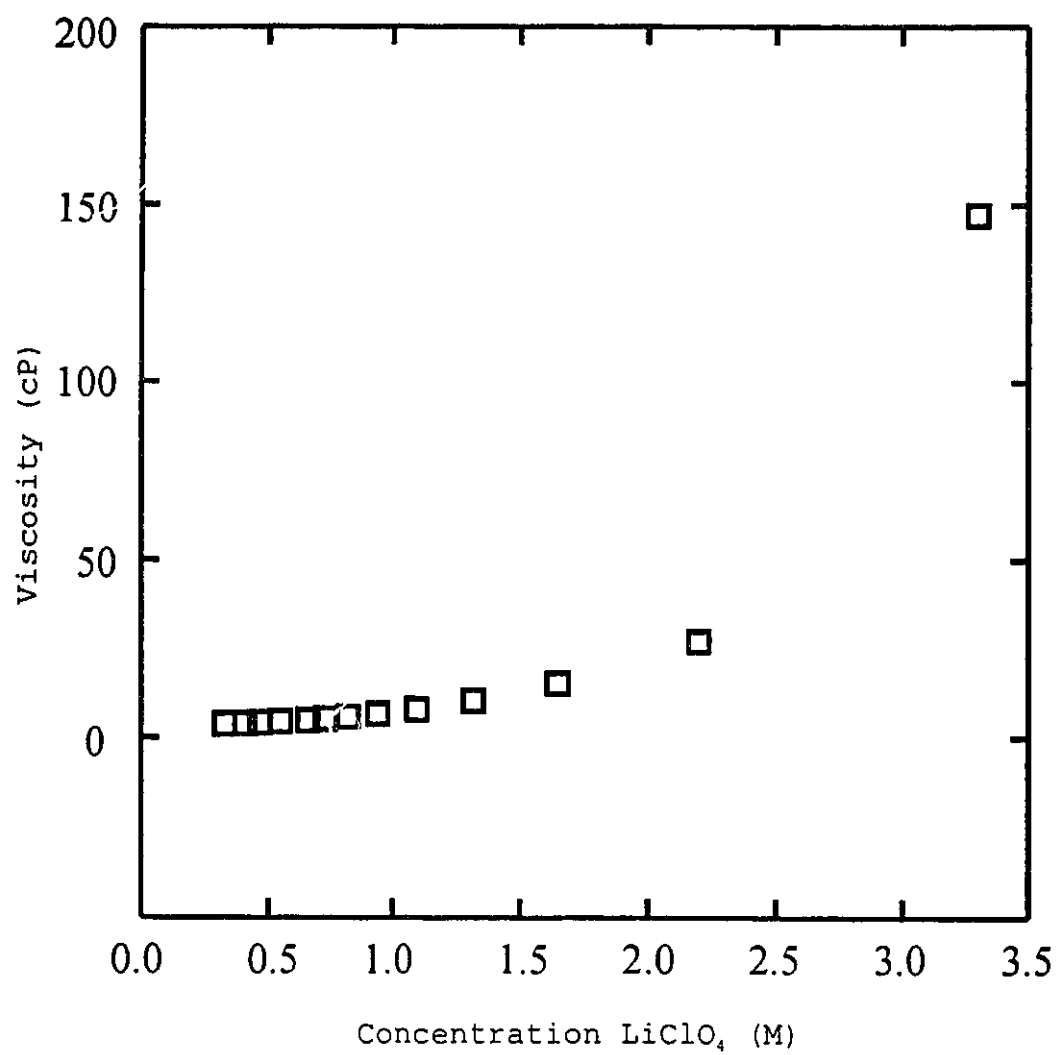
Figure 7.3 Concentration dependence of viscosity for the binary-solvent solution EC/PC/LiClO$_4$
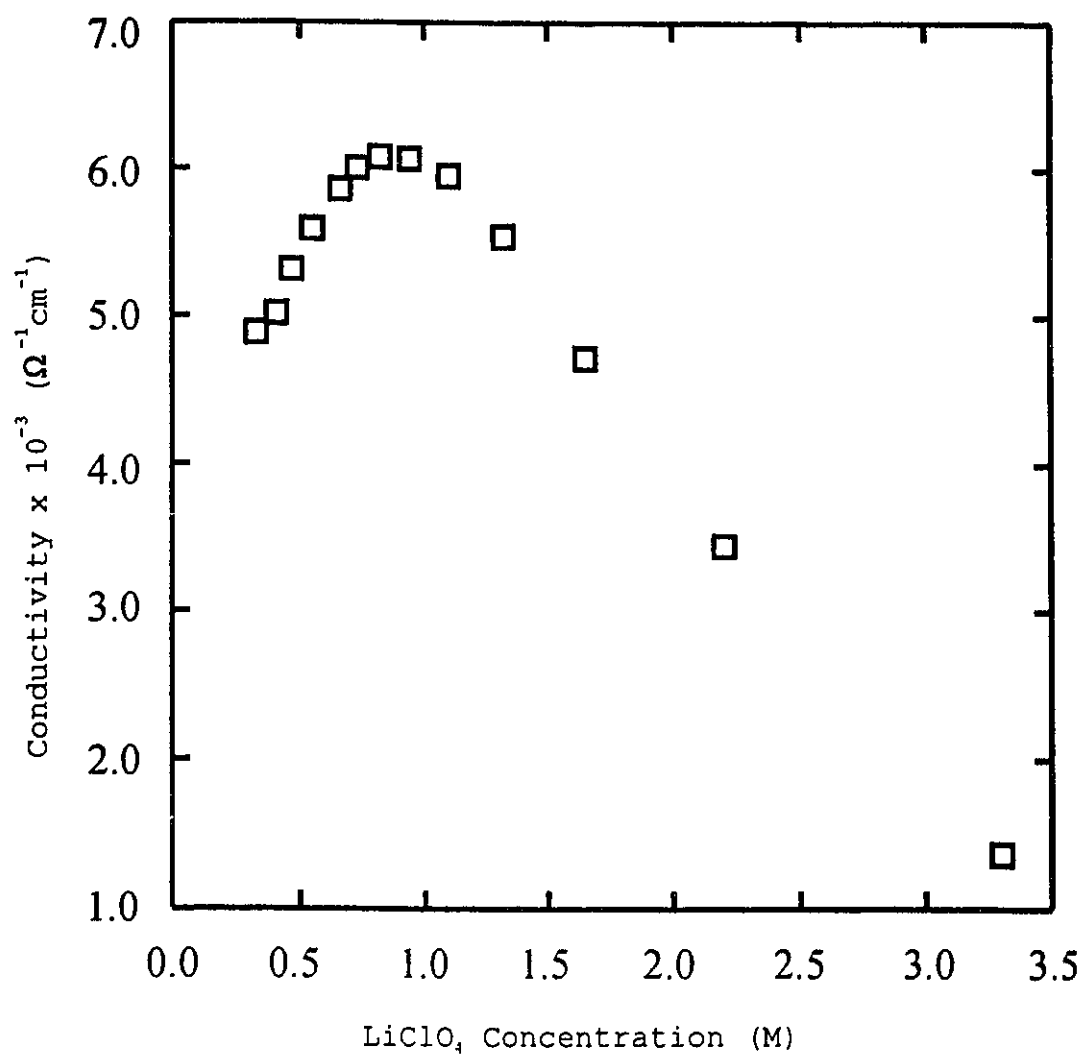
Figure 7.4 Concentration dependence of conductivity for the binary-solvent solution EC/PC/LiClO$_4$
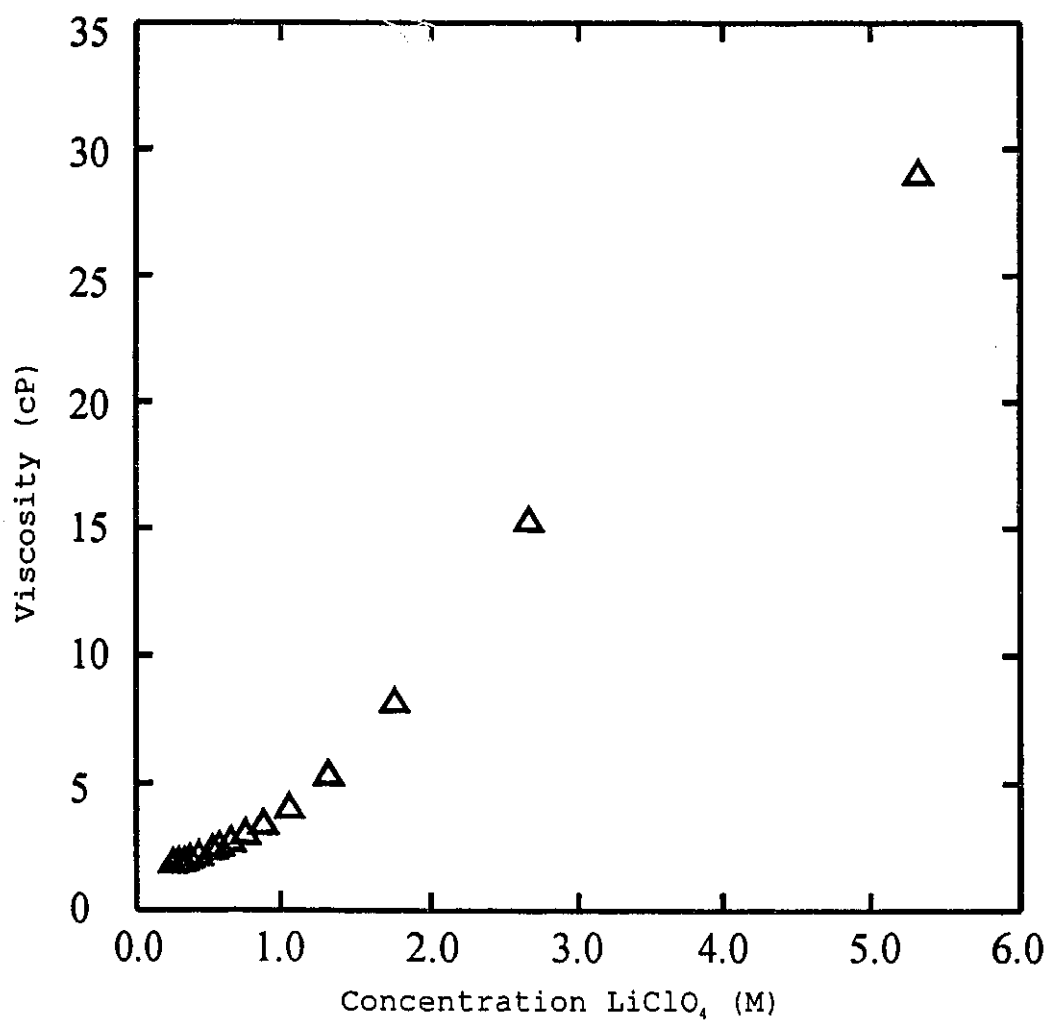
Figure 7.5 Concentration dependence of viscosity for the binary-solvent solution EC/DEC/LiClO$_4$
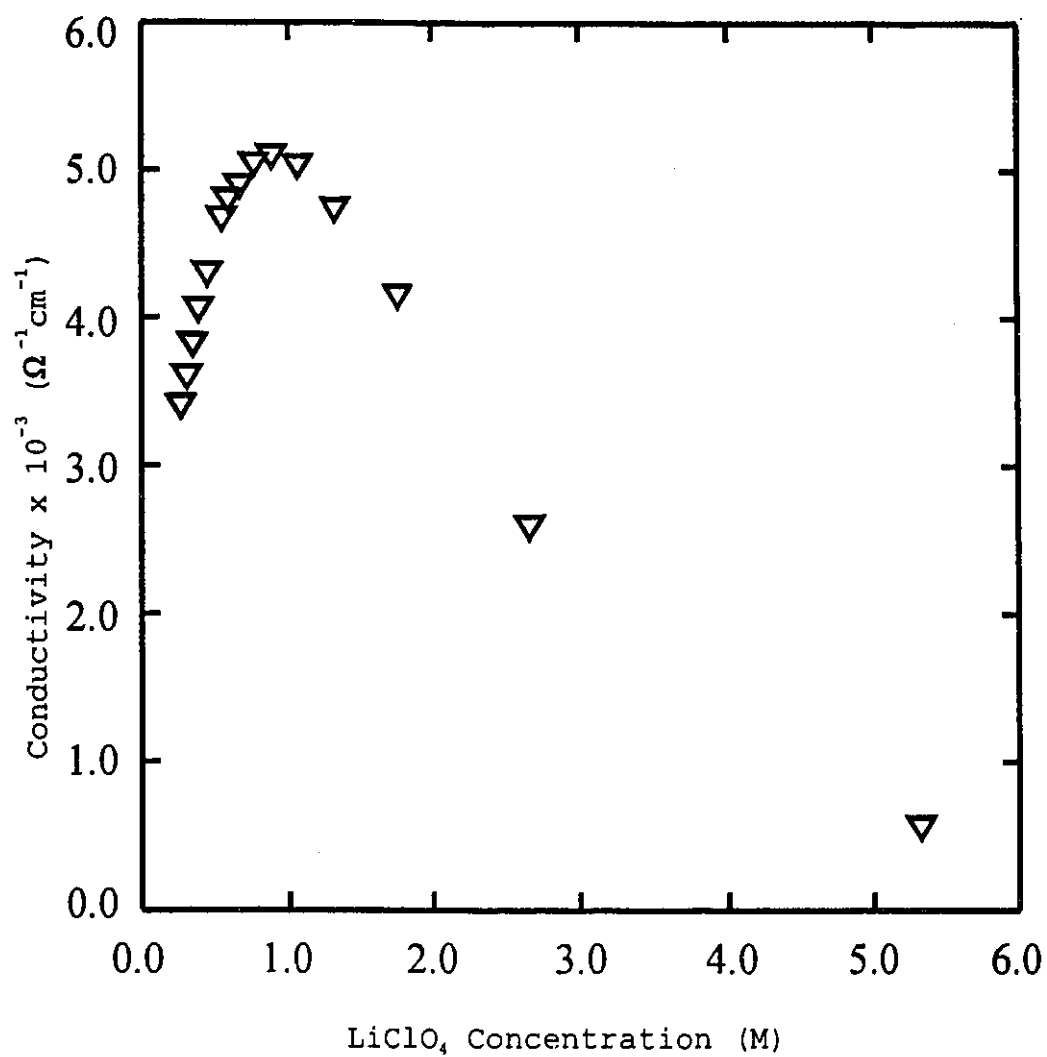
Figure 7.6 Concentration dependence of conductivity for the binary-solvent solution EC/DEC/LiClO$_4$

concentration. The viscosity data for the EC/DEC/LiClO$_4$, Figure 7.5, electrolyte behaved in the same manner as the EC/PC/LiClO$_4$ electrolyte, where the viscosity increased with increased lithium perchlorate concentration. For lithium perchlorate concentrations from 0.26 M (EC/DEC/LiClO$_4$ = 20/20/1) to 5.3 M (EC/DEC/LiClO$_4$ = 1/1/1), viscosity changes from 1.84 cP to 29.0 cP.

Conductivity, Figure 7.4, increases with increasing lithium perchlorate concentration in the EC/PC/LiClO$_4$ electrolyte until a maximum of 6.1 kΩ^{-1}cm^{-1} is reached at 0.82 M LiClO$_4$ (EC/PC/LiClO$_4$ = 8/8/1). After which the conductivity decreases rapidly between 0.82 M and 3.3 M to a minimum of 1.4 kΩ^{-1}cm^{-1}. In a similar fashion, the conductivity of EC/DEC/LiClO$_4$, Figure 7.6, increases with increasing lithium perchlorate concentration until a maximum of 5.1 kΩ^{-1}cm^{-1} is obtained at a lithium perchlorate concentration of 0.88 M (EC/DEC/LiClO$_4$ = 6/6/1). Once again the conductivity drops off rapidly between the lithium perchlorate concentrations of 0.88 M and 5.32 M reaching a minimum conductivity of 0.57 kΩ^{-1}cm^{-1}

It is informative to take a close look at the curve from the EC/PC/LiClO$_4$ viscosity data. Notably, the viscosity remains relatively constant from 0.33 M (EC/PC/LiClO$_4$ = 20/20/1) to 0.82 M (EC/PC/LiClO$_4$ = 8/8/1). The change in viscosity over this range is approximately 2 cP. For lithium

perchlorate concentration range between 0.82 M and 3.3 M the viscosity increases form 5.9 cP to 147 cP, giving a total change in viscosity of approximately 141 cP. This rapid increase in viscosity may be attributed to the association of Li^+ cations with ClO_4^- anions producing the formation of solvated complexes[7]. Evidence for the formation of these solvated complexes can be provided by the conductivity measurements and Raman spectroscopy. When lithium perchlorate is added to the solvent mixtures, the dissociated Li^+ are associated with individual EC and PC molecules. As these associated species form, the ions are accommodated in the voids available in the solvent, which contributes to the overall structural enhancement[8]. As mentioned, the conductivity increases with increased lithium perchlorate concentration until a maximum is obtained at 0.82 M ($EC/PC/LiClO_4$ = 8/8/1) lithium perchlorate. This can be qualitatively explained as resulting from a favourable combination of the high dielectric constant binary solvent along with the small change in viscosity in this binary system[9]. With the high dielectric binary solvent, lithium perchlorate will have a large degree of ion dissociation. Increase of lithium perchlorate concentration beyond 0.82 M causes the conductivity to drop off quickly. This decrease in ionic conductivity is due to the influence of viscosity on the mobility of Li^+ which reduces the mobility and the

number of Li· charge carriers. An increase in viscosity is attributed to the formation of ion pairs[10,11] and ion aggregates evidence is supported by the Raman spectroscopic data.

The viscosity data from the EC/DEC/LiClO$_4$ tells a different story from that of the EC/PC/LiClO$_4$ electrolyte. The viscosity remains relatively constant over a greater range than EC/PC/LiClO$_4$, from 0.26 M (EC/DEC/LiClO$_4$ = 20/20/1) to 1.32 M (EC/DEC/LiClO$_4$ = 4/4/1) the change in viscosity over this range is approximately 3.5 cP. For lithium perchlorate concentration range between 1.32 M and 5.32 M the viscosity increases form 5.30 cP to 29.0 cP, giving a total change in viscosity of approximately 23.7 cP.

7.5 TEMPERATURE DEPENDANCE OF VISCOSITY AND CONDUCTIVITY IN BINARY-SOLVENT ELECTROLYTES SOLUTIONS

It is known that aprotic solvents show high permittivities, low viscosities, and strong temperature dependence[12]. The performance of the electrolytes over a large temperature range is of interest in practical applications. Results for the temperature dependence of viscosity and conductivity are presented in Figures 7.7-7.10. Data was collected over the temperature range of −30
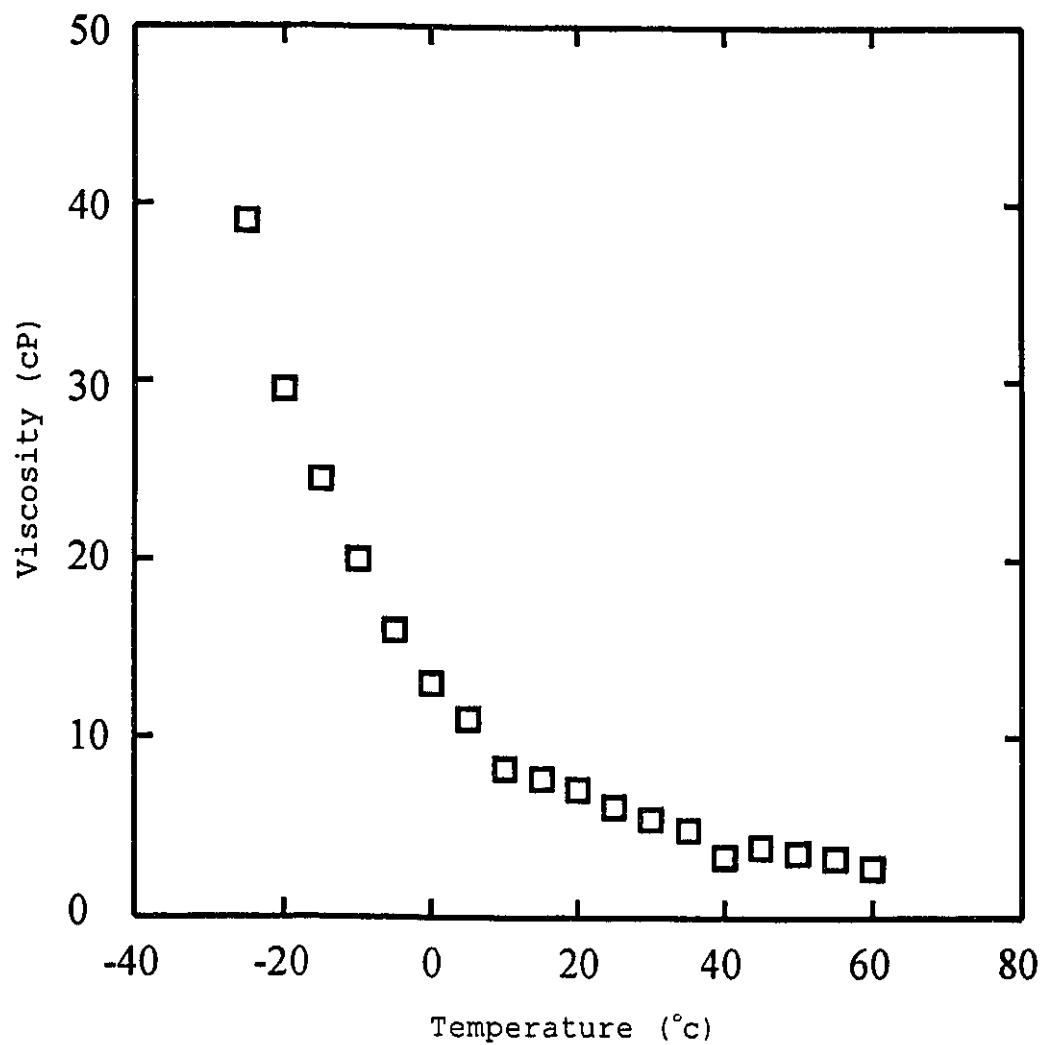
Figure 7.7 Temperature dependence of viscosity for the binary-solvent solution EC/PC/LiClO₄
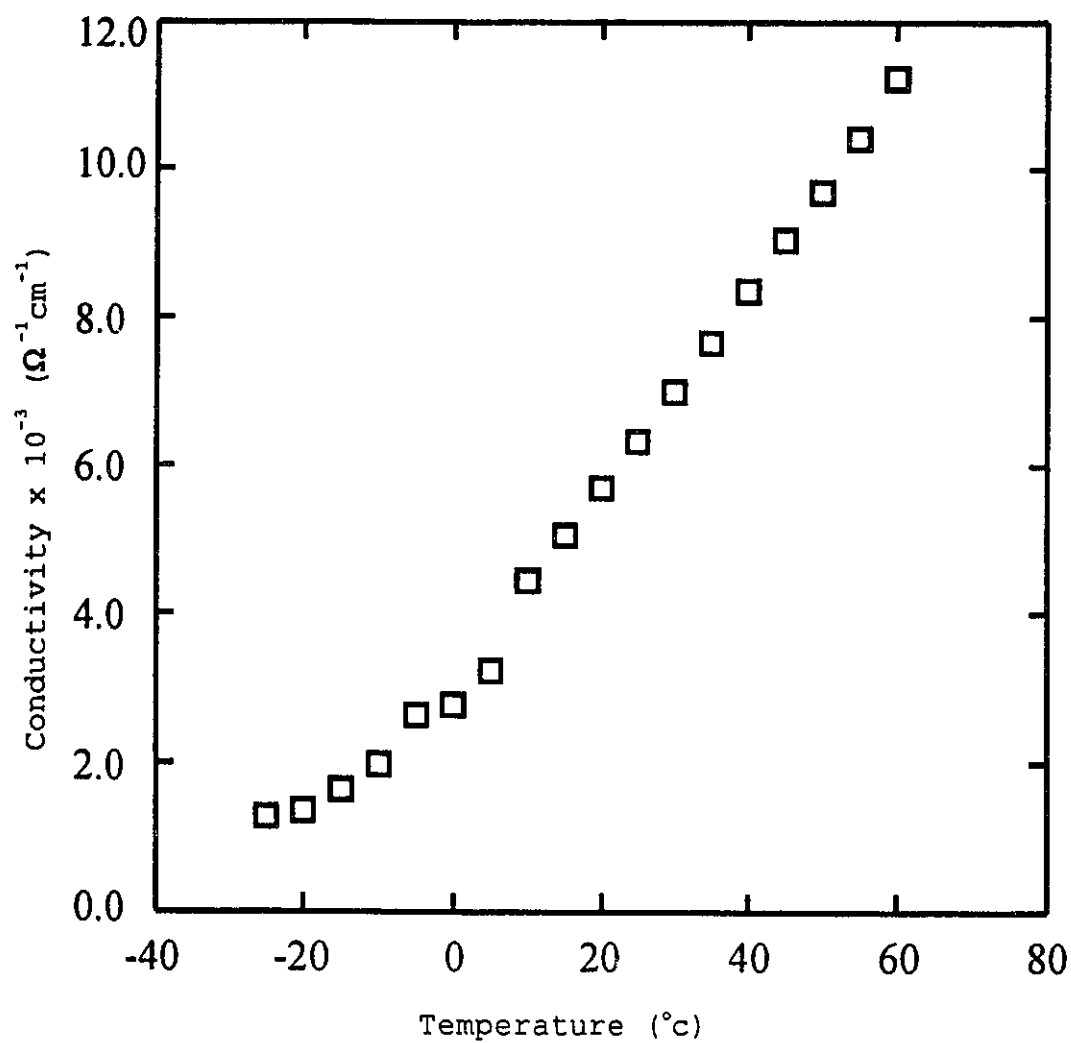
Figure 7.8 Temperature dependence of conductivity for the binary-solvent solution EC/PC/LiClO$_4$
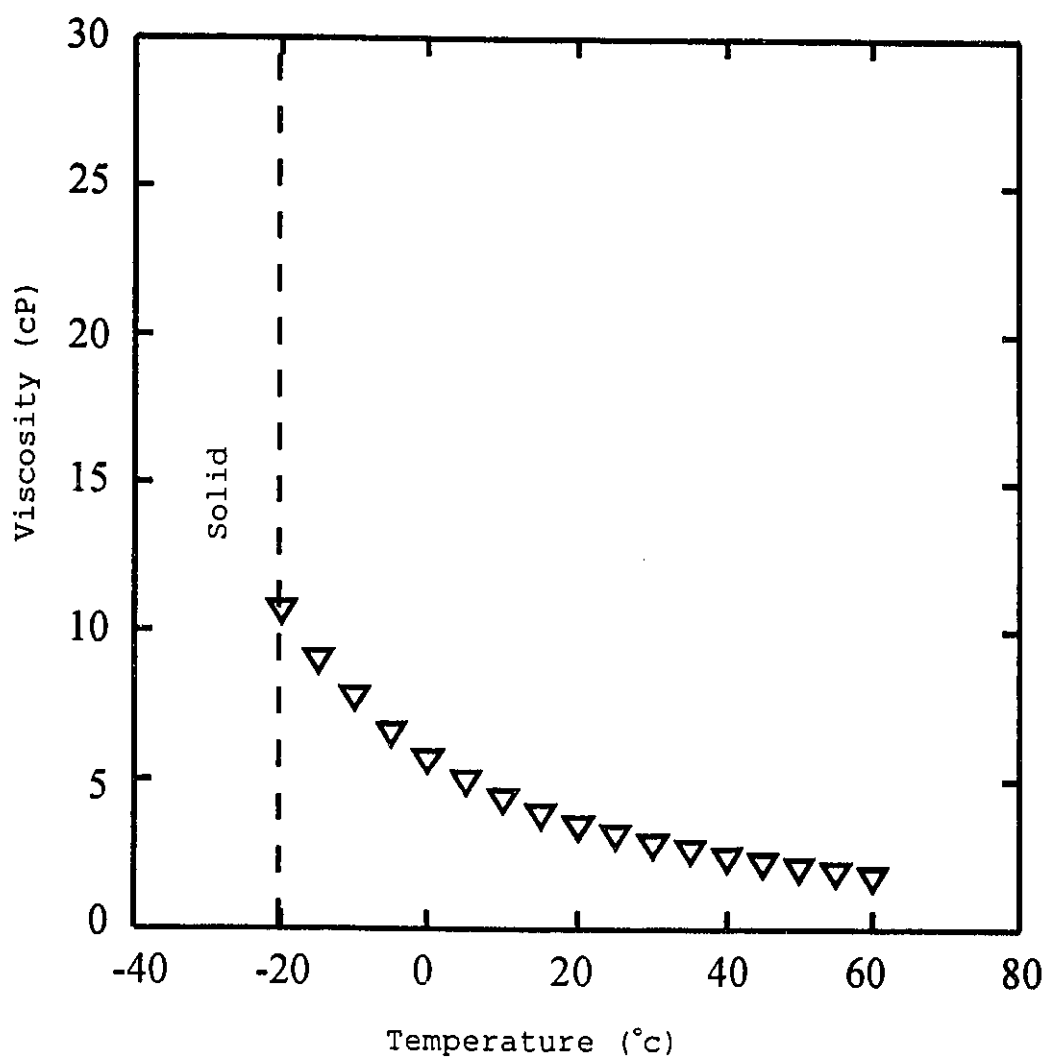
Figure 7.9 Temperature dependence of viscosity for the binary-solvent solution EC/DEC/LiClO$_4$
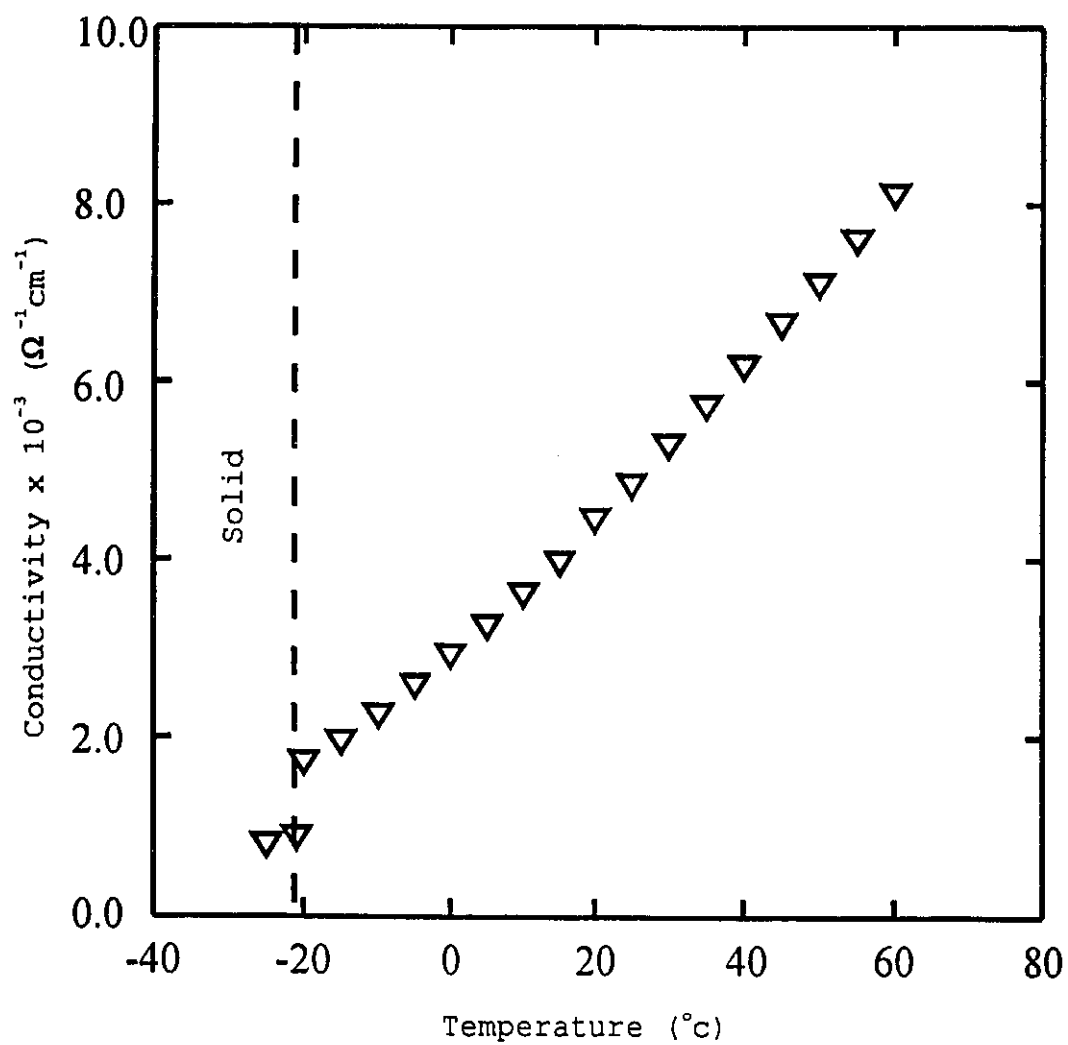
Figure 7.10 Temperature dependence of conductivity for the binary-solvent solution EC/DEC/LiClO$_4$

ºC to 60 ºC, which is the expected temperature range that would be useful in practical cells. The concentration of lithium perchlorate in all measurements are at maximum conductivity for the particular binary-solvent electrolyte solution.

Both the dielectric constant and the viscosity increase as the temperature is lowered[13]. For the electrolyte solutions $EC/PC/LiClO_4$ and $EC/DEC/LiClO_4$ the maximum conductivity decreases rather rapidly with decreasing temperature, indicating that both dielectric constant and solvent viscosity may be acting together to reduce these properties as the temperature is lowered. The effect has been explained as being predominantly due to the viscosity increase with decreasing temperature. When the temperature was lowered to -22 ºC during the viscosity and conductivity measurements of the $EC/DEC/LiClO_4$ solution, a solid formed around the cylinder walls in the viscometer cell and the conductivity sample cell. The formation of the solid prevented further viscosity measurements and the conductivity dropped off dramatically. The liquid component was separated from the solid component, the solid was then rinsed with DEC solvent. Raman spectroscopy was performed on each of the components to determine the composition. Figure 7.11 compares the unseparated (bottom), the liquid phase (middle), and the solid phase (top). Recalling the band
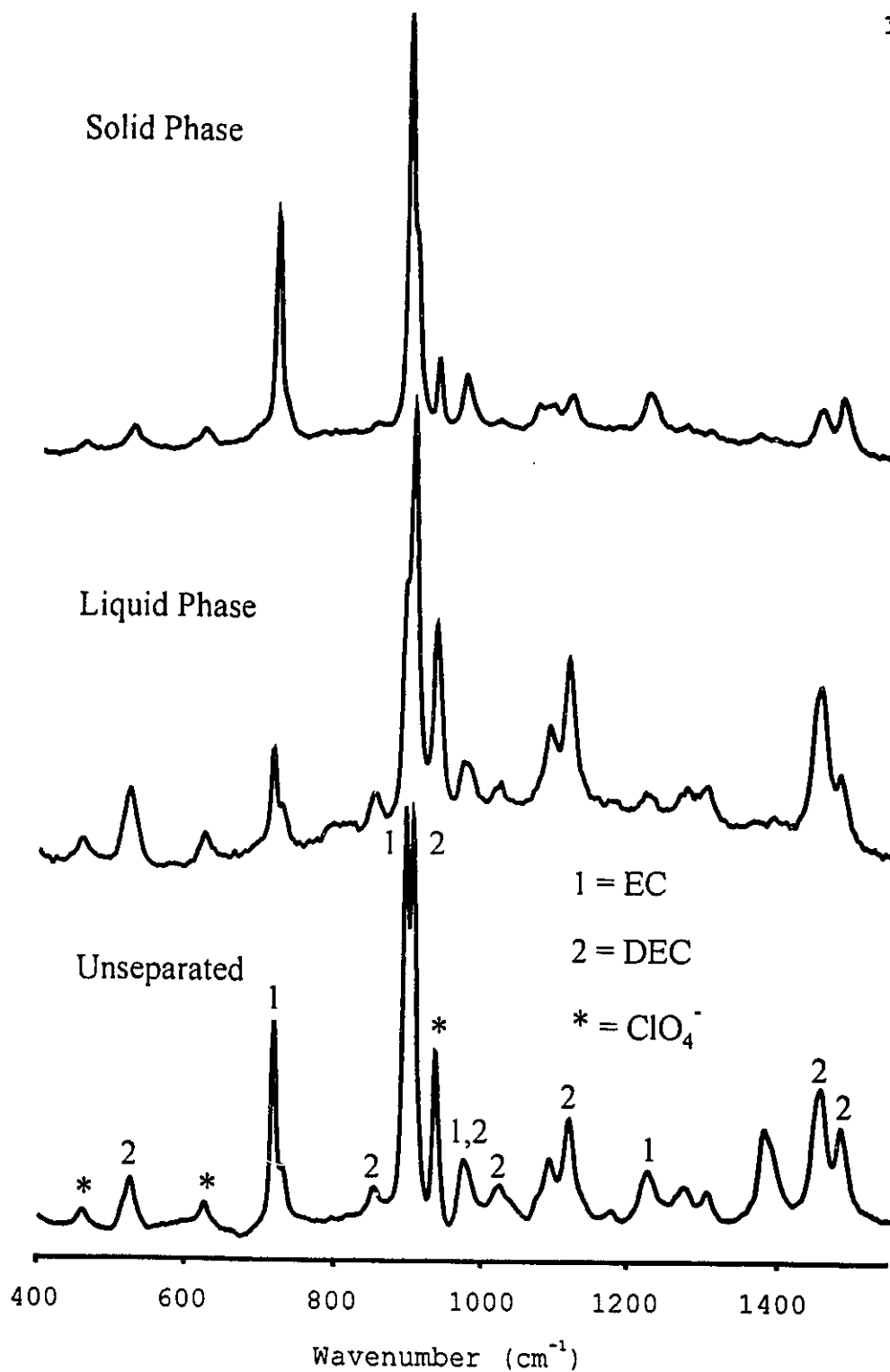
Figure 7.11 Raman spectroscopy of the separated components of the EC/DEC/LiClo4 solution

assignments for EC and DEC that were established in chapters 3 and 4, the solid phase is comprised predominantly of EC and contains only a small amount perchlorate anion. On the other hand, the liquid phase is comprised mainly of the DEC solvent along with dissolved perchlorate anion as indicated by the bands associated with the perchlorate anion.

7.6 ETHYLENE CARBONATE CONCENTRATION DEPENDENCE OF VISCOSITY AND CONDUCTIVITY IN BINARY-SOLVENT ELECTROLYTE SOLUTIONS

From the lithium perchlorate concentration dependence of viscosity and conductivity, it was found that a lithium perchlorate concentration of approximately 0.8 M gave the highest conductivity for the solutions $EC/PC/LiClO_4$, and $EC/DEC/LiClO_4$. Considering that ethylene carbonate was chosen for its positive influence on the conductivity of the electrolyte solutions, the ethylene carbonate concentration dependence of conductivity and viscosity is studied. In this case, the binary solvent solutions of $EC/PC/LiClO_4$, $EC/DEC/LiClO_4$, and $EC/DMC/LiClO_4$ are considered.

Conductivity and viscosity results for three types of binary-solvent electrolyte solutions with a lithium perchlorate concentration of 0.8 M ($EC/PC/LiClO_4$, $EC/DEC/LiClO_4$, $EC/DMC/LiClO_4$) with varying %EC content at 25 ºC are presented in Figures 7.12 and 7.13. The viscosity
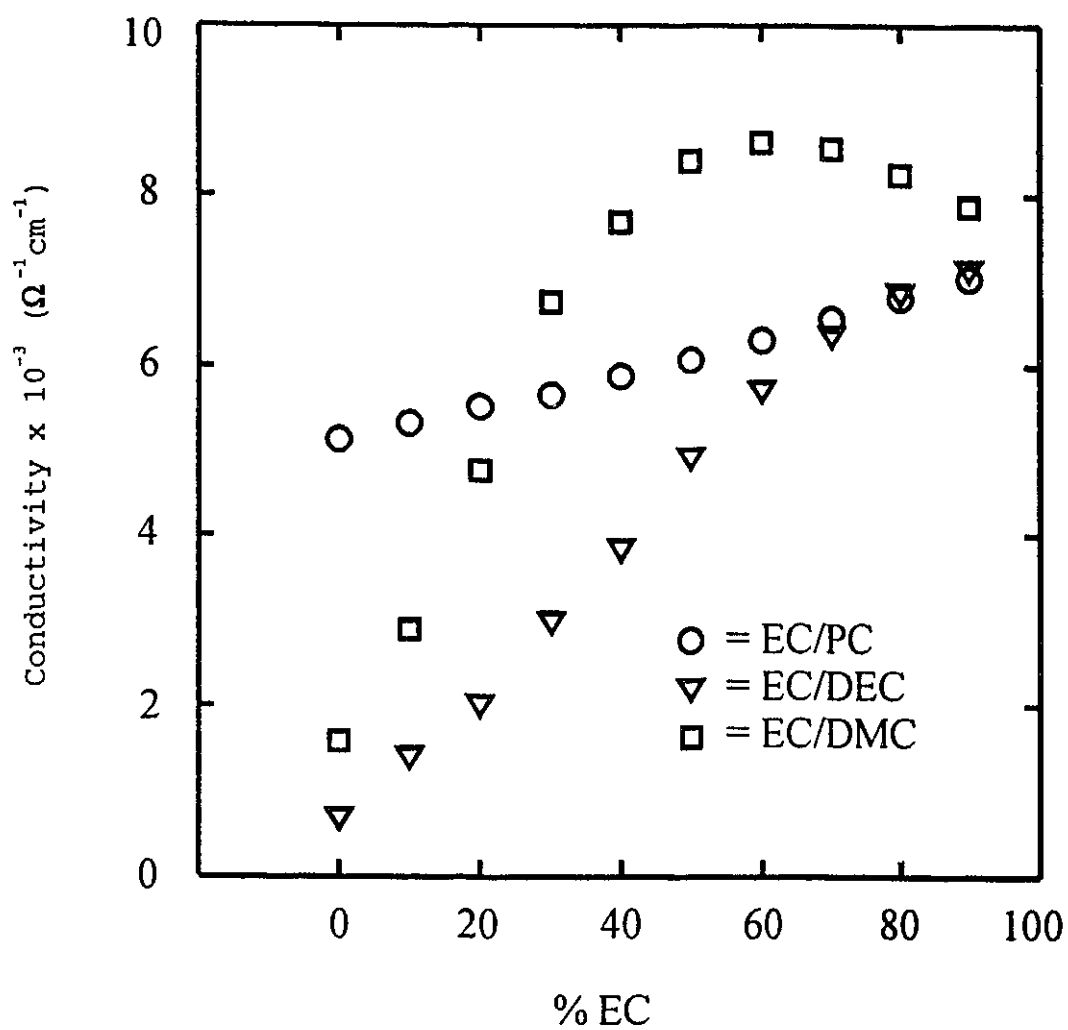
Figure 7.12 EC Concentration dependence of conductivity for
the binary-solvent 0.8 M solutions:
EC/PC/LiClO₄, EC/DEC/LiClO₄, and EC/DMC/LiClO₄
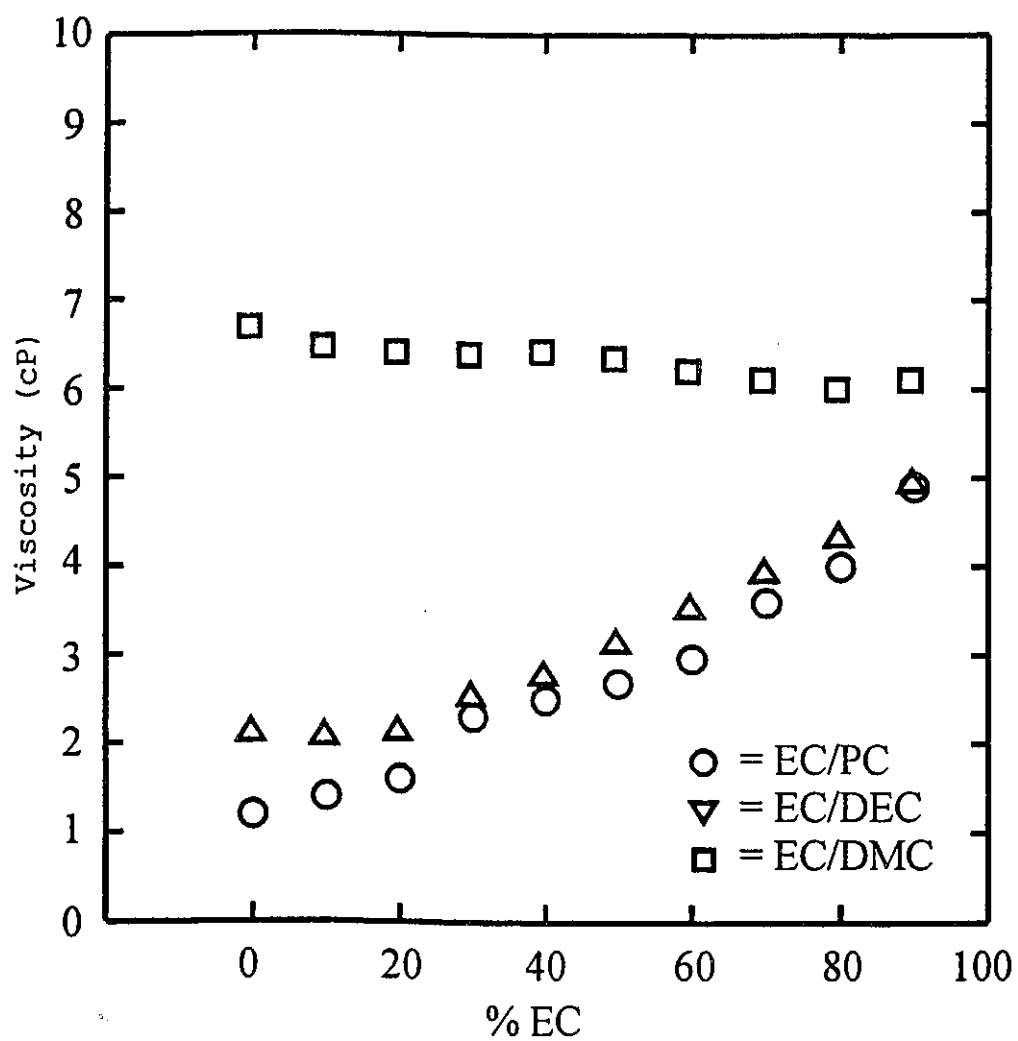
Figure 7.13 EC Concentration dependence of viscosity for the binary-solvent 0.8 M solutions: EC/PC/LiClO$_4$, EC/DEC/LiClO$_4$, and EC/DMC/LiClO$_4$

measurements show that there is small change in the EC/PC/LiClO$_4$ electrolytes (remains constant at around 6 cP), while the binary solvents of EC/DEC/LiClO$_4$ and EC/DMC/LiClO$_4$ show a continuous increase in viscosity with increasing EC content (viscosity of pure EC could not be measured since it is a solid at room temperature). The viscosity curves, Figure 7.12, gives insight into the solvent-solvent interactions within the electrolyte solution.

Pure EC possesses intermolecular association, as observed through dielectric constant measurements[14]. The behaviour of the EC/PC electrolyte solution viscosity suggests that the interaction between EC and PC is such that the basic network of intermolecular association resembles that of pure PC or EC and remains relatively unaffected, the similarity in the structure of PC and EC allows the viscosity to remain constant even at 90% EC content. Results from the viscosity measurements of the binary-solvents mixtures of EC/DEC and EC/DMC suggests that the intermolecular association in EC disrupted and the individual EC and DEC (or DMC) molecules are loosely bound together to give rise to a less structured solution. Similar behaviour has been observed in binary solvent electrolytes made up of EC and tetrahydrofuran (THF)[15] and also systems comprised of water and formamide[16].

The conductivity results for the three binary-solvent

electrolytes with varying EC content are presented in figure 7.12. The conductivity increases with increasing EC content in the solvent mixtures. Conductivity passes through a maximum at around 60 vol% EC in EC/DMC, while the conductivity increases at a relatively constant rate where the maximum appears to occur upon reaching pure EC.

The appearance of the conductivity maximum in the EC/DMC solvent mixture can be qualitatively explained as arising from a favourable combination of high dielectric solvent EC and the low viscosity of DMC. The binary-solvent EC/DMC solution had the highest conductivity, this can be explained by the size of the primary solvation shell. Assuming that the solvent-Li$^+$ is non selective, the solvation shell of EC/DMC mixture will be the smallest thus providing the greatest mobility and therefore conductivity.

7.7 THESIS SUMMARY

In the present thesis the interactions that occur between components within an electrolyte solution were studied. An important aspect of this thesis was the application of theoretical methods combined with experimental results to provide a model that describes the interactions that occur within a solution comprised of lithium perchlorate dissolved in organic solvents.

Lithium perchlorate was found to form ion-pairs in concentrated electrolyte solutions. Evidence of ion-pairing was provided by Raman spectroscopy and *ab initio* quantum chemical calculations. Calculated ground state energies of the bidentate ion-pair are predicted to be stable in the gas phase by a relatively high energy and therefore can be expected to form ion-pairs in solution. The $Li^+ClO_4^-$ ion-pair is predicted to prefer a bidentate C_{2v} geometry over a monodentate C_{3v} or tridentate C_{3v} geometry according to adequate levels of theory (HF and MP2 with basis sets having polarization functions: HF/6-31+G*, HF/6-311+G*, MP2/6-31+G*, and MP2/6-311+G*). *Ab initio* calculations of the fundamental vibrations for the perchlorate anion were found to be very accurate when compared to the experimental Raman spectra. The subsequent splitting of the fundamental vibrations for the T_d anion upon coordination in a bidentate

C_{2v} geometry is predicted.

To facilitate the analysis of the solutions, a complete vibrational analysis was carried out using experimental vibrational spectroscopy and *ab initio* vibrational calculations. The resulting description of the individual vibrational modes are used to provide insight into the interaction between solvent and electrolyte. The properties of the resulting binary solvent solutions upon dissolving lithium perchlorate in EC combined with one of PC, DEC, or DMC is discussed in detail. The interactions that occur within the binary-solvent solution when going from a dilute to a concentrated solution is discussed in terms of conductivity, viscosity, and spectral changes.

The lithium cation was found to coordinate to the carbonyl oxygen of the solvents. From experimental evidence combined with theoretical calculations, a coordination number (solvation number) of 4 - 6 solvent molecules around the lithium cation is suggested.

Conductivity was found to increase with the increase in electrolyte concentration for all solutions until a maximum was reached at approximately 0.8 M. After which the conductivity decreased dramatically. This was explained by the increased occurrence of contact ion-pairs and aggregates forming in solution.

REFERENCES

1. Deng, Z.; Irish, D. E. *Can. J. Chem.* **1991**, *69*, 1766.

2. Deng, Z.; Irish, D. E. *Faraday Trans.* **1992**, *88*, 2891.

3. Blint, R. *J. Electrochem. Soc.* **1995**, *142*, 696.

4. Strasser, J.; Medina, C.; Xu, M.; Eyring, E. M.; Petrucci, S. *J. Phys. Chem.* **1991**, *95*, 1453.

5. Dzidic, I.; Kebarle, P. *J. Phys. Chem.*, **1970**, *74*, 1466.

6. Woodin, R. L.; Beauchamp, J. L. *J. Am. Chem. Soc.*, **1978**, *100*, 501.

7. Kumar, G.; Janakiraman; Namboodiri, N.; Gangadharan; Kanagaraj; Saminathan; Sharief, N. *J. Chem. Eng. Data*, **1991**, *36*, 467.

8. Salomon, M.; Uchiyama, M.; Xu, M.; Petrucci, S. *J. Phys. Chem.*, **1989**, *93*, 4374.

9. **Blomgren, G. E.,** *Lithium Batteries*, **Academic Press, New York, J. P. Gabano ed., 1983, pp 13-41.**

10. Jansen, M. J.; Yeager, H. L. *J. Phys. Chem.* **1974**, *78*, 1380.

11. Ishikawa, M.; Wen, S.-Q.; Matsuda, Y. *Journal of Power Sources*, **1993**, *45*, 229.

12. Barthel, J.; Gores, H. J. *Pure Appl. Chem.* **1985**, *57*, 1071.

13. Blomgren, G. E. in J. P. Gabano (ed.), *Lithium Batteries*, New York, 1983, Ch. 2.

14. Shedlovsky, T. *J. Am. Chem. Soc.*, **1932**, *54*, 1411.

15. Prabhu, P. V. S. S.; Kumar, T. P.; Namboodiri, P. N. N.; Gangadharan, R. *J. Appl. Electrochem.* **1992**, *23*, 151.

16. Lal Bahadur, Ramanamurti, M. V. *J. Electrochem. Soc.* **1981**, *128*, 339.

APPENDICES

APPENDIX I

GAUSSIAN 92 OUTPUT EXAMPLE (ClO$_4^-$, HF/6-31G)

Entering Link 1 = L1.EXE PID=   2142.

                    Copyright (c) 1992, Gaussian, Inc.
                         All Rights Reserved.

This work is based on the Gaussian 90(TM) system (copyright
1990 Gaussian, Inc.), the Gaussian 88(TM) system (copyright
1988 Gaussian, Inc.), the Gaussian 86(TM) system (copyright
1986 Carnegie Mellon University), and the Gaussian 82(TM)
system (copyright 1983 Carnegie Mellon University). Gaussian
is a federally registered trademark of Gaussian, Inc.

This software is provided under written license and may be
used, copied, transmitted, or stored only in accord with that
written license.

The following legend is applicable only to US Government
contracts under DFARS:

                    RESTRICTED RIGHTS LEGEND

Use, duplication or disclosure by the US Government is subject
to restrictions as set forth in subparagraph (c)(1)(ii) of the
Rights in Technical Data and Computer Software clause at DFARS
252.227-7013.

Gaussian, Inc.
Carnegie Office Park, Building 6, Pittsburgh, PA 15106 USA

The following legend is applicable only to US Government
contracts under FAR:

                    RESTRICTED RIGHTS LEGEND

Use, reproduction and disclosure by the US Government is subject
to restrictions as set forth in subparagraph (c) of the
Commercial Computer Software - Restricted Rights clause at FAR
52.227-19.

Gaussian, Inc.
Carnegie Office Park, Building 6, Pittsburgh, PA 15106 USA

Cite this work as:
Gaussian 92, Revision E.1, M. J. Frisch, G. W. Trucks,
M. Head-Gordon, P. M. W. Gill, M. W. Wong, J. B. Foresman,
B. G. Johnson, H. B. Schlegel, M. A. Robb, E. S. Replogle,
R. Gomperts, J. L. Andres, K. Raghavachari, J. S. Binkley,
C. Gonzalez, R. L. Martin, D. J. Fox, D. J. Defrees, J. Baker,

J. J. P. Stewart, and J. A. Pople, Gaussian, Inc.,
Pittsburgh PA, 1992.

```
*******************************************************
Gaussian 92:   486-Windows-G92RevE.1   30-Jun-1993
                    12-Jan-1995
*******************************************************
Default route:  Tran=Conventional MaxDisk=13107200
-----------------
# RHF/6-31G opt
-----------------
1/10=7,29=10000/1,3;
2/12=2,17=6,18=5/2;
3/5=1,6=6,11=1,25=20,30=1/1,2,3,11,20;
4/7=1/1;
5/5=1/2;
6/7=2,8=2,9=2,10=2,28=1/1;
7/29=1/1,2,3,16;
1/10=7/3(1);
99//99;
2//2;
3/5=1,6=6,11=1,25=20,30=1/1,2,3,11,20;
4/5=5,7=1,16=2/1;
5/5=1/2;
7//1,2,3,16;
1//3(-5);
3/5=1,6=6,11=1,30=1,39=1/1,3;
6/7=2,8=2,9=2,10=2,28=1/1;
99/9=1/99;
-----------------
Perchlorate ion.
-----------------
Symbolic Z-matrix:
    Charge =-1 Multiplicity = 1
O
Cl    1    r1
O     2    r2      1     109.47
O     2    r3      1     109.47   3    -120.   0
O     2    r4      1     109.47   3    120.    0
        Variables:
  r1                    1.85
  r2                    1.85
  r3                    1.85
  r4                    1.85
```

GradGradGradGradGradGradGradGradGradGradGradGradGradGradGradGradGr
adGrad
 Berny optimization.
 Initialization pass.
```
                         ---------------------------
                         !   Initial Parameters    !
                         ! (Angstroms and Degrees) !
---------------------------
---------------------------
```

!	Name	Value	Derivative information (Atomic
Units)	!		

!	r1	1.85	estimate D2E/DX2
!			
!	r2	1.85	estimate D2E/DX2
!			
!	r3	1.85	estimate D2E/DX2
!			
!	r4	1.85	estimate D2E/DX2
!			

Initial trust radius is 3.000D-01.
Number of steps in this run= 20 maximum allowed number of steps= 100.

GradGradGradGradGradGradGradGradGradGradGradGradGradGradGradGradGr adGrad

---

Z-MATRIX (ANGSTROMS AND DEGREES)

CDJ	Cent	Atom	N1	Length/X	N2	Alpha/Y	N3	Beta/Z
1	1	O						
2	2	Cl	1	1.850000(	1)			
3	3	O	2	1.850000(	2)	1	109.470(	5)
4	4	O	2	1.850000(| 3)	1	109.470(| 6)	3 -120.000(8)	0
5	5	O	2	1.850000(| 4)	1	109.470(| 7)	3 120.000(9)	0

Z-Matrix orientation:

Center Number	Atomic Number	Coordinates (Angstroms)		
		X	Y	Z
1	8	0.000000	0.000000	0.000000
2	17	0.000000	0.000000	1.850000
3	8	1.744210	0.000000	2.466630
4	8	-0.872105	-1.510530	2.466630
5	8	-0.872105	1.510530	2.466630

Distance matrix (angstroms):

	1	2	3	4	5

```
1  O    0.000000
2  Cl   1.850000   0.000000
3  O    3.021015   1.850000   0.000000
4  O    3.021015   1.850000   3.021060   0.000000
5  O    3.021015   1.850000   3.021060   3.021060   0.000000
```

                        Interatomic angles:
```
     O1-Cl2-O3=109.47          O1-Cl2-O4=109.47
O3-Cl2-O4=109.4724
     O1-Cl2-O5=109.47          O3-Cl2-O5=109.4724
O4-Cl2-O5=109.4724
```

```
Stoichiometry      ClO4(1-)
Framework group    C3V[C3(OCl),3SGV(O)]
Deg. of freedom    3
Full point group                      C3V      NOp  6
Largest Abelian subgroup              CS       NOp  2
Largest concise Abelian subgroup CS   CS       NOp  2
```
                        Standard orientation:

```
Center     Atomic              Coordinates (Angstroms)
Number     Number          X            Y            Z
```

```
   1          8          0.000000    0.000000   -1.849982
   2         17          0.000000    0.000000    0.000018
   3          8          0.000000    1.744210    0.616648
   4          8          1.510530   -0.872105    0.616648
   5          8         -1.510530   -0.872105    0.616648
```

```
Rotational constants (GHZ):      3.4619948      3.4619948
3.4619166
Isotopes: O-16,Cl-35,O-16,O-16,O-16
Standard basis: 6-31G     (S, S=P, 6D, 7F)
There are    33 symmetry adapted basis functions of A'  symmetry.
There are    16 symmetry adapted basis functions of A"  symmetry.
Crude estimate of integral set expansion from redundant
integrals=1.164.
Integral buffers will be       8192 words long.
Raffenetti 1 integral format.
Two-electron integral symmetry is turned on.
     49 basis functions      134 primitive gaussians
     25 alpha electrons       25 beta electrons
        nuclear repulsion energy       222.8697247895 Hartrees.
One-electron integrals computed using PRISM.
The smallest eigenvalue of the overlap matrix is  2.929D-02
DipDrv:  will hold 34 matrices at once.
Out2e will use a cutoff of  1.00D-10
      345888 integrals produced for a total of       345888.
Out2e will use a cutoff of  1.00D-10
           0 integrals produced for a total of       345888.
CNDO Guess failed.  Using Huckel.
Initial guess orbital symmetries:
       Occupied  (A1) (A1) (E)  (E)  (A1) (A1) (E)  (E)  (A1) (A1)
                 (E)  (E)  (A1) (A1) (E)  (E)  (A1) (E)  (E)  (E)  (E)
                 (A1) (A2) (E)  (E)
       Virtual   (A1) (A1) (E)  (E)  (A1) (E)  (E)  (A1) (A1) (A1)
                 (E)  (E)  (A1) (A1) (E)  (E)  (E)  (E)  (E)  (E)
```

```
                         (E) (E) (E)
Requested convergence on RMS density matrix=1.00D-08 within  64
cycles.
Requested convergence on MAX density matrix=1.00D-06.
SCF Done:  E(RHF) =   -758.300971351     A.U. after   12 cycles
              Convg  =     0.2761D-08            -V/T =  2.0000
              S**2   =     0.0000
```

****
****

                Population analysis using the SCF density.

****
****

Orbital Symmetries:
        Occupied (A1) (A1) (E) (E) (A1) (A1) (E) (E) (A1) (A1)
                  (E) (E) (A1) (A1) (E) (E) (A1) (E) (E) (A2) (E)
                  (E) (E) (E) (A1)
        Virtual   (A1) (A1) (E) (E) (A1) (E) (E) (A1) (E) (E) (E)
                  (E) (A1) (A2) (E) (E) (A1) (E) (E) (A1) (A1) (E)
                  (E) (A1)
 The electronic state is 1-A1.
 Alpha occ. eigenvalues -- -104.79571 -20.44011 -20.44010
-20.44010 -20.44010
 Alpha occ. eigenvalues -- -10.53610 -8.00121 -8.00121
-8.00121 -1.18995
 Alpha occ. eigenvalues --   -1.06169 -1.06169 -1.06168
-0.84631 -0.44687
 Alpha occ. eigenvalues --   -0.44687 -0.44687 -0.34180
-0.34180 -0.32026
 Alpha occ. eigenvalues --   -0.32025 -0.32025 -0.29109
-0.29109 -0.29109
 Alpha virt. eigenvalues --   0.25734   0.30457   0.30458
0.30458   0.81760
 Alpha virt. eigenvalues --   0.81760   0.81760   0.83238
1.26692   1.26692
 Alpha virt. eigenvalues --   1.38902   1.38902   1.38902
1.41872   1.41873
 Alpha virt. eigenvalues --   1.41873   1.42207   1.54117
1.54117   1.54118
 Alpha virt. eigenvalues --   1.79570   1.79572   1.79572
2.23699
          Condensed to atoms (all electrons):
               1   2   3   4   5
    1 O   8.457952   0.059714 -0.008161 -0.008161 -0.008161
    2 Cl   0.059714 15.788406   0.059715   0.059715   0.059715
    3 O   -0.008161   0.059715   8.457950 -0.008160 -0.008160
    4 O   -0.008161   0.059715 -0.008160   8.457950 -0.008160
    5 O   -0.008161   0.059715 -0.008160 -0.008160   8.457950
 Total atomic charges:
               1
```

```
1 O   -0.493183
2 Cl   0.972735
3 O   -0.493184
4 O   -0.493184
5 O   -0.493184
```
Sum of Mulliken charges=  -1.00000
Atomic charges with hydrogens summed into heavy atoms:
```
             1
1 O   -0.493183
2 Cl   0.972735
3 O   -0.493184
4 O   -0.493184
5 O   -0.493184
```
Sum of Mulliken charges=  -1.00000
Electronic spatial extent (au):  <R**2>=   487.1457
Charge=     -1.0000 electrons
Dipole moment (Debye):
    X=       0.0000    Y=       0.0000    Z=       0.0001   Tot=
0.0001
Quadrupole moment (Debye-Ang):
    XX=    -43.0607    YY=    -43.0607    ZZ=    -43.0604
    XY=      0.0000    XZ=      0.0000    YZ=      0.0000
Octapole moment (Debye-Ang**2):
    XXX=      0.0000    YYY=     -4.1261    ZZZ=      5.8349    XYY=
0.0000
    XXY=      4.1261    XXZ=     -2.9176    XZZ=      0.0000    YZZ=
0.0000
    YYZ=     -2.9176    XYZ=      0.0000
Hexadecapole moment (Debye-Ang**3):
XXXX=   -192.9466 YYYY=   -192.9466 ZZZZ=   -192.4951 XXXY=
0.0000
XXXZ=      0.0000 YYYX=      0.0000 YYYZ=      0.6277 ZZZX=
0.0000
ZZZY=      0.0000 XXYY=    -64.3155 XXZZ=    -64.7586 YYZZ=
-64.7586
XXYZ=     -0.6277 YYXZ=      0.0000 ZZXY=      0.0000
N-N= 2.228697247895D+02 E-N=-2.260317839610D+03   KE=
7.583272742554D+02
 Symmetry A'   KE= 6.288179493399D+02
 Symmetry A"   KE= 1.295093249155D+02
 ***** AXES RESTORED TO ORIGINAL SET *****
```

-

| Center | Atomic | | Forces (Hartrees/Bohr) | |
| Number | Number | X | Y | Z |

-

1	8	0.000000000	0.000000000	
-0.002872206				
2	17	0.000000000	0.000000000	
-0.000003171				
3	8	0.002707110	0.000000000	
0.000958459				

```
     4        8        -0.001353555    -0.002344426
0.000958459
     5        8        -0.001353555     0.002344426
0.000958459
```

-

```
            MAX    0.002872206    RMS    0.001483034
```


```
         Internal Coordinate Forces (Hartree/Bohr or radian)
  Cent Atom N1    Length/X    N2    Alpha/Y    N3    Beta/Z
     J
```


```
   1  O
   2  Cl   1    0.002872(   1)
   3  O    2    0.002872(   2)  1  0.000005(  5)
   4  O    2    0.002872(   3)  1  0.000005(  6)  3  0.000000(
8)  0
   5  O    2    0.002872(   4)  1  0.000005(  7)  3  0.000000(
9)  0
```


```
            MAX    0.002872206    RMS    0.001914590
```

GradGradGradGradGradGradGradGradGradGradGradGradGradGradGradGradGr
adGrad
 Berny optimization.
 Search for a local minimum.
 Step number   1 out of a maximum of   20
 All quantities printed in internal units (Hartrees-Bohrs-Radians)
 Second derivative matrix not updated -- first step.
 The second derivative matrix:
                      r1   r2   r3   r4
         r1   0.22543
         r2   0.00000   0.22543
         r3   0.00000   0.00000   0.22543
         r4   0.00000   0.00000   0.00000   0.22543
     Eigenvalues ---   0.22543   0.22543   0.22543   0.22543
 RFO step: Lambda=-1.46251099D-04.
 Linear search not attempted -- first point.
 Variable   Old X   -DE/DX   Delta X   Delta X   Delta X
New X
                                   (Linear)   (Quad)   (Total)
     r1   3.49599   0.00287   0.00000   0.01273   0.01273
3.50873
     r2   3.49599   0.00287   0.00000   0.01273   0.01273
3.50872
     r3   3.49599   0.00287   0.00000   0.01273   0.01273
3.50872
```

```
    r4          3.49599   0.00287   0.00000   0.01273   0.01273
3.50872
            Item                  Value      Threshold  Converged?
Maximum Force               0.002872    0.000450     NO
RMS     Force               0.002872    0.000300     NO
Maximum Displacement        0.012733    0.001800     NO
RMS     Displacement        0.012731    0.001200     NO
Predicted change in Energy=-7.307817D-05
```

GradGradGradGradGradGradGradGradGradGradGradGradGradGradGradGradGr
adGrad

```
--------------------------------------------------------------
------
                        Z-MATRIX (ANGSTROMS AND DEGREES)
 CD Cent Atom  N1     Length/X     N2     Alpha/Y     N3     Beta/Z
    J
--------------------------------------------------------------
------
   1   1  O
   2   2  Cl    1   1.856738(  1)
   3   3  O     2   1.856737(  2)    1  109.470(  5)
   4   4  O     2   1.856737(  3)    1  109.470(  6)    3 -120.000(
8)   0
   5   5  O     2   1.856737(  4)    1  109.470(  7)    3  120.000(
9)   0
--------------------------------------------------------------
------
                    Z-Matrix orientation:
--------------------------------------------------------------
 Center     Atomic           Coordinates (Angstroms)
 Number     Number         X            Y            Z
--------------------------------------------------------------
    1          8        0.000000     0.000000     0.000000
    2         17        0.000000     0.000000     1.856738
    3          8        1.750561     0.000000     2.475613
    4          8       -0.875281    -1.516031     2.475613
    5          8       -0.875281     1.516031     2.475613
--------------------------------------------------------------
                Distance matrix (angstroms):
                    1          2          3          4          5
  1  O       0.000000
  2  Cl      1.856738   0.000000
  3  O       3.032017   1.856737   0.000000
  4  O       3.032017   1.856737   3.032061   0.000000
  5  O       3.032017   1.856737   3.032061   3.032061   0.000000
                    Interatomic angles:
        O1-Cl2-O3=109.47          O1-Cl2-O4=109.47
O3-Cl2-O4=109.4724
        O1-Cl2-O5=109.47          O3-Cl2-O5=109.4724
O4-Cl2-O5=109.4724
  Stoichiometry    ClO4(1-)
  Framework group  C3V[C3(OCl),3SGV(O)]
```

Deg. of freedom   3
Full point group   C3V   NOp   6
Largest Abelian subgroup   CS   NOp   2
Largest concise Abelian subgroup CS   NOp   2
                    Standard orientation:

Center   Atomic   Coordinates (Angstroms)
Number   Number   X   Y   Z
----
   1   8   0.000000   0.000000   -1.856719
   2   17   0.000000   0.000000   0.000018
   3   8   0.000000   1.750561   0.618893
   4   8   1.516031   -0.875281   0.618893
   5   8   -1.516031   -0.875281   0.618893

Rotational constants (GHZ):   3.4369164   3.4369164
3.4368402
Isotopes: O-16,Cl-35,O-16,O-16,O-16
Standard basis: 6-31G   (S, S=P, 6D, 7F)
There are   33 symmetry adapted basis functions of A' symmetry.
There are   16 symmetry adapted basis functions of A" symmetry.
Crude estimate of integral set expansion from redundant
integrals=1.164.
Integral buffers will be   8192 words long.
Raffenetti 1 integral format.
Two-electron integral symmetry is turned on.
   49 basis functions   134 primitive gaussians
   25 alpha electrons   25 beta electrons
       nuclear repulsion energy   222.0610488008 Hartrees.
One-electron integrals computed using PRISM.
The smallest eigenvalue of the overlap matrix is 2.981D-02
DipDrv: will hold 34 matrices at once.
Out2e will use a cutoff of 1.00D-10
       345299 integrals produced for a total of   345299.
Out2e will use a cutoff of 1.00D-10
         0 integrals produced for a total of   345299.
Initial guess read from the read-write file:
Initial guess orbital symmetries:
       Occupied   (A1) (A1) (E) (E) (A1) (A1) (E) (E) (A1) (A1)
                  (E) (E) (A1) (A1) (E) (E) (A1) (E) (E) (A2) (E)
                  (E) (E) (E) (A1)
       Virtual   (A1) (A1) (E) (E) (A1) (E) (E) (A1) (E) (E) (E)
                  (E) (A1) (A2) (E) (E) (A1) (E) (E) (A1) (A1) (E)
                  (E) (A1)
Requested convergence on RMS density matrix=1.00D-08 within 64
cycles.
Requested convergence on MAX density matrix=1.00D-06.
SCF Done: E(RHF) = -758.301098395   A.U. after   9 cycles
           Convg =   0.1657D-08   -V/T = 2.0000
           S**2   =   0.0000
   ***** AXES RESTORED TO ORIGINAL SET *****

-
Center   Atomic   Forces (Hartrees/Bohr)

Number	Number	X	Y	Z
1	8	0.000000000	0.000000000	-0.002123007
2	17	0.000000000	0.000000000	-0.000003243
3	8	0.002000950	0.000000000	0.000708750
4	8	-0.001000475	-0.001732874	0.000708750
5	8	-0.001000475	0.001732874	0.000708750

	MAX	0.002123007	RMS	0.001096222

Internal Coordinate Forces (Hartree/Bohr or radian)

Cent Atom N1	Length/X	N2	Alpha/Y	N3	Beta/Z
J					

1	O									
2	Cl	1	0.002123(	1)						
3	O	2	0.002123(	2)	1	0.000004(	5)			
4	O	2	0.002123(	3)	1	0.000004(	6)	3	0.000000(8)	0
5	O	2	0.002123(	4)	1	0.000004(	7)	3	0.000000(9)	0

	MAX	0.002123007	RMS	0.001415219

GradGradGradGradGradGradGradGradGradGradGradGradGradGradGradGradGr
adGrad
 Berny optimization.
 Search for a local minimum.
 Step number   2 out of a maximum of 20
 All quantities printed in internal units (Hartrees-Bohrs-Radians)
 Update second derivatives using information from points 1 2
 Trust test= 1.74D+00 RLast= 2.55D-02 DXMaxT set to 7.64D-02
 The second derivative matrix:

	r1	r2	r3	r4
r1	0.18377			
r2	-0.04165	0.18378		
r3	-0.04165	-0.04165	0.18378	
r4	-0.04165	-0.04165	-0.04165	0.18378

 Maximum step size (0.076) exceeded in linear search.

```
            -- Step size scaled by   0.970
            -- Skip Quadratic or steepest descent search.
       Quartic linear search produced a step of   3.00000.
       Steepest descent instead of Quadratic search.
```

Variable	Old X	-DE/DX	Delta X	Delta X	Delta X
New X					
			(Linear)	(Quad)	(Total)
r1	3.50873	0.00212	0.03820	0.00000	0.03820
3.54692					
r2	3.50872	0.00212	0.03819	0.00000	0.03819
3.54692					
r3	3.50872	0.00212	0.03819	0.00000	0.03819
3.54692					
r4	3.50872	0.00212	0.03819	0.00000	0.03819
3.54692					

Item		Value	Threshold	Converged?
Maximum	Force	0.002123	0.000450	NO
RMS	Force	0.002123	0.000300	NO
Maximum	Displacement	0.038198	0.001800	NO
RMS	Displacement	0.038194	0.001200	NO

Predicted change in Energy=-1.716565D-04

GradGradGradGradGradGradGradGradGradGradGradGradGradGradGradGradGr
adGrad

```
----------------------------------------------------------------
------
```

				Z-MATRIX	(ANGSTROMS AND DEGREES)			
CD Cent J	Atom	N1	Length/X	N2	Alpha/Y	N3	Beta/Z

```
----------------------------------------------------------------
------
```

1	1	O								
2	2	Cl	1	1.876951(	1)					
3	3	O	2	1.876947(	2)	1	109.470(	5)		
4	4	O	2	1.876947(	3)	1	109.470(	6)	3	-120.000(

8)   0

| 5 | 5 | O | 2 | 1.876947(| 4) | 1 | 109.470(| 7) | 3 | 120.000(|

9)   0

```
----------------------------------------------------------------
------
```

Z-Matrix orientation:

Center Number	Atomic Number	Coordinates (Angstroms)		
		X	Y	Z
1	8	0.000000	0.000000	0.000000
2	17	0.000000	0.000000	1.876951
3	8	1.769616	0.000000	2.502563
4	8	-0.884808	-1.532533	2.502563
5	8	-0.884808	1.532533	2.502563

Distance matrix (angstroms):

		1	2	3	4	5
1	O	0.000000				
2	Cl	1.876951	0.000000			
3	O	3.065023	1.876947	0.000000		
4	O	3.065023	1.876947	3.065065	0.000000	
5	O	3.065023	1.876947	3.065065	3.065065	0.000000

Interatomic angles:

O1-Cl2-O3=109.47   O1-Cl2-O4=109.47
O3-Cl2-O4=109.4724
      O1-Cl2-O5=109.47   O3-Cl2-O5=109.4724
O4-Cl2-O5=109.4724
Stoichiometry   ClO4(1-)
Framework group   C3V[C3(OCl),3SGV(O)]
Deg. of freedom   3
Full point group   C3V   NOp 6
Largest Abelian subgroup   CS   NOp 2
Largest concise Abelian subgroup CS   NOp 2
                Standard orientation:

Center	Atomic	Coordinates (Angstroms)		
Number	Number	X	Y	Z
1	8	0.000000	0.000000	-1.876932
2	17	0.000000	0.000000	0.000019
3	8	0.000000	1.769616	0.625631
4	8	1.532533	-0.884808	0.625631
5	8	-1.532533	-0.884808	0.625631

Rotational constants (GHZ):   3.3632949   3.3632949
3.3632242
Isotopes: O-16,Cl-35,O-16,O-16,O-16
Standard basis: 6-31G   (S, S=P, 6D, 7F)
There are   33 symmetry adapted basis functions of A' symmetry.
There are   16 symmetry adapted basis functions of A" symmetry.
Crude estimate of integral set expansion from redundant
integrals=1.164.
Integral buffers will be   8192 words long.
Raffenetti 1 integral format.
Two-electron integral symmetry is turned on.
     49 basis functions   134 primitive gaussians
     25 alpha electrons   25 beta electrons
        nuclear repulsion energy   219.6698527486 Hartrees.
One-electron integrals computed using PRISM.
The smallest eigenvalue of the overlap matrix is 3.139D-02
DipDrv: will hold 34 matrices at once.
Out2e will use a cutoff of 1.00D-10
     343574 integrals produced for a total of   343574.
Out2e will use a cutoff of 1.00D-10
          0 integrals produced for a total of   343574.
Initial guess read from the read-write file:
Initial guess orbital symmetries:
      Occupied (A1) (A1) (E) (E) (A1) (A1) (E) (E) (A1) (A1)
                (E) (E) (A1) (A1) (E) (E) (A1) (E) (E) (A2) (E)
                (E) (E) (E) (A1)
      Virtual   (A1) (A1) (E) (E) (A1) (E) (E) (A1) (E) (E) (E)

```
                    (E) (A1) (A2) (E) (E) (A1) (E) (E) (A1) (A1) (E)
                    (E) (A1)
Requested convergence on RMS density matrix=1.00D-08 within  64
cycles.
Requested convergence on MAX density matrix=1.00D-06.
SCF Done:  E(RHF) =  -758.301261342     A.U. after    9 cycles
           Convg  =    0.4302D-08              -V/T =  2.0000
           S**2   =    0.0000
 ***** AXES RESTORED TO ORIGINAL SET *****
```

```
-------------------------------------------------------------------
-
 Center     Atomic                    Forces (Hartrees/Bohr)
 Number     Number           X               Y               Z
-------------------------------------------------------------------
-
    1          8       0.000000000     0.000000000
-0.000052759
    2         17       0.000000000     0.000000000
-0.000003480
    3          8       0.000049581     0.000000000
0.000018747
    4          8      -0.000024791    -0.000042938
0.000018747
    5          8      -0.000024791     0.000042938
0.000018747
-------------------------------------------------------------------
-
         MAX     0.000052759    RMS     0.000027355
-------------------------------------------------------------------
------
          Internal Coordinate Forces (Hartree/Bohr or radian)
 Cent Atom N1     Length/X    N2     Alpha/Y      N3      Beta/Z
    J
-------------------------------------------------------------------
------
    1  O
    2  Cl   1   0.000053(  1)
    3  O    2   0.000053(  2)  1   0.000004(  5)
    4  O    2   0.000053(  3)  1   0.000004(  6)  3   0.000000(
8)  0
    5  O    2   0.000053(  4)  1   0.000004(  7)  3   0.000000(
9)  0
-------------------------------------------------------------------
------
          MAX     0.000052994    RMS     0.000035369
```

GradGradGradGradGradGradGradGradGradGradGradGradGradGradGradGradGr
adGrad

Berny optimization.
Search for a local minimum.
Step number   3 out of a maximum of   20
All quantities printed in internal units (Hartrees-Bohrs-Radians)
Update second derivatives using information from points 1 2 3
The second derivative matrix:

	r1	r2	r3	r4
r1	0.18261			
r2	-0.04281	0.18262		
r3	-0.04281	-0.04281	0.18262	
r4	-0.04281	-0.04281	-0.04281	0.18262
Eigenvalues ---	0.05419	0.22543	0.22543	0.22543

RFO step: Lambda= 0.00000000D+00.
Quartic linear search produced a step of 0.02729.

Variable	Old X	-DE/DX	Delta X	Delta X	Delta X
New X					
			(Linear)	(Quad)	(Total)
r1	3.54692	0.00005	0.00104	0.00000	0.00104
3.54797					
r2	3.54692	0.00005	0.00104	0.00000	0.00104
3.54796					
r3	3.54692	0.00005	0.00104	0.00000	0.00104
3.54796					
r4	3.54692	0.00005	0.00104	0.00000	0.00104
3.54796					

Item		Value	Threshold	Converged?
Maximum	Force	0.000053	0.000450	YES
RMS	Force	0.000053	0.000300	YES
Maximum	Displacement	0.001042	0.001800	YES
RMS	Displacement	0.001042	0.001200	YES

Predicted change in Energy=-1.177260D-07
Optimization completed.
    -- Stationary point found.

                    ! Optimized Parameters   !
                    ! (Angstroms and Degrees) !

 !   Name   Value   Derivative information (Atomic
Units)   !

 !   r1   1.877   -DE/DX =   0.000053
    !
 !   r2   1.8769 -DE/DX =   0.000053
    !
 !   r3   1.8769 -DE/DX =   0.000053
    !
 !   r4   1.8769 -DE/DX =   0.000053
    !

]GradGradGradGradGradGradGradGradGradGradGradGradGradGradGradGradG
radGrad
 Standard basis: 6-31G   (S, S=P, 6D, 7F)
 There are   33 symmetry adapted basis functions of A'   symmetry.
 There are   16 symmetry adapted basis functions of A"   symmetry.
 Crude estimate of integral set expansion from redundant
integrals=1.164.
     49 basis functions   134 primitive gaussians
     25 alpha electrons   25 beta electrons
        nuclear repulsion energy   219.6698527486 Hartrees.
 DipDrv: will hold 34 matrices at once.

 ****
 ****

         Population analysis using the SCF density.

 ****
 ****

 Orbital Symmetries:
       Occupied (A1) (A1) (E) (E) (A1) (A1) (E) (E) (A1) (A1)
                 (E) (E) (A1) (A1) (E) (E) (A1) (E) (E) (A2) (E)
                 (E) (E) (E) (A1)
       Virtual   (A1) (A1) (E) (E) (A1) (E) (E) (A1) (E) (E) (E)
                 (E) (A1) (A2) (E) (E) (A1) (E) (E) (A1) (A1) (E)
                 (E) (A1)
  The electronic state is 1-A1.
 Alpha occ. eigenvalues -- -104.78295 -20.44221 -20.44219
-20.44219 -20.44219
 Alpha occ. eigenvalues -- -10.52315 -7.98833 -7.98833
-7.98833 -1.17410
 Alpha occ. eigenvalues --   -1.05699 -1.05699 -1.05699
-0.85040 -0.43796
 Alpha occ. eigenvalues --   -0.43796 -0.43796 -0.34133
-0.34133 -0.32187
 Alpha occ. eigenvalues --   -0.32187 -0.32187 -0.29095
-0.29095 -0.29095
 Alpha virt. eigenvalues --   0.25233   0.29922   0.29922
0.29922   0.82149
 Alpha virt. eigenvalues --   0.82149   0.82149   0.83945
1.26938   1.26938
 Alpha virt. eigenvalues --   1.38772   1.38772   1.38772
1.41167   1.41167
 Alpha virt. eigenvalues --   1.41167   1.42122   1.53276
1.53276   1.53277
 Alpha virt. eigenvalues --   1.78493   1.78495   1.78495
2.21431
          Condensed to atoms (all electrons):
               1   2   3   4   5
    1 O   8.433154   0.056653 -0.006695 -0.006695 -0.006695
    2 Cl   0.056653 15.894487   0.056654   0.056654   0.056654
    3 O   -0.006695   0.056654   8.433157 -0.006695 -0.006695

```
4   O    -0.006695    0.056654   -0.006695    8.433157   -0.006695
5   O    -0.006695    0.056654   -0.006695   -0.006695    8.433157
```
Total atomic charges:
```
            1
1   O    -0.469722
2   Cl    0.878899
3   O    -0.469726
4   O    -0.469726
5   O    -0.469726
```
Sum of Mulliken charges=   -1.00000
Atomic charges with hydrogens summed into heavy atoms:
```
            1
1   O    -0.469722
2   Cl    0.878899
3   O    -0.469726
4   O    -0.469726
5   O    -0.469726
```
Sum of Mulliken charges=   -1.00000
Electronic spatial extent (au): <R**2>=   498.3801
Charge=   -1.0000 electrons
Dipole moment (Debye):
```
    X=      0.0000    Y=      0.0000    Z=      0.0001   Tot=
0.0001
```
Quadrupole moment (Debye-Ang):
```
    XX=    -42.9519   YY=    -42.9519   ZZ=    -42.9516
    XY=      0.0000   XZ=      0.0000   YZ=      0.0000
```
Octapole moment (Debye-Ang**2):
```
    XXX=     0.0000   YYY=    -3.8804   ZZZ=      5.4873   XYY=
0.0000
    XXY=     3.8804   XXZ=    -2.7439   XZZ=      0.0000   YZZ=
0.0000
    YYZ=    -2.7439   XYZ=     0.0000
```
Hexadecapole moment (Debye-Ang**3):
```
XXXX=   -196.3926 YYYY=   -196.3926 ZZZZ=   -195.7428 XXXY=
0.0000
XXXZ=      0.0000 YYYX=      0.0000 YYYZ=      0.9083 ZZZX=
0.0000
ZZZY=      0.0000 XXYY=    -65.4642 XXZZ=    -66.1057 YYZZ=
-66.1057
XXYZ=     -0.9083 YYXZ=      0.0000 ZZXY=      0.0000
```
N-N= 2.196698527486D+02 E-N=-2.254065917221D+03 KE=
7.582644274830D+02
Symmetry A'   KE= 6.287581435599D+02
Symmetry A"   KE= 1.295062839231D+02
1|1|GINC-UNK|FOPT|RHF|6-31G|Cl1O4(1-)|PCUSER|12-Jan-1995|1||#
RHF/6-31
 G OPT||Perchlorate
ion.||-1,1|O|Cl,1,r1|O,2,r2,1,109.47|O,2,r3,1,109.4

7,3,-120.,0|O,2,r4,1,109.47,3,120.,0||r1=1.87695143|r2=1.87694746|
r3=1

.87694746|r4=1.87694746||Version=486-Windows-G92RevE.1|State=1-A1|
HF=-
```

```
758.3012613|RMSD=4.302e-009|RMSF=2.736e-005|Dipole=0.,0.,0.000039|
PG=C
 O3V [C3(O1Cl1),3SGV(O1)]||@
```

THE MORE PROGRESS PHYSICAL SCIENCES MAKE, THE MORE THEY TEND TO
ENTER
THE DOMAIN OF MATHEMATICS, WHICH IS A KIND OF CENTRE TO WHICH
THEY ALL
CONVERGE. WE MAY EVEN JUDGE THE DEGREE OF PERFECTION TO WHICH A
SCIENCE HAS ARRIVED BY THE FACILITY WITH WHICH IT MAY BE
SUBMITTED
TO CALCULATION.

                                     -- ADOLPHE QUETELET, 1796-1874
 Job cpu time: 0 days 0 hours 33 minutes 2.0 seconds.
 File lengths (MBytes): RWF=   5 Int=   4 D2E=   0 Chk=   1
Scr=   1
 Normal termination of Gaussian 92.

APPENDIX II

ATOMIC DISPLACEMENTS FOR FREQUENCY CALCULATIONS

The program Gaussian92 produces vast amounts of results listed in the appropriate matrices. In the case of this work, the overlying theme was the prediction of harmonic vibrational frequencies. After a geometry has been found that can be minimized to an ground state structure, a frequency calculation can then be attempted. This is done by inputting the minimized ground state energy structure then adding the key-word "freq" to the command line.

The frequency calculations results are given in wavenumbers and are accompanied by a matrix describing the atomic displacements in the Cartesian coordinate system relative to the ground state geometry. An algorithm was written to read in the ground state geometry then read in the displacement coordinates for each frequency. The atomic displacements are subtract (or added) to the ground state geometry producing the distorted molecule which represents the atoms involved in the particular vibration. The program then displayed the results graphically. The distorted molecule pertaining to the frequency superimposed on the ground state geometry.

The following is the original code written in the Pascal programing language.

```
{ --------------------------------------------------------

                  P T O L E M Y

Displays normal modes of a molecule from data obtained
from vibrational calculations graphically

--------------------------------------------------------}

{$R+}

program Ptolemy;


uses
     crt, graph,dos;

const
     AcceptedChars = [];                        { Active Keys }
     AcceptedExt = [char(59), char(60), char(61), char(62),
char(63),
          char(114),char(64), char(65), char(86), char(87),
char(88),
               char(67), char(66), char(91), char(68),
char(93),char(25)  ];


  Fonts : array[0..4] of string[13] =
  ('DefaultFont', 'TriplexFont', 'SmallFont',
'SansSerifFont', 'GothicFont');

  { The five predefined line styles supported }
  LineStyles : array[0..4] of string[9] =
  ('SolidLn', 'DottedLn', 'CenterLn', 'DashedLn',
'UserBitLn');
  { The two text directions available }
  TextDirect : array[0..1] of string[8] = ('HorizDir',
'VertDir');

  { The Horizontal text justifications available }
  HorizJust  : array[0..2] of string[10] = ('LeftText',
'CenterText', 'RightText');

  { The vertical text justifications available }
```

```
    VertJust   : array[0..2] of string[10] = ('BottomText',
'CenterText', 'TopText');



type
    TypeCharacterSet = set of char;
    CoordArray = array[1 .. 60,1 .. 8] of real;
    L_Matrix   = array[1 .. 60,2 .. 4] of real;

var
        NumAtoms      : integer; { Size of Molecule to be
inputed }
        Coord         : CoordArray; { Input containing
GroundState Coord. }
        Excoord       : L_Matrix;   { Input containing  atomic
displacements}
    GraphDriver : integer;   { The Graphics device driver }
    GraphMode   : integer;   { The Graphics mode value }
    MaxX, MaxY  : word;      { The maximum resolution of the
screen }
    ErrorCode   : integer;   { Reports any graphics errors }
    MaxColor    : word;      { The maximum color value
available }
    OldExitProc : Pointer;   { Saves exit procedure address
}
        Frequency     : integer;   { frequency of the normal
mode }
        P             : pointer;   { Image Memory pointer }
        size          : word;      { Image Memory size }
            KeyHit    : char;      { Key board control }
    ExtKeyHit, done  : boolean;   {      ''       }
                Zoom  : real;


{$F+}
procedure MyExitProc;
begin
    ExitProc := OldExitProc; { Restore exit procedure
address }
    CloseGraph;                 { Shut down the graphics
system }
end; { MyExitProc }
{$F-}

procedure Initialize(var Done : boolean);
{ Initialize graphics and report any errors that may occur }
var
        InGraphicsMode : boolean; { Flags initialization of
```

```
graphics mode }
     PathToDriver   : string;   { Stores the DOS path to
*.BGI & *.CHR }
begin
     done := false;
     { when using Crt and graphics, turn off Crt's
memory-mapped writes }
     DirectVideo := False;
     OldExitProc := ExitProc;                  { save previous
exit proc }
     ExitProc := @MyExitProc;                  { insert our
exit proc in chain }
     PathToDriver := '';
     repeat

{$IFDEF Use8514}                               { check for
Use8514 $DEFINE }
     GraphDriver := IBM8514;
     GraphMode := IBM8514Hi;
{$ELSE}
     GraphDriver := Detect;                    { use
autodetection }
{$ENDIF}

     InitGraph(GraphDriver, GraphMode, PathToDriver);
     ErrorCode := GraphResult;            { preserve error
return }
     if ErrorCode <> grOK then            { error? }
     begin
              Writeln('Graphics error: ',
GraphErrorMsg(ErrorCode));
              if ErrorCode = grFileNotFound then   { Can't
find driver file }
          begin
            Writeln('Enter full path to BGI driver or type
<Ctrl-Break> to quit:');
            Readln(PathToDriver);
            Writeln;
          end
          else
          Halt(1);                             { Some other
error: terminate }
     end;
     until ErrorCode = grOK;
     MaxColor := GetMaxColor;   { Get the maximum allowable
drawing color }
     MaxX := GetMaxX;           { Get screen resolution
values }
     MaxY := GetMaxY;
```

```
end; { Initialize }

function Int2Str(L : LongInt) : string;
{ Converts an integer to a string for use with OutText,
OutTextXY }
var
     St : string;
begin
     Str(L, St);
     Int2Str := St;
end; { Int2Str }

procedure DefaultColors;
{ Select the maximum color in the Palette for the drawing
color }
begin
     SetColor(MaxColor);
end; { DefaultColors }

procedure DrawBorder;
{ Draw a border around the current view port }
var
     ViewPort : ViewPortType;
begin
     DefaultColors;
     SetLineStyle(SolidLn, 0, NormWidth);
     GetViewSettings(ViewPort);
     with ViewPort do
     Rectangle(0, 0, x2-x1, y2-y1);
end; { DrawBorder }

procedure FullPort;
{ Set the view port to the entire screen }
begin
     SetViewPort(0, 0, MaxX, MaxY, ClipOn);
end; { FullPort}

procedure MainWindow(Header : string);
{ Make a default window and view port for demos }
begin
     DefaultColors;                              { Reset the
colors }
     ClearDevice;                                { Clear the
screen }
     SetTextStyle(DefaultFont, HorizDir, 1);    { Default text
font }
     SetTextJustify(CenterText, TopText);       { Left justify
text }
     FullPort;                                  { Full screen
```

```
view port }
      OutTextXY(MaxX div 2, 2, Header +Int2str(frequency));
      { Draw the header }
      { Draw main window }
      SetViewPort(0, TextHeight('M')+4, MaxX,
MaxY-(TextHeight('M')+4), ClipOn);
      DrawBorder;                             { Put a border
around it }
      { Move the edges in 1 pixel on all sides so border
isn't in the view port }
      SetViewPort(1, TextHeight('M')+5, MaxX-1,
MaxY-(TextHeight('M')+5), ClipOn);
end; { MainWindow }

procedure StatusLine(Msg : string);
{ Display a status line at the bottom of the screen }
begin
      FullPort;
      DefaultColors;
      SetTextStyle(DefaultFont, HorizDir, 1);
      SetTextJustify(CenterText, TopText);
      SetLineStyle(SolidLn, 0, NormWidth);
      SetFillStyle(EmptyFill, 0);
      Bar(0, MaxY-(TextHeight('M')+4), MaxX, MaxY);        {
Erase old status line }
      Rectangle(0, MaxY-(TextHeight('M')+4), MaxX, MaxY);
      OutTextXY(MaxX div 2, MaxY-(TextHeight('M')+2),
      msg );
      { Go back to the main window }
      SetViewPort(1, TextHeight('M')+5, MaxX-1,
MaxY-(TextHeight('M')+5), ClipOn);
end; { StatusLine }



procedure GetKey(var Key : char;                { Read in Key
commands }
                   var Extended : boolean;
                   Acceptable,
                   ExtendedAcceptable : TypeCharacterSet;
                   CAPSOn : boolean);

const
      ExtendedKey = chr(0);
      beep = chr(7);

function CharOk( Key : char;
                   Extended : boolean;
```

```
                     Acceptable,
                     ExtendedAcceptable : TypeCharacterSet) :
boolean;
     begin {CharOk}
          CharOk := (Extended and (Key in
ExtendedAcceptable)) or
                     ((not Extended) and (Key in Acceptable))
     end;

begin { GetKey }
     repeat
          key := readkey;
          Extended := (Key = ExtendedKey);
          if Extended
               then
                     Key := readkey
               else
                    if CAPSOn
                         then
                                   Key := upcase(Key);
          if not CharOk(Key, Extended, Acceptable,
ExtendedAcceptable)
               then
               write(Beep)
     until CharOk(Key, Extended, Acceptable,
ExtendedAcceptable)
end; { GetKey }




Procedure Execute(     HitKey : Char;
                    var
                         ExtKeyHit : boolean;
                    var Done : boolean);



     procedure loadcoord;

     var
         GroundName : string[8];
         GroundFile : string[25];
         GroundInput : text;
         A,B : integer;
         vibration : string;


     begin      { loadcoord }
         MainWindow('Loading Coordinates....');
```

```
            StatusLine('   ');
            RestoreCRTMode;
            clrscr;
            gotoXY(8,12);
            write('Enter file name: ');
            readln(GroundName);
            GroundFile :=
concat('C:\FORCE\',GroundName,'.PAS');
            assign(GroundInput, GroundFile);
            reset(GroundInput);
            readln(GroundInput, Frequency);
            readln(GroundInput, NumAtoms);
            for A := 1 to NumAtoms do
            begin
                  for B := 1 to 8 do
                  begin
                        read(GroundInput, Coord[A,B]);
                        Coord[A,B] := Coord[A,B]*10;
                  end;

            end;

            for A := 1 to NumAtoms do
            begin
                  for B := 2 to 4 do
                  begin
                        read(GroundInput, Excoord[A,B]);
                        Excoord[A,B] := Coord[A,B] -
Excoord[A,B]*10;

                  end;

            end;
            SetGraphMode(GetGraphMode);
            close(GroundInput);
            zoom := 100;

            StatusLine('Plot[F2] Rotate-X[F3] Rotate-Y[F4]
Rotate-Z[F5] New[F6] Quit[F7]');
         end;{-LoadCoord-}

        procedure New;
        begin
              clrscr;
              loadCoord;
        end;

     Procedure PlotCoord;
```

```pascal
        var
              X_obs,Y_obs,X_ext,Y_ext : array[1 .. 60] of
integer;
              H,W,A,B,C,D,X1,X2,Y1,Y2 : integer;
              Beta,Conn,View : real;
              CurPort : ViewPortType;



     begin    { plotcoord }
           ClearDevice;
           FullPort;
           { Paint Screen }
           ClearDevice;
           GetViewSettings(CurPort);

           MainWindow('Frequency(wavenumbers): ');
              view := 6;

              H := GetMaxY div 2;
              W := GetMaxX div 2;
              Beta := W/(sin(pi/View)/cos(pi/View));
            Size := ImageSize(50,40,590,430);
              for A := 1 to NumAtoms do
              begin
                 X_obs[A] := W - round(Beta*(1/(Zoom -
Coord[A,2]))*Coord[A,3]);
                 Y_obs[A] := round(Beta*(1/(Zoom -
Coord[A,2]))*Coord[A,4]) + H;

              end;

              for A := 1 to NumAtoms do

              begin
                 X_ext[A] := W - round(Beta*(1/(Zoom -
Excoord[A,2]))*Excoord[A,3]);
                 Y_ext[A] := round(Beta*(1/(Zoom -
Excoord[A,2]))*Excoord[A,4]) + H;
              end;
              for C := 1 to NumAtoms do
                begin
                  A := C;
                  X1 := X_obs[A];
                  Y1 := Y_obs[A];
                   X2 := X_ext[A];
                   Y2 := Y_ext[A];
                      Conn := Coord[A,1];
                  for D := 1 to NumAtoms do
```

```
            begin
                        A := D;
                        if conn = Coord[A,5] then
                        begin
                         setcolor(4);
                         line(X2,Y2,X_ext[A],Y_ext[A]);
                         setcolor(7);
                          line(X1,Y1,X_obs[A],Y_obs[A]);

                end;
                        if conn = Coord[A,6] then
                        begin
                         setcolor(4);
                         line(X2,Y2,X_ext[A],Y_ext[A]);
                         setcolor(7);
                          line(X1,Y1,X_obs[A],Y_obs[A]);

                end;
                        if conn = Coord[A,7] then
                        begin
                         setcolor(4);
                         line(X2,Y2,X_ext[A],Y_ext[A]);
                         setcolor(7);
                          line(X1,Y1,X_obs[A],Y_obs[A]);

                end;
                        if conn = Coord[A,8] then
                        begin
                         setcolor(4);
                         line(X2,Y2,X_ext[A],Y_ext[A]);
                         setcolor(7);
                          line(X1,Y1,X_obs[A],Y_obs[A]);

                end;

                end;
            end;
        GetMem(P, size);
        GetImage(50,40,590,430,P^);
        PutImage(320,240, P^, XORPut);
        PutImage(320,240, P^, XORPut);
        FreeMem(P, Size);
        StatusLine('Load[F1]  Plot[F2] Rotate-X[F3]
Rotate-Y[F4] Rotate-Z[F5] Menu[F10]');

        end; { plotCoord }
```

```
        { -next set of procedures calculate the rotation
matrix in order to
        rotate the molecule in 10 degree increments    }

        procedure RotateX;

    var
        x : real;
      A,B,C,D : integer;

    begin    { rotate X }

        x := 18;
        for A := 1 to NumAtoms do
        begin
              Coord[A,3] := Coord[A,3]*cos(pi/x) +
Coord[A,4]*sin(pi/x);
              Coord[A,4] := Coord[A,4]*cos(pi/x) -
Coord[A,3]*sin(pi/x);
              Excoord[A,3] := Excoord[A,3]*cos(pi/x) +
Excoord[A,4]*sin(pi/x);
              Excoord[A,4] := Excoord[A,4]*cos(pi/x) -
Excoord[A,3]*sin(pi/x);
            end;
        PutImage(320,240, P^, XORPut);
        Plotcoord;

    end;    { rotate X}


    procedure reverseX;

    var
       x : real;
       a,b  : integer;
    begin
        x := 18;
        for a:= 1 to NumAtoms do
        begin
              Coord[a,3] := Coord[a,3]*cos(pi/x) -
Coord[a,4]*sin(pi/x);
              Coord[a,4] := Coord[a,4]*cos(pi/x) +
Coord[a,3]*sin(pi/x);
              Excoord[a,3] := Excoord[a,3]*cos(pi/x) -
Excoord[a,4]*sin(pi/x);
              Excoord[a,4] := Excoord[a,4]*cos(pi/x) +
Excoord[a,3]*sin(pi/x);
            end;
        PutImage(320,240, P^, XORPut);
```

```
        plotcoord;
end; { reverseX }


procedure RotateY;

var
     y : real;
   A,B : integer;

begin
     y := 18;
     for A := 1 to NumAtoms do
     begin
          Coord[A,2] := Coord[A,2]*cos(pi/y) +
Coord[A,4]*sin(pi/y);
          Coord[A,4] := Coord[A,4]*cos(pi/y) -
Coord[A,2]*sin(pi/y);
          Excoord[A,2] := Excoord[A,2]*cos(pi/y) +
Excoord[A,4]*sin(pi/y);
          Excoord[A,4] := Excoord[A,4]*cos(pi/y) -
Excoord[A,2]*sin(pi/y);
          end;
          PutImage(320,240, P^, XORPut);
          Plotcoord;
     end; { RotateY }


procedure reverseY;
var
   y : real;
   a,b : integer;
begin

     y := 18;
     for a := 1 to NumAtoms do
     begin
          Coord[a,2] := Coord[a,2]*cos(pi/y) -
Coord[a,4]*sin(pi/y);
          Coord[a,4] := Coord[a,4]*cos(pi/y) +
Coord[a,2]*sin(pi/y);
          Excoord[a,2] := Excoord[a,2]*cos(pi/y) -
Excoord[a,4]*sin(pi/y);
          Excoord[a,4] := Excoord[a,4]*cos(pi/y) +
Excoord[a,2]*sin(pi/y);
          end;
     PutImage(320,240, P^, XORPut);
     plotcoord;
     end;  { reversY }
```

```
procedure RotateZ;

var
     z : real;
   A,B : integer;

begin

     Z := 18;
     for A := 1 to NumAtoms do
     begin
           Coord[A,2] := Coord[A,2]*cos(pi/z) +
Coord[A,3]*sin(pi/z);
           Coord[A,3] := Coord[A,3]*cos(pi/z) -
Coord[A,2]*sin(pi/z);
           Excoord[A,2] := Excoord[A,2]*cos(pi/z) +
Excoord[A,3]*sin(pi/z);
           Excoord[A,3] := Excoord[A,3]*cos(pi/z) -
Excoord[A,2]*sin(pi/z);
        end;
                 PutImage(320,240, P^, XORPut);

     Plotcoord;
   end; { rotate Z}


procedure reverseZ;
var
   z : real;
   a,b : integer;
begin
     z := 18;
     for a := 1 to NumAtoms do
     begin
           Coord[a,2] := Coord[a,2]*cos(pi/z) -
Coord[a,3]*sin(pi/z);
           Coord[a,3] := Coord[a,3]*cos(pi/z) +
Coord[a,2]*sin(pi/z);
           Excoord[a,2] :=ExCoord[a,2]*cos(pi/z) -
Excoord[a,3]*sin(pi/z);
           Excoord[a,3] := Excoord[a,3]*cos(pi/z) +
Excoord[a,2]*sin(pi/z);
        end;
                 PutImage(320,240, P^, XORPut);

     plotcoord;
   end;   { reverseZ }
```

```
Procedure Animate;

    var
        X_obs,Y_obs,X_ext,Y_ext : array[1 .. 60] of
integer;
        H,W,A,B,X1,X2,Y1,Y2 : integer;
        Beta,Conn,View : real;
        CurPort : ViewPortType;
        P1, P2 : pointer;


procedure PlotGround;

var
    Cg,Dg : integer;

begin { plotground }
    for Cg := 1 to NumAtoms do
    begin
        A := Cg;
        X1 := X_obs[A];
        Y1 := Y_obs[A];
        Conn := Coord[A,1];
        for Dg := 1 to NumAtoms do
        begin
            A := Dg;
            if conn = Coord[A,5] then
            begin
                setcolor(14);
                line(X1,Y1,X_obs[A],Y_obs[A]);

            end;
            if conn = Coord[A,6] then
            begin
                setcolor(14);
                line(X1,Y1,X_obs[A],Y_obs[A]);

            end;
            if conn = Coord[A,7] then
            begin
                setcolor(14);
                line(X1,Y1,X_obs[A],Y_obs[A]);

            end;
            if conn = Coord[A,8] then
            begin
                setcolor(14);
                line(X1,Y1,X_obs[A],Y_obs[A]);

            end;
```

```
                 end;
           end;{ plotground }
     end;

     procedure PlotExcited;

     var
           Cx,Dx : integer;

     begin { plotExcited }
           for Cx := 1 to NumAtoms do
           begin
                 A := Cx;
                 X2 := X_ext[A];
                 Y2 := Y_ext[A];
                 Conn := Coord[A,1];
                 for Dx := 1 to NumAtoms do
                 begin
                       A := Dx;
                       if conn = Coord[A,5] then
                       begin
                             setcolor(14);
                             line(X2,Y2,X_ext[A],Y_ext[A]);

                       end;
                       if conn = Coord[A,6] then
                       begin
                             setcolor(14);
                             line(X2,Y2,X_ext[A],Y_ext[A]);

                       end;
                       if conn = Coord[A,7] then
                       begin
                             setcolor(14);
                             line(X2,Y2,X_ext[A],Y_ext[A]);

                       end;
                       if conn = Coord[A,8] then
                       begin
                             setcolor(14);
                             line(X2,Y2,X_ext[A],Y_ext[A]);

                       end;

                 end;
           end;
     end; { plotExcited }
```

```
begin   { Animate }
      ClearDevice;
      FullPort;
      { Paint Screen }
      ClearDevice;
      GetViewSettings(CurPort);

      MainWindow('Frequency: ');
      StatusLine('Press F2 to abort....');
      view := 6;

      H := GetMaxY div 2;
      W := GetMaxX div 2;
      Beta := W/(sin(pi/View)/cos(pi/View));

      for A := 1 to NumAtoms do
      begin
            X_obs[A] := W - round(Beta*(1/(Zoom -
Coord[A,2]))*Coord[A,3]);
            Y_obs[A] := round(Beta*(1/(Zoom -
Coord[A,2]))*Coord[A,4]) + H;

      end;

      for A := 1 to NumAtoms do

      begin
            X_ext[A] := W - round(Beta*(1/(Zoom -
Excoord[A,2]))*Excoord[A,3]);
            Y_ext[A] := round(Beta*(1/(Zoom -
Excoord[A,2]))*Excoord[A,4]) + H;
      end;

  { -Animation of Molecule -- }
            ClearDevice;
        repeat
            PlotGround;
            Size := ImageSize(50,40,590,430);
      GetMem(P1, size);
            GetImage(50,40,590,430,P1^);
            PutImage(320,240,P1^,Normalput);
            Delay(5);
            FreeMem(p1, size);
            ClearDevice;
            GetMem(p2, size);
            PlotExcited;
            GetImage(50,40,590,430,P2^);
            PutImage(320,240,P2^,Normalput);
            Delay(5);
```

```
                    FreeMem(P2, size);
                    cleardevice;
                until keypressed;

       end; { Animate }

       procedure Menu1;
       begin
             StatusLine('New[F6] Quit[F7] Zoom[F8] Animate[F9]
Menu[shft-F10]');
       end;
       procedure Menu2;
       begin
             StatusLine('Load[F1] Plot[F2] Rotate-X[F3]
Rotate-Y[F4] Rotate-Z[F5] Menu[F10]');
       end;

       procedure ZoomIn;

       begin
             Zoom := Zoom + 5;
             PlotCoord;
       end;

       Procedure ZoomOut;

       begin
             Zoom := Zoom - 5;
             if Zoom < 15 then Zoom := 100 else
             PlotCoord;
       end;

       procedure  print;


          var
                X_obs,Y_obs,X_ext,Y_ext : array[1 .. 60] of
integer;
                H,W,A,B,C,D,X1,X2,Y1,Y2 : integer;
                Beta,Conn,View : real;
                CurPort : ViewPortType;



       begin   { Print }
           ClearDevice;
           FullPort;
           { Paint Screen }
           ClearDevice;
```

```
{GetViewSettings(CurPort);}
SetBkColor(white);

 view := 6;

   H := GetMaxY div 2;
   W := GetMaxX div 2;
   Beta := W/(sin(pi/View)/cos(pi/View));
  Size := ImageSize(50,40,590,430);
   for A := 1 to NumAtoms do
   begin
     X_obs[A] := W - round(Beta*(1/(Zoom -
Coord[A,2]))*Coord[A,3]);
       Y_obs[A] := round(Beta*(1/(Zoom -
Coord[A,2]))*Coord[A,4]) + H;

   end;

   for A := 1 to NumAtoms do

   begin
       X_ext[A] := W - round(Beta*(1/(Zoom -
Excoord[A,2]))*Excoord[A,3]);
       Y_ext[A] := round(Beta*(1/(Zoom -
Excoord[A,2]))*Excoord[A,4]) + H;
   end;
   for C := 1 to NumAtoms do
     begin
       A := C;
       X1 := X_obs[A];
       Y1 := Y_obs[A];
        X2 := X_ext[A];
        Y2 := Y_ext[A];
        Conn := Coord[A,1];
       for D := 1 to NumAtoms do
       begin
                A := D;
                if conn = Coord[A,5] then
                begin
                  setcolor(8);
                  setlinestyle(3,0,ThickWidth);
                  line(X2,Y2,X_ext[A],Y_ext[A]);
                  setcolor(8);
                  setlinestyle(0,0,ThickWidth);
                   line(X1,Y1,X_obs[A],Y_obs[A]);

        end;
                if conn = Coord[A,6] then
                begin
```

```
                        setcolor(8);
                        setlinestyle(3,0,ThickWidth);
                        line(X2,Y2,X_ext[A],Y_ext[A]);
                        setcolor(8);
                        setlinestyle(0,0,ThickWidth);
                         line(X1,Y1,X_obs[A],Y_obs[A]);

                end;
                    if conn = Coord[A,7] then
                    begin
                     setcolor(8);
                     setlinestyle(3,0,ThickWidth);
                     line(X2,Y2,X_ext[A],Y_ext[A]);
                     setcolor(8);
                     setlinestyle(0,0,ThickWidth);
                      line(X1,Y1,X_obs[A],Y_obs[A]);

                end;
                    if conn = Coord[A,8] then
                    begin
                     setcolor(8);
                     setlinestyle(3,0,Thickwidth);
                     line(X2,Y2,X_ext[A],Y_ext[A]);
                     setlinestyle(0,0,Thickwidth);
                     setcolor(8);
                      line(X1,Y1,X_obs[A],Y_obs[A]);

                end;

              end;
          end;
      GetMem(P, size);
      GetImage(50,40,590,430,P^);
      PutImage(320,240, P^, XORPut);
      PutImage(320,240, P^, XORPut);
      FreeMem(P, Size);
      end; { print }
```

```
    { read in key command and execute the appropiate procedure
}

  Begin   { execute }
```

```
      if ExtKeyHit then
          case ord(KeyHit) of
              59 : LoadCoord;           { F1 }
              60 : PlotCoord;           { F2 }
              61 : RotateX;             { F3 }
              62 : RotateY;             { F4 }
              63 : RotateZ;             { F5 }
              64 : New;                 { F6 }
              65 : Done := true;        { F7 }
              91 : ZoomIn;              { shft - F8 }
              66 : ZoomOut;             { F8 }
              67 : Animate;             { F9 }
              86 : reverseX;            { shft - F3 }
              87 : reverseY;            { shft - F4 }
              88 : reverseZ;            { shft - F5 }
              68 : Menu1;               { F10 }
              93 : Menu2;               { shft - F10 }
              25 : print;               { alt - P }


          end
  end; { execute }

  { ----- M A I N    P R O G R A M ----- }

begin
     initialize(Done);

     StatusLine('Load Coordinates[F1]  Quit[F7]');
     repeat
          GetKey(KeyHit, ExtKeyHit, AcceptedChars,
AcceptedExt, false);
          Execute(KeyHit, ExtKeyHit,Done);
     until Done;
     closegraph;
     restorecrtmode;
end.
```

The molecule produced graphically on the screen could be rotated, enlarged, and shrunk. The disired picture is then simply sreen-dumped into the Windows clipboard which then imported Corel Draw! and manipulated to give the disired figure.

Gaussian 92 also produced infrared intensities and Raman activities. For the theoretical Raman spectra, the frequency energies as the x-axis were plotted with Raman activities as the y-axis in the program Sigma Plot. The resulting bar graph was imported into Corel Draw. The appearance of band width was artificially reproduced by using Spectra Calc and fitting an isolated band of the experimental spectrum with a gaussian curve fitting routine. The resulting gaussian was then imported into the Corel Draw file containing the bar graph of the theoretical Raman spectrum. To produce the various intensities of each predicted band, the importanted gaussian curve was simply adjusted according to the predicted intensity.

Vita Auctoris

Name: Barry Klassen

Birthdate: June 2, 1964 Canada (Winnipeg, Manitoba)

Education: B.A. (History) University of Manitoba, 1987

B.Sc.(Chemistry) University of Lethbridge, 1990

Ph.D.(chemistry) University of Windsor, 1996

Publications:

D. Battisti, G. A. Nazri, B. Klassen, and R. Aroca, "Vibrational Studies of Lithium Perchlorate in Propylene Carbonate Solutions" *J. Phys. Chem.*, **1993,**97, 5826.

R. T. Boeré, B. Klassen, and K. H. Moock, "Organometallic Thiazenes. Oxidative addition of S_4N_4 to Low-Valent Metals; ^{15}N NMR of $CpCoS_2N_2$ and $Cp*CoS_2N_2$" *J. Organomet. Chem.*,1993, *467*, 127.

I. Gobernado-Mitre, B. Klassen, and R. Aroca, "Vibrational Spectral and Structure of Perchlorinated Metal-Free Phthalocyanine and Lutetium Bisphthalocyanine", *J. Raman Spectroscopy,* 1993, *24*, 903.

B. Klassen, G. A. Nazri, and R. Aroca, "Lithium Perchlorate, Ab initio Study of the Spectral and Structural Changes Associated with Ion Pairing", *J. Phys. Chem.* In Press.

B. Klassen, G. A. Nazri, and R. Aroca, "Vibrational and Transport Properties of a Binary Solvent Electrolyte" *J. Phys. Chem.* Submitted.

B. Klassen, G. A. Nazri, and R. Aroca, " Structural Study of Ethylene, Propylene, Dimethyl, and Diethyl Carbonates, Applying ab Initio Molecular Orbital Calculations and Vibrational Spectroscopy", *J. Phys. Chem.* Submitted.